Università degli Studi
di Pisa

Facoltà di Ingegneria
Corso di Laurea in Ingegneria Aerospaziale

École Polytechnique Fédérale
de Lausanne

Faculté Sciences et Technique de l'Ingénieur
Génie Mécanique

Master Thesis

Atmosphere Re-Entry Simulation Using Direct Simulation Monte Carlo (DSMC) Method

Supervisors:

Prof. Luca D'Agostino
Università di Pisa

Dr. Pénélope Leyland
École Polytechnique Fédérale de Lausanne

Candidate:

Francesco Pellicani

19 July 2016

Abstract

Aerothermodynamic investigations of hypersonic re-entry vehicles provide crucial information to other key disciplines like structures and materials, assisting the development of efficient and lightweight thermal protection systems (TPS). Under the transitional flow regime, where chemical and thermal nonequilibrium are predominant, the most innovative numerical method for such studies has been the direct simulation Monte Carlo (DSMC) numerical technique. In the 50 years since its invention, the acceptance and applicability of the DSMC method have increased significantly. Extensive verification and validation efforts have led to its greater acceptance, whereas the increase in computer speed has been the main factor behind its greater applicability. As the performance of a single processor reaches its limit, massively parallel computing is expected to play an even stronger role in its future development.

In this study, the Monte Carlo simulator OpenFOAM and Sparta have been studied and benchmarked against numerical and theoretical data for inert and chemically reactive flows and the same will be done against experimental data in the near future.

The results show the validity of the data found with the DSMC. The best setting of the fundamental parameters used by a DSMC simulator are presented for each software and they are compared with the guidelines deriving from the theory behind the Monte Carlo method. In particular the number of particles per cell was found to be the most relevant parameter to achieve valid and optimized results. It is shown how a simulation with a mean value of one particle per cell gives sufficiently good results with very low computational resources. This achievement aims to reconsider the correct investigation method in the transitional regime where both the direct simulation Monte Carlo (DSMC) and the computational fluid-dynamics (CFD) can work,

but with a different computational effort.

In parallel the results deriving from this study have been presented in terms of vibration / electron / electronic and translation / rotational temperature, pressure, Mach number and specie number density required to start a design of a thermal shield.

"Re-entry is perhaps one of the most difficult problems one can imagine. It is certainly a problem that constitutes a challenge to the best brains workings in these domains of modern aerophysics"

Theodhor von Karman, 1956

Acknowledgements

I wish to thank Pénélope Leyland, Jérémy Raphaël Mora-Monteros and Nikhil Banerji for the precious guidance and continual encouragement in doing my thesis.

Special thanks also to the Interdisciplinary Aerodynamic Group and all its members for their help and kindness and, most of all, for having given me the opportunity this research work at the École Polytechnique Fédérale de Lausanne.

Contents

Nomenclature

Latin Symbol

a	Speed of sound, m/s
k	Convective transmission coefficient, W/mK
c	Molecular velocity, m/s
d	Molecular diameter, m
i	Vibrational quantum level, dimensionless
k_B	Boltzmann constant, $m^2 kg\, s^{-2} K^{-1}$
Kn	Knudsen number, λ/L
l	Characteristic length, m
Ma	Mach number, U/a
m	Mass, kg
n	Number density, m^{-3}
p	Scalar pressure, N/m^2
$\dot{q}$	Scalar heat flux, W/m^2
R	Universal gas constant, $J/K\, mol$
Re	Reynolds number, $\rho UL/\mu$

T	Temperature, K
t	Time, s
U	Freestream velocity, m/s
Z	Relaxation number, dimensionless
e	Multiplied 10 to the power of
h	Hours
u, v, w	Velocity vector components, m/s
x, y, z	Spatial Cartesian co-ordinates, m

Greek Symbols

α	Angle of attack, degree
γ	Ratio of specific heats, dimensionless
ε	Energy
λ	Molecular mean free path, m
μ	Viscosity, Ns/m^2
ξ	Collision cross-section, m^2
ρ	Mass density, kg/m^3
σ	Collision cross section, m^2

Superscripts

’	Minutes

Subscripts

∞	Freestream conditions

Abbreviations

p	Particles
t	Time
c	Cell size
O	OpenFOAM
S	Sparta
ref.	Reference
max	Maximum
Diff.	Difference
abs.	Absolute
%	Percentage

Acronyms

AIAA	American Institute of Aeronautics and Astronautics
CFD	Computational Fluid Dynamics
DSMC	Direct Simulation Monte Carlo
NASA	National Aeronautics and Space Administration
NTC	No-Time-Counter
OpenFOAM	Open Field Operation And Manipulation
Sparta	Stochastic PArallel Rarefied-gas Time-accurate Analyzer
QK	Quantum-Kinetic
TC	Time Counter
TCE	Total Collision Energy
TPS	Thermal Protection System
VHS	Variable Hard Sphere

VSS	Variable Soft Sphere
2D	Two-dimensional
3D	Three-dimensional
EPFL	École polytechnique fédérale de Lausanne

1 Introduction

> "You know, there is nothing we can do about damage to the TPS [Thermal Protection System]. If it has been damaged it's probably better not to know. I think the crew would rather not know. Don't you think it would be better for them to have a happy successful flight and die unexpectedly during entry than to stay in orbit, knowing that there was nothing to be done, until the air ran out?"

These are the words of the Director of Mission Operations of NASA, Jon C. Harpold, before Columbia's disaster in February 2003 [35].

It is clear the fundamental importance of the thermal protection system in space missions, moreover when you have to penetrate an atmosphere, whether it be the Earth's one or that of another planet. In fact, if the space exploration starts with the launch of probes in the low orbits around the Earth, modern acknowledgments and the level of technologies achieved, push interest toward the exploration of extraterrestrial bodies with unmanned and mostly manned missions. In order to explore other planets, moons or asteroids and perhaps bring back samples or men from these bodies, aerospace engineers have to deal with the difficulty to make spacecrafts survive until the end of its mission where probably the hardest phase is the atmosphere crossing. Conditions are always extreme there because of the heat, pressure and chemical activity which they encounter. It is evident that spacecrafts have to be protected during atmosphere entry. This is achieved by installing a TPS on the vehicle.

The heat-shields introduction for space applications started with the development of the German V-2 rocket during the Second World War [11]. From that moment technology in the TPS field has improved enormously and nowadays several strategies of thermal protection management have been developed. They can be classified in three main categories: passive, semi-passive and active systems.

Passive thermal protection implies control of the temperature and the heat by conduction through the spacecraft structural materials and radiation from its surface.

Semi-passive systems are characterized by phase change of the shield materials (ablative material).

The active cooling consists of either circulating a fluid in the TPS material in order to increase heat transport or injecting a fluid directly into the boundary layer which increases its thickness and therefore reduces convective heating.

The kind of thermal protection system utilized depends on the speed of entry of the capsule, the chemical composition of the atmosphere, the shape of the exposed surface, which influences the thickness of the boundary layer, and the distance of the shock wave.

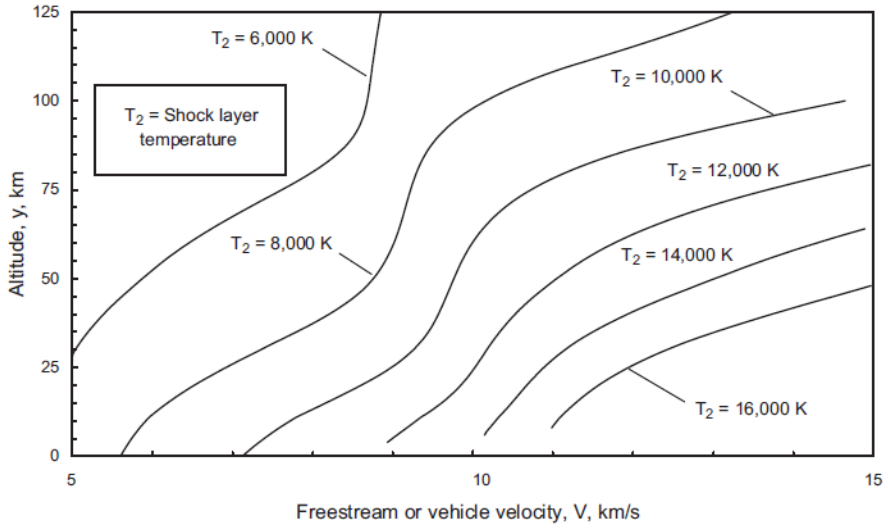

Figure 1.1 Shock Layer Temperature as a Function of Re-entry Parameter Freestream Velocity and Altitude [78]

Since the 1970s, estimation of the heating environment experienced by atmospheric entry vehicles was achieved using analytical formula that rely on theoretical and empirical correlations. It is clear that such a simplified hypothesis induces large error margins and consequently a higher safety factor has to be maintained when designing the TPS . However thermal protection materials, besides withstanding aerodynamic, chemical and thermal loads, have to be both as light as possible, and as simple and as cheap as possible. The importance of the weight factor in space engineering has no need to be explained. The simplicity and the cheapness is related to the fact that the TPS covers almost all the vehicle surface and is consumed each mission. That is why there is the need to improve this field of space engineering to build a model as closest as

possible to what happens in reality in order to obtain exact previsions of what a thermal shield will encounter during its lifetime. This is done passing from the use of analytical formulas to numerical simulations, which now are the main tool of investigation in this field.

A numerical simulation tries to reproduce a particular event. In this case it is important to have detailed knowledge of what happens to a spacecraft which passes through the environment that surrounds a celestial body. Space vehicles entering the atmosphere undergo not only different velocity regimes, hypersonic, supersonic and subsonic, but also different flow regimes, free molecular flow, transition, and continuum. Each of these flow regimes must be considered during the vehicle aerothermodynamic design.

At the highest altitudes, the interaction of the vehicle with the atmospheric air is characterized by free molecular flow. In this regime, the air molecules collide and interact with the vehicle's surface. However, collisions of reflected particles from the surface with freestream particles are not likely to occur. As the vehicle enters deeper into the Earth's atmosphere, the mean free path decreases and collisions between particles reflected from the vehicle's surface and the incoming freestream particles can no longer be ignored. As a result, the flow in this condition defines the transition flow regime, i.e., transition between the free molecular flow regime and the continuum flow regime. In the transition flow regime, the contribution of aerodynamic forces and heat flux to the vehicle surface start to increase rapidly with decreasing altitude, causing large changes in the aerodynamic characteristics of the vehicle when compared with those observed in the free molecular flow. At such altitudes, strong shock waves are formed in front of the vehicle and new flow features such as thermodynamic and chemical nonequilibrium become important for the correct prediction of heating rates and pressure loads acting on the vehicle's surface. As the vehicle continues to enter into the atmosphere, it finally reaches a dense atmosphere characterized by the continuum flow regime. In this regime, the flow around the vehicle is examined by means of a macroscopic model that considers the air as a continuum and the description of the flow is made in terms of spatial and temporal variations of the macroscopic properties, such as velocity, pressure, density and temperature.

1.1 Project Objectives

The purpose of this thesis is to investigate the conditions encountered by a spacecraft entering the atmosphere. The aim is to report the values needed for starting the design of an optimized thermal shield. Therefore a design which can start from data very close to the real conditions experienced by a vehicle during the crossing of the atmosphere without the need of a safety factor higher than the standard one to prevent any inertness.

This study focuses on the higher zones of the atmosphere, where the flow is rarefied. In particular, the zone investigated is characterized by the transitional regime. This kind of flow is above the validity upper limit for the Navier-Stockes equations but below the level at which the flow falls into the free molecular regime. In pursuit of this goal, flows are investigated by employing the direct simulation Monte Carlo (DSMC) method.

The use of this kind of method in the study of hypersonic spacecrafts atmosphere entry at high altitude has been recently implemented in some software, so it is quite a new technique used to deal with these kinds of phenomena. In particular, the Interdisciplinary Aerodynamic Group at the École Polytechnique Fédérale de Lausanne, which is the research group that suggested this study, had never studied this topic before using the DSMC. Therefore the preliminary target is to discover how this solver works and to find the best setting to be used to have accurate results but at the same time efficient in terms of time, power and resources consumption. In particular, two types of software are taken into consideration, OpenFOAM and Sparta with the additional aim to establish which is the best between the two to be used in the future for this kind of simulation.

The subject of the study is the Hayabusa capsule, a probe launched by the Japan Aerospace Exploration Agency (JAXA) which landed on the asteroid 25143 Itokawa and came back to the Earth in 2010. The subject of the simulations is not the relevant point, considering that the Hayabusa mission has already taken place and also with success. The main objective is to analyze the types of software, to find out how they work, to establish the right simulations setting and to extract all the useful data needed for future thermal shield design. The choice of Hayabusa is dictated by the collection of some aerodynamic data made at the point H3 of its re-entry trajectory. This point, at an altitude of 78,8 km with respect to the Earth's surface, is entirely in the transitional regime so it provides some experimental data to be compared with the values obtained from the DSMC. In this way, it is possible also to validate the program and guarantee the production of correct results, considering the absence of experience in this field of application.

In addition another tool of investigation in the field of fluid dynamics simulations want to be studied, that is the DSMC, to understand if it can be a valid alternative to the classical CFD in terms of results and computational resources used.

The main objectives of this thesis are described below:

- Discover how DSMC OpenFOAM and Sparta software work
- Determine the optimized setting for OpenFOAM and Sparta simulations

- Verification and validation of the DSMC solver for rarefied hypersonic reacting flows applied to real cases of atmospheric re-entry
- Comparison of OpenFOAM and Sparta in order to establish the best one to be used for future DSMC of atmospheric entry
- Extraction of data useful to start the design of a thermal shield
- Comparison between two tools of investigation in the fluid dynamics field, CFD and DSMC.

1.2 Thesis Outline

The current chapter serves as an overall introduction to the interest that prompted this study and to give an overview of the goals we set. The rest of the document is structured as follows:

Chapter 2 introduces the numerical simulations technique used in the fluid-dynamic studies with its relative field of validity and presents in detail the Direct Simulation Monte Carlo method.

Chapter 3 describes the OpenFOAM and Sparta software, and the relative DSMC solvers used in the study.

Chapter 4 gives a description of the model used, in particular it presents an overview of the mission, the mesh, the chemistry and physics model and the boundary conditions considered.

Chapter 5 shows the results of the sensitivity study and presents the best setting in terms of results and resources consumed for each software considered. The analysis is conducted over the fundamental parameter governing a DSMC simulation: the number of particles per cell, the time step and the cell size.

Chapter 6 presents the validation of the results derived from OpenFOAM and Sparta, the comparison of the two and with the theoretical data and provides a set of values necessary to start the design of the Thermal Protection System (TPS).

Chapter 7 draws the conclusions for the present work.

2 Fluid-Dynamics Numerical Simulations

Nowadays studies about the environment each kind of machine encounters when traveling in a fluid, as said in Chapter 1, are done using software which can simulate operational conditions. These are called numerical simulators.

2.1 Continuous Regime Simulations

The world is full of objects which move in a fluid, like for example a car, nowadays a very common object, or a boat or a plane. The development of technology achived in the most advanced models of these vehicles like in Formula 1 or in a supersonic fighter aircraft, is a clear indicator of the amount and depth of the analysis that has been done, fundamental in the building of such a machine for the choice of the kind of structure, shape and materials. The level of knowledge achieved in all these fields is possible thanks to the increase of the computational capacity which enables the introduction of the fluid numerical simulation.

The numerical simulations for all the machines moving on the Earth's surface or in its proximity are conducted using software which can simulate the fluid field with the Navier-Stockes equations. This kind of subject is called computational fluid dynamics, usually abbreviated as CFD. In CFD computers are used to perform the calculations required to simulate the interaction of liquids and gases with surfaces defined by boundary conditions.

In all of CFD software the same basic procedure is followed. During pre-processing the geometry (physical boundaries) of the problem is defined. The volume occupied by the fluid is divided into discrete cells (the mesh). The physical modeling to be used is defined, for example you can use the equations of motion together with enthalpy, radiation and species conservation. Then

boundary conditions are defined. This involves specifying the fluid behavior and properties at the boundaries of the problem. For transient problems, the initial conditions are also defined. Then simulation is started and the equations are solved iteratively as a steady-state or transient. Finally a post-processor is used for the analysis and visualization of the results.

2.2 Limits of Continuous Flow Regime

The majority of common machines move on the Earth or in its proximity, even considering planes that fly at a relativly high altitude, but really irrelevant if you think about the vastness of space. In fact, space vehicles, which are the subjects of this study, undergo different flow regimes, as well as different velocity regimes, and not only the continuum, the name given to the motion inside a dense fluid, like the one present in the lower zones of the Earth's atmosphere. Each of these flow regimes must be considered during vehicle design.

The basic criterion that determines the flow regime (collisionless, transition or continuum [12]) is determined by the Knudsen number (2.1).

$$K_n \triangleq \frac{\lambda}{l} \quad (2.1)$$

where λ is the mean free path traveled by particles between collisions and l is the characteristic length of the body.

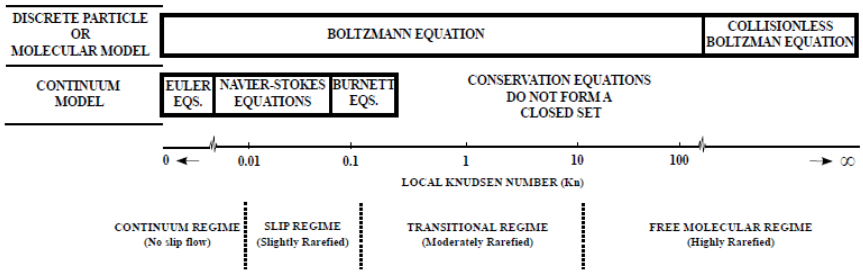

Figure 2.1 Fluid Dynamic Regimes (adapted from Ref. [1]).

Figure 2.1 presents the limits of typical mathematical formulations expressed in terms of the local Knudsen number. A flow is defined in the continuum regime when the Knudsen number approaches zero. On the other hand, a flow is defined in the free molecular flow when the Knudsen number tends to infinity. In the continuum model or macroscopic model, the general

expressions of the fundamental conservation principles that govern the motion of gases are valid for all flow regimes. However, when the Knudsen number increases, these expressions do not form a system of equations in a closed form. The application of conservation equations requires additional information concerning the shear stress tensor and the heat flux vector expressed in terms of macroscopic quantities. The Euler equations for inviscid flow assume that the flow is in local thermodynamic equilibrium, with the velocity distribution function at any point equal to the Maxwellian distribution function. This is the limiting case as the Knudsen number tends to zero. The model expressed by the Navier-Stokes-Fourier equations, called continuum model is assumed to be valid when the Knudsen number is relatively small. In this case, the velocity distribution function can differ from the Maxwellian distribution function. However, the deviation is still small enough so that the transport coefficients, obtained from the Chapman-Enskog theory, are valid [2]. Usually, the terms in the Navier-Stokes-Fourier expressions represent the conservation of linear momentum, mass, and energy in viscous fluids and they are usually applied to the study of Newtonian fluids, where the shear stress tensor is linearly proportional to the deformation rate tensor. Boyd et al. [3; 4] have shown that the difference between the velocity distribution function and the Maxwellian distribution function is significant for a local Knudsen number higher than 0.05, indicating that both the Chapman-Enskog theory and the Navier-Stokes equations are no longer valid. This problem of the failure of the Navier-Stokes equations has an alternative approach consisting in the Chapman-Enskog expansion to a high order to obtain the Burnett equations [5; 6]. However, the application of the Burnett equations has presented additional difficulties with the formulation of the numerical instability and boundary conditions [8]. Furthermore, the Burnett equations increase the order of the differential equations that govern the momentum and energy transport in the gas. These equations are more difficult to solve numerically, and has no solution when the degree of rarefaction is sufficiently high. Moreover the Burnett equations may not satisfy the second law of thermodynamics in certain situations, such as a negative dissipation function or the presence of a heat flux in an isothermal gas [9]. A detailed description of the use of the Burnett equations to solve problems of rarefied hypersonic flow is available in references [10] and [13].

In the microscopic model or molecular model, the gas is treated as an ensamble of particles where the position and velocity of these particles are described individually. Such a system requires the solution of the Boltzmann equation [14]. Analytical solutions of the Boltzmann equation are possible only for collisonless flow, i.e., when the Knudsen number approaches infinity. However, analytical difficulties are present when the Knudsen number is finite. The Boltzmann equation is an integral-differential equation with the velocity distribution function as the only dependent variable. In contrast, the Navier-Stokes-Fourier equations have flow velocity and thermodynamic properties as dependent variables. The reduced number of dependent variables in the Boltzmann equation increases the number of independent variables from the physical space to that of phase

space. Thus for example, a one-dimensional monoatomic gas problem at steady state becomes a three-dimensional gas in phase space. Analytical solutions of the Boltzmann equation usually involve one independent macroscopic variable, simple molecular models and flows with small disturbances. However, rarefied hypersonic flow problems are correlated with complex physical effects, such as chemical reactions and thermal radiation, which have not yet been incorporated into the Boltzmann formulation. Consequently the development of physically-based numerical methods have been stimulated by the mathematical difficulties encountered with the direct solution of the Boltzmann equation. Nowadays, the most widely used technique to compute gas flows at molecular level and to provide solutions to the Boltzmann equation are the molecular dynamics method (MD) [15; 16] and the direct simulation Monte Carlo (DSMC) method [1; 17]. For the purpose of this study, only the DSMC method will be presented and discussed herein.

2.3 Direct Simulation Monte Carlo Method

The direct simulation Monte Carlo method (DSMC) was almost exclusively developed by Bird [1] between 1960 and 1980 and has become one of the most important numerical techniques for solving rarefied gas flows in the transition regime. The DSMC method has its basis on physical concepts of rarefied gases and on the physical assumptions that form the basis for the derivation of the Boltzmann equation [14]. However, the DSMC method is not derived directly from the Boltzmann equation. As both, the DSMC method and the Boltzmann equation are based on classical kinetic theory, then the DSMC method is subject to the same restrictions of Boltzmann equation, i.e., restrictions related to diluted gases and the assumption of molecular chaos. The DSMC method models the flow as a collection of particles or molecules. Each particle is classified with a position, velocity and internal energy [66]. The state of the particle is stored and modified with the time as the particles move, collide and interact with the surface in the simulated physical domain. The assumption of dilute gas (where the mean molecular diameter is much smaller than the mean molecular space in the gas) allows the molecular motion to be decoupled from the molecular collisions. The particles movement is modeled deterministically, while collisions are treated statistically. Since it is impossible to simulate the real number of particles in the computational domain, a small number of representative particles are used and each one represents a large number of real particles. Simulations can contain from thousands to millions of DSMC particles simulators in rarefied flow problems. A computational grid, representing the physical space to be investigated, is necessary in order to use this method. Each cell provides a convenient reference for the sampling of the macroscopic gas properties and for the choice of the potential collision pairs.

2.3.1 Basic Algorithm of the DSMC Method

The DSMC algorithm can be briefly divided into four individual main steps [58]:

- move particles over the time step Δt
- apply boundary conditions such as introducing new particles at inflow boundaries and removing particles at outflow boundaries
- organize particles into cells and perform collisions
- sample average particle information.

Figure 2.2 shows the basic algorithm followed by all DSMC solvers.

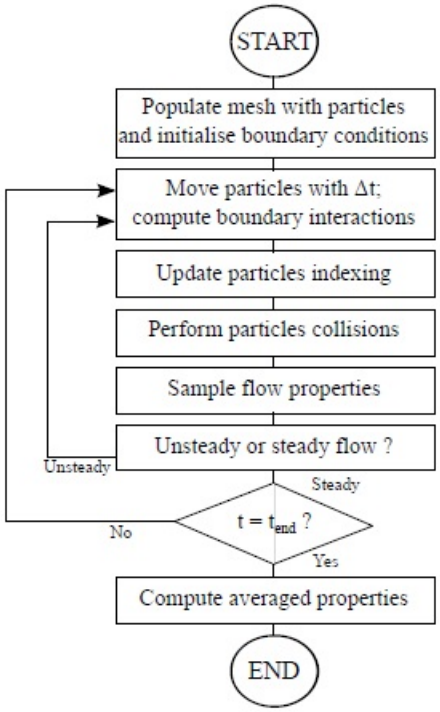

Figure 2.2 Scheme of the Standard DSMC Algorithm

2.3.2 DSMC Method Physical Model

This section describes the most frequently used physical models implemented in DSMC calculations for the study of hypersonic reentry flows. The purpose is to describe the concepts at the base of the physical phenomena modeling boundary conditions, molecular and collision models, rotational and vibrational energy exchange and chemical reactions.

Boundary Conditions Model

In gas dynamic problems, there are basically two types of boundary conditions: those specified by freestream macroscopic properties, and those defined by the physical behavior of a solid surface that interacts with the particles. In the molecular-discrete approach, the first boundary type deals with the inlet and outlet of particles through a given boundary. The main idea of the inlet procedure is to define the flux and thermal state of the molecules that are moving into the simulated domain. The outlet procedure simply consists of removing the particles that leave the domain. Obviously, both procedures must be consistent with the desired flow conditions.

The second boundary type deals with gas-surface interactions, which can modify the thermal state of the impinging particles. The first gas-surface interaction model for kinetic theory was proposed by Maxwell in 1879 [33]. In this model, two types of interactions are considered: specular and diffuse. Specular reflection is perfectly elastic with the particle velocity component normal to the surface being reversed, while those parallel to the surface remain unchanged. Thus, the angle of reflection is the same as the angle of incidence. Usually, the specular boundary condition is considered to represent a perfectly smooth surface or symmetry plane. A diffuse reflection represents a microscopically rough surface in which the particle's post-interaction velocity is not related to its pre-interaction velocity. The post-interaction velocity is computed based on thermal equilibrium with the local surface temperature and the direction of the velocity vector is chosen with equal probability in all directions according to the Maxwellian distribution function. In the diffuse gas-surface interaction model just one accommodation coefficient is required and the scattering angle is independent of the particle's incoming angle. Accommodation coefficients depend upon the fluid, surface material and surface roughness. Theoretical and experimental works have shown [34; 37] that when particles are reflected from a solid surface they show evidence of a preferential direction of reflection resulting in an offset elliptical scattering distribution as shown in Figure 2.3. This behavior is poorly represented by the Maxwell model and in order to circumvent this issue, a phenomenological model was proposed by Cercignani and Lampis in 1971 [38].

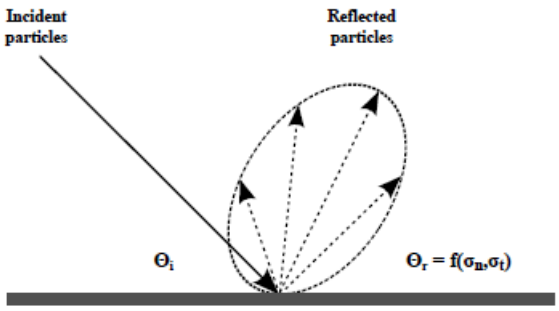

Figure 2.3 Reflection of Particles from a Solid Surface

The Cercignani-Lampis (CL) model is based on the definition of the coefficients α_n and α_t that represent the accommodation coefficients for the kinetic energy associated with the normal and tangential components of velocity. In addition, the scattering angle is a permanent function of the incoming particle angle. This model is relatively simple and produces results similar to the experimental data [39]. A DSMC application of the CL model was proposed by Lord in 1990 [40] through a relatively simple algorithm. In addition, Lord later extended the CLL model to account for rotational and vibrational energy exchange at the surface along with the capability to have diffuse reflections with incomplete energy accommodation [41; 42]. The CLL model is currently implemented in the DSMC solver analyzed.

Molecular Model

A particle's behavior during the collision process depends on the choice of the intermolecular force field. A simple molecular model that is accurate enough for the majority of hypersonic calculations is the inverse power law. In this model, the inter-molecular force is modeled as the inverse of the repulsive power force as follows,

$$Fn = \frac{C}{r^{\eta}} \quad (2.2)$$

where r is the distance between the particles involved in the collision and C and η are constants. In addition, the model proposed in (2.2) corresponds to a Maxwellian gas for $\eta = 5$ and the Hard Sphere model (HS) is obtained by setting$\eta \rightarrow \infty$. In hypersonic flow simulations, millions or billions of particles/molecules are considered and a simple molecular model is required for engineering purposes. In this scenario, the HS model is the simplest and most computationally-efficient alternative. In the HS molecular model, the collision cross section is invariant for a

single gas specie. The scattering angle is isotropic and the post-collision relative velocity is sampled to form a uniform solid angle distribution. Nevertheless, the HS molecular model is not realistic, since the total collision cross-section σ_T does not depend on the relative velocity of the pair of particles involved in the collision process. When the intermolecular potential law is given by (2.4), the theory of Chapman-Enskog provides a direct relationship between the coefficient of viscosity and the gas temperature given by,

$$\mu \propto T^{\omega} \quad (2.3)$$

where ω=1/2(η +3)/(η -1) and η represents a free parameter. According to (2.3), the coefficient of viscosity has a fixed temperature exponent. This exponent is 1 for the Maxwell model and 0.5 for the HS model. Alternative molecular models, based on the HS model, have been proposed. These models have proven very successful at efficiently computationally reproducing the correct viscosity of a gas. The first alternative model was the Variable Hard Sphere (VHS) model proposed by Bird [97]. The VHS model treats particles as "hard-spheres" with respect to the distribution of the scattering angle, i.e., all directions are equally possible for the post-collision velocity in a reference frame based on the center of mass. Moreover, the total cross-section σ_T varies with the relative speed of colliding particles. The VHS model is the most popular molecular model used in DSMC applications. In the VHS model, the collision cross-section is defined as,

$$\sigma \equiv \pi d^2 \propto \left(\frac{1}{2} m_r c_r^2\right)^{-\omega} \quad (2.4)$$

where m_r represents the reduced mass, c_r the relative speed of colliding particles and ω an exponent to be defined subsequently. The collision cross section σ varies with temperature and the relative speed between the particles,

$$\sigma \propto c_r^{-4(\eta-1)} \propto T^{-2/(\eta-1)} \quad (2.5)$$

A comparison of (2.4) and (2.5) shows that ω is related to the exponent of the inverse power law molecular force as follows:

$$\omega = \frac{2}{\eta - 1} \quad (2.6)$$

where ω is equal to zero for the HS model,1/4 for the inverse power law model, and1/2 for the Maxwell model.

Koura and Matsumoto [44; 45] further improved the VHS model and introduced the Variable Soft Sphere (VSS) molecular model. The VSS model considers anisotropic post-collision scattering. Hassan and Hash [46] introduced the Generalized Hard Sphere (GHS) molecular model. The GHS molecular model takes into account both attractive and repulsive parts of the particle-particle interaction. Since the GHS model can reproduce the effects of the attractive portion of an interaction potential, the model is suitable to simulate low temperature flows that are dominated by attractive collisions [48; 49] and are diffusion-driven.

Collision Model

There are a number of techniques for simulating collisions in the DSMC method. Among them, the Time Counter (TC) [17], Null Collision (NC) [29; 30], NTC method [31], and the Generalised Scheme [32]. Bird's NTC technique is the most widely used collision scheme and it will be discussed here. The establishment of the correct collision rate is essential in the DSMC approach. From the kinetic theory, it can be shown that the number of collisions (N_{coll}) pairs to be simulated in a cell over the time step $\triangle t$ is as follows:

$$N_{coll} = \frac{1}{2}\frac{Nn(\overline{\sigma_T c_r})\Delta t}{V_c} \quad (2.7)$$

where n is the number density, N is the number of particles in the cell, σ_T is the collision cross section, and c_r is the relative velocity. In order to determine the total number of collisions during the time step $\triangle t$, the average product of the mean relative velocity c_r and the collision cross section σ_T must be calculated for all possible collision pairs. For such calculations, the numerical code that employs this procedure would have a computational time proportional to N^2. In order to overcome this issue, Bird [17] introduced the parameter $(\sigma_T c_r)_{max}$ where the subscript max denotes the largest value for the product in the cell and it should be updated during a binary collision if the real product $\sigma_T c_r$ is greater than $(\sigma_T c_r)_{max}$. In addition, the parameter $(\sigma_T c_r)_{max}$ is used to determine a real collision according to the following operations:

1. A pair of particles is randomly chosen within a cell volume

2. The product of the mean relative velocity c_r and the collision cross σ_T for the colliding pair is calculated

3. If the product $\sigma_T c_r$ is greater than $(\sigma_T c_r)_{max}$, the maximum value is updated

4. The probability of a collision occuring is given by:

$$P_{coll} = \frac{\sigma_T c_r}{(\sigma_T c_r)_{max}} \quad (2.8)$$

if the probability P_{coll} is greater than R_f, then the pair of particles is accepted for collision, where R_f is a uniform random number ranging from0 to1. Otherwise, a new pair is randomly chosen and the procedure is repeated. This acceptance-rejection method to select the collision pair of particles is described in detail by Bird [1].

5. If the pair of particles is accepted for the collision process, then cell time is advanced by an increment δt by setting

N_{coll}= 1,

$$\delta t = \frac{2}{N n \sigma_T c_r} \quad (2.9);$$

6. The number of collisions are calculated in the cell until the sum of δt is slightly higher than the time step $\triangle t$.

The procedure described above is called Time Counter (TC) and it was proposed by Bird in 1976 [17]. Despite reproducing the correct non-equilibrium collision rate with an optimal computational performance, the TC technique can lead to some problems under extreme non-equilibrium conditions, such as in strong shock waves. The acceptance of low probability collisions, i.e., pairs with a small value of $\sigma_T c_r$, results in large δt values. Consequently, the time increment sum can exceed $\triangle t$ by unacceptable amounts. From a computational aspect, as reported by Baganoff and McDonald [50], the total number of simulated collisions may be very different from one cell to another. Besides, this number is unknown until time step $\triangle t$ is determined. Such an implementation makes the numerical vectorisation of the collision procedure a difficult task.

In order to overcome this problem, Bird [31] proposed the collision model named No Timer Counter (NTC). NTC and TC techniques have the same selection rule for the collision pair, which is based on the acceptance-rejection method; however, in the NTC technique the maximum number N_{coll} of collisions to be selected over $\triangle t$ in a cell is set before the selection of the colliding pairs. In this new collision method, the time count is replaced by an explicit dependence of N_{coll} on the time step, i.e., the number of collisions does not depend on the choice of pairs or particular values of $\sigma_T c_r$. In this new approach, this number of collisions is given by:

$$N_{coll} = \frac{1}{2} \frac{N \overline{N} F_N (\sigma_T c_r)_{max} \Delta t}{V_c} \quad (2.10)$$

where F_N is the number of real molecules represented by each simulated molecule, N is the number of particles within a cell, and $\overline{N}$ is a mean value of N. The collision probability for each chosen pair is given by (2.10). Additional information about the NTC method are available in Ref. [1].

Energy Exchange Model

The thermal nonequilibrium may have a significant influence on the amount of chemical reactions produced during atmospheric entry. In this scenario, it is of great importance that the model used in the energy exchange between kinetic and internal modes is physically realistic. For polyatomic gases, the energy exchange cannot be computed accurately using a simple collision model. The internal energy transfer between the various modes is usually implemented into the DSMC method by the phenomenological model introduced by Borgnakke and Larsen [51]. In this model, the probability of an inelastic collision determines the rate at which energy is transferred between translational and rotational mode after an inelastic collision. A fraction φ of the translational collisions are assumed to be inelastic, and the rest of the collisions $(1-\varphi)$ are considered as elastic. The fraction φ can be interpreted as the average probability of the energy exchange between rotational or vibrational modes for translational collisions. This average probability can be determined from measurements of relaxation times. The relaxation time is a function of local flow properties and may be related to the relaxation number (or collision number) Z. The relaxation or collision number Z is usually defined as:

$$Z = \frac{\tau}{\tau_c} \quad (2.10)$$

where τ is the relaxation time and τ_c is the mean collision time. The collision number is the average number of molecular collisions that are required for a particular mode to obtain equilibrium energy. Therefore, given this number, the average probability φ for each mode in a given collision is conveniently defined as

$$\varphi = \frac{1}{Z} \quad (2.11)$$

Usually, DSMC calculations employ the rotational collision number Z_{rot}=5. In other words, it means that, on average, rotational energy relaxation occurs once every five collisions. In general, this is a good approximation for engineering problems; however, more realistic models for a rotational collision number as a function of the translational temperature or translational energy have been proposed[52; 53]. Lumpkin et al. [54] have noted that the mechanisms of

energy transfer used in DSMC calculations affect the energy transfer rate. According to them, the value of the collision number used in the DSMC should be approximately half of that determined experimentally and employed in a continuum computation. In this scenario, the following equation should be applied:

$$Z_{rot}^{DSMC} = \frac{Z_{rot}^{cont}}{1 + \frac{\varsigma_{rot}}{\varsigma_{tra}}} \quad (2.12)$$

where ς_{rot} and ς_{tra} are the degrees of freedom for rotational and translational energy, respectively. The vibrational modes of a gas are activated when the particles that compose the fluid are sufficiently excited. This situation may occurs in the presence of strong compressibility effects and high temperature regions provoked by shock waves. In DSMC calculations, it is commonly accepted that the vibrational energy can only assume discrete quantum levels, as proposed by Haas et al. [55] and Bergemann and Boyd [56]. In the present study, the vibrational energy redistribution occurs before rotational and translational energy exchange and a serial application of the quantum Larsen- Borgnakke method is considered here.

The vibrational collision number Z_v can then be calculated as [57]:

$$Z_{vib} = \left(\frac{\Theta_d}{T_c}\right)^{\omega} \left[Z_{ref}\left(\frac{\Theta_d}{T_{Z_{ref}}}\right)^{-\omega}\right] \exp\left[\left(\frac{\Theta_d}{T_c}\right)^{\frac{1}{3}} - 1\right] / \left[\left(\frac{\Theta_d}{T_{Z_{ref}}}\right)^{\frac{1}{3}} - 1\right] \quad (2.13)$$

where Θ_d represents the characteristic dissociation temperature, T_c is a "quantised collision temperature" defined as:

$$T_c = \frac{i_{max}\Theta_v}{\frac{7}{2} - \omega} \quad (2.14),$$

i_{max} is the maximum quantum level available to the particle and Z_{ref} is the vibrational collision number at a reference temperature $T_{Z_{ref}}$, which is usually taken to be the characteristic vibrational temperature, Θ_v, as cited in Ref. [112]. Once the vibrational collision number has been calculated, the particle is tested for vibrational energy exchange and is accepted if

$$\frac{1}{Z_{vib}} > R_f \quad (2.15)$$

where R_f is a random number between 0 and 1. An integer post-collision vibrational quantum level i^* is chosen uniformly between 0 and the maximum possible level i^*_{max} and the acceptance-rejection method is used to select a value of i^* using a quantised version of the Larsen-Borgnakke probability ratio [56]:

$$\frac{P}{P_{max}} = \left(1 - \frac{i^* k_B \Theta_v}{E_c}\right)^{\frac{3}{2}-\omega_{rs}} \quad (2.16)$$

where ω_{rs} is the average viscosity exponent of the collision pair r and s, E_c is:

$$E_c = \left(\frac{C_1}{T_{Zref}^{\omega}}\right) \exp\left(C_2 T_{Zref}^{-\frac{1}{3}}\right) \quad (2.17)$$

where C_1 and C_2 are constants which can be found in Appendix A of Ref. [1], and $T_{Z_{ref}}$ is set as Θ_v. The total energy of the colliding pair is reduced accordingly and particle r is then considered for relaxation into rotational and translational modes using the standard Larsen-Borgnakke method. When particles are initialized, introduced at a freestream boundary, or reflected at a diffuse surface, they must be assigned a vibrational energy. First, a quantum level is chosen by analogy to how rotational energy is chosen for a diatomic molecule, i.e.

$$i = \left[\frac{-\ln(R_f)\, T_{vib}}{\Theta_v}\right] \quad (2.18)$$

where T_{vib} is the vibrational temperature, and then the vibrational energy of the particle is assigned from the relation:

$$\varepsilon_{vib} = i k_B \Theta_v \quad (2.19)$$

2.3.3 Chemistry Model

A considerable number of chemistry models relevant to hypersonic aerothermodynamics have been developed like Rebick and Levine [60] model, vibrational bias model [61], threshold line model [62], maximum entropy model [63], and the total collision energy model (TCE) model [1; 64; 65]. Introduced by Bird [64], the TCE model became the most commonly used chemistry model for DSMC simulations of rarefied hypersonic reacting flows. This model is based on a modified Arrhenius rate coefficient of the form:

$$C = a T^b \exp\left(\frac{\varepsilon_{act}}{k_B T}\right) \quad (2.20)$$

where a and b are constants, and ε_{act} is the activation energy of the reaction. The probability of a reaction, P, is obtained by integrating the equilibrium distribution function for the total collision energy and equating it to the chemical rate coefficient,

$$C = \langle \sigma c_r \rangle \int_{\epsilon_{act}}^{\infty} P\left(\varepsilon_c\right) f_B\left(\varepsilon_c\right) d\varepsilon_c \quad (2.21)$$

where σ is the elastic cross section, c_r is the relative velocity, and $f_B\left(\varepsilon_c\right)$ is the equilibrium Boltzmann distribution function for the total collision energy, ε_c. The total collision energy consists of the translational collision energy, and the sum of the rotational and vibrational energies of the two colliding particles considered for a reaction. In this case, the reaction probability for the TCE model is given by:

$$P_{TCE} = A\frac{\left(\varepsilon_c - \varepsilon_{act}\right)^{\psi}}{\left(\varepsilon_c\right)^{\chi}} \quad (2.22)$$

where

$$A = \frac{a\varepsilon\sqrt{\frac{1}{2}m_r\pi}(\varsigma + 2 - \omega)}{\sigma_{ref}\left[\left(2-\omega\right)k_B T_{ref}\right]^{\omega} k_B^b \left(2-\omega\right)\Gamma(\varsigma + b + 3/2)} =$$

$$= B\frac{(\varsigma + 2 - \omega)}{\left(2-\omega\right)\Gamma(\varsigma + b + 3/2)} \quad (2.23)$$

the parameters ω, σ_{ref} and T_{ref} are employed in the Variable Hard Sphere collision model [1], ς is the average number of rotational and vibrational degrees of freedom, and m_r is the reduce mass of two colliding particles. In addition, ε=1 for collisions of two particles of the same species, and ε=1/2 for different species. The exponents in (2.22) is given by:

$$\psi = b + 1/2 + \varsigma \quad (2.24)$$

and

$$\chi = 1 + \varsigma - \omega \quad (2.25)$$

The TCE model was extended [67, 68] to take into account the coupling between vibrational energy and collision-induced dissociation. This model extension, called Vibrationally Favored Dissociation (VFD), includes an additional dependence of the reaction probability on the vibrational

energy of the reactant particle. The Total Collision Energy model is highly phenomenological and employs equilibrium kinetic theory to convert the conventional Arrhenius rate coefficients, defined in terms of macroscopic gas temperature, into collision probabilities which are a function of the collision energy at microscopic level. In addition, this model is dependent on the availability of experimental data to fit the Arrhenius rate coefficient equation.

DSMC being a particle-based method, is of fundamental importance to develop a molecular level chemistry model that predicts equilibrium and non-equilibrium reaction rates using only kinetic theory and fundamental molecular properties. In doing so, Bird recently proposed a chemical reactions model based solely on the fundamental properties of the two colliding particles, i.e., total collision energy, the quantised vibrational levels, and the molecular dissociation energies. These models link chemical reaction and cross sections to the energy exchange process and the probability of transition between vibrational energy states. The Larsen-Borgnakke [51] procedures and the principle of microscopic reversibility are used to derive a simple model for recombination and reverse reactions. Called "Quantum-Kinetic", this DSMC chemistry model has been developed since 2009 [111; 69–73].

3 DSMC Software

3.1 OpenFOAM

OpenFOAM (Open source Field Operation And Manipulation) is a C++ toolbox for the development of customized numerical solvers, and pre-/post-processing utilities for the solution of continuum mechanics problems, from complex fluid flows involving chemical reactions, turbulence and heat transfer, to acoustics, solid mechanics and electromagnetic [75]. The code is released as free and open source software under the GNU General Public License. OpenFOAM is developed primarily by OpenCFD Ltd.

The version used in this study is OpenFOAM 2.3.1

3.1.1 *dsmcFoam* Solver

The *dsmcFoam* code is employed in the present work to solve moderate rarefied non-reacting hypersonic flows over complex geometries. This new freeware, based on Bird's algorithm [1], has been developed to solve complex engineering problems [74]. The main features of the *dsmcFoam* code contain particle initialization in arbitrary geometries, the capability to perform both steady state and transient DSMC simulations, particle tracking in unstructured meshes, and unlimited parallel processing. OpenFOAM provides also powerful meshing tools, such as the *snappyHexMesh*, allowing to the user build complex structured and unstructured meshes for use in DSMC simulations. In addition, force measurements tools like heat flux measurement tools provide a very useful way to calculate the external forces acting on a body and the quantity of heat it is receiving during the re-entry phase. Post-processing is carried out using a variety of post-processing software, among which Paraview is the software provided by OpenFOAM.

The main features of the *dsmcFoam* solver are summarized in the list below:

- Arbitrary 2D/3D/axi-symmetric geometries;
- Mesh generation, walls/freestream properties extraction, and force and heat measurements tools;
- Availability of different boundaries conditions, such as freestream, vacuum, cyclic, and specular/diffuse/CLL models for gas-surface interactions;
- Steady state and transient simulations;
- Automatic sub-cells generation;
- Post-processing and dumping file capability.

When using the *dsmcFoam* solver, six main step may are employed:

1. Build or import the computational mesh;
2. Set up the freestream properties, boundary conditions, and time step size;
3. Fill the mesh with DSMC particles with *dsmcInitialise*;
4. Start the simulation using the command *dsmcFoam*;
5. Enable the time averaging process once the steady state solution has been archived;
6. Perform the post-processing, using the Paraview or other software.

3.2 Sparta

Sparta, acronym for Stochastic PArallel Rarefied-gas Time-accurate Analyzer, is a Direct Simulation Montel Carlo code that models rarefied gases, using collision, chemistry, and boundary condition models [23].

Sparta can model systems with only a few particles up to millions or billions. It uses a hierarchical Cartesian grid to track and group particles for 3D or 2D or axisymmetric models. Objects embedded in the gas are represented as triangulated surfaces and cut through grid cells. Sparta

runs efficiently on single-processor desktop or laptop machines, but is designed for parallel computers. This includes distributed- or shared-memory parallel machines as well as commodity clusters. Sparta was developed at Sandia National Laboratories, a US Department of Energy (DOE) laboratory. It is written in C++ which is used at a hi-level to structure the code and its options in an object-oriented fashion. The kernel computations use simple data structures and C-like code for efficiency. It run on any machine that compiles C++ and supports the MPI message-passing library. The code is a freely-available open-source code, distributed under the terms of the GNU (GNU's Not Unix) operative system Public License, or sometimes by request under the terms of the GNU Lesser General Public License (LGPL), which means the code is completely modifiable.

3.2.1 Sparta DSMC Solver

The main features of the Sparta solver are summarized in the list below:

Models

- 3D or 2D or 2D-axisymmetric domains;
- Variety of global boundary conditions;
- Create particles within flow volume;
- Emit particles from simulation box faces due to flow properties;
- Emit particles from simulation box faces due to profile defined in file;
- Emit particles from surface elements due to normal and flow properties;
- Ambipolar approximation for ionized plasmas.

Geometry

- Cartesian, heirarchical grids with multiple levels of local refinement;
- Create grid from input script or read from file;
- Embed triangulated (3D) or line-segmented (2D) surfaces in grid, read in from file.

Gas-Phase Collisions and Chemistry

- Collisions between all particles or pairs of species groups within grid cells;
- Collision models: VSS (Variable Soft Sphere), VHS (Variable Hard Sphere), HS (Hard Sphere);
- Chemistry models: TCE (Total Collision Energy), QK (Quantum Kinetic).

Surface Collisions and Chemistry

- collisions: specular or diffuse.

Performance

- Grid cell weighting of particles;
- Adaptation of the grid cells between runs;
- On-the-fly adaptation of the grid cells;
- Static load-balancing of grid cells or particles;
- Dynamic load-balancing of grid cells or particles.

Diagnostics

- Global boundary statistics;
- Per grid cell statistics;
- Per surface element statistics;
- Time-averaging of global, grid, surface statistics.

Output

- Log file of statistical info;
- Dump files (text or binary) of per particle, per grid cell, per surface element values;
- Binary restart files;
- On-the-fly rendered images and movies of particles, grid cells, surface elements.

Pre- and Post-Processing

- Various pre- and post-processing serial tools are packaged with SPARTA;
- Separate toolkit, written by Sparta developers, called Pizza.py which provides tools for doing setup, analysis, plotting, and visualization for SPARTA simulations.

4 Model Building

4.1 Hayabusa Mission

The study is conducted on the Hayabusa capsule and to be precise on the point H3 of its re-entry trajectory. All the data used for the simulation are the original ones of the mission. In particular the geometry used is the Hayabusa's original one and the initial conditions are the ones measured from Hayabusa at the point considered.

The choice of Hayabusa for this study is due to the fact that during its re-entry it collects some data at certain points, as anticipated. These provide real data for starting the simulations and, at the same time, data to make a comparisons for the validation of the results obtained. This is necessary to know if the simulations are correct or not.

Moreover it experienced a direct re-entry in the Earth's atmosphere characterized by very high entry velocity. These are very critical conditions which are typical of extraterrestrial mission re-entry, so interesting for actual space mission targets.

4.1.1 Mission Overview

The Hayabusa capsule was an unmanned spacecraft developed by the Japan Aerospace Exploration Agency (JAXA) to return a sample of material from a small near-Earth asteroid, named 25143 Itokawa, to Earth for further analysis [24]. The scientific aim of Hayabusa was to achieve a deeper knowledge of the asteroids that include in their rocks the story of the Universe from the Big Bang. Until that moment, the only extra-terrestrial celestial body from which it has been gathered samples is the Moon. However asteroids are believed to be small enough to have preserved the state of the early solar system and are sometimes referred to as celestial fossils. A

soil sample from an asteroid can give clues about the raw materials that made up planets and asteroids in their formative years, and about the state of the inside of a solar nebula around the time of the birth of the planets.

Hayabusa was the first spacecraft designed to deliberately land on an asteroid and then take off again. And that was only the second time in history a spacecraft descended to the surface of an asteroid (NASA's Near Earth Asteroid Rendezvous-Shoemaker spacecraft landed on asteroid Eros on February 12, in 2001. But it was not designed as a lander and was eventually deactivated after it arrived). For this reason the mission has also some technological targets. Hayabusa was designed as a flying test-bed to research several new engineering technologies necessary for develop the autonomous navigation, atmospheric re-entry, electrical propulsion (it used a ion thruster) and obviously for returning planetary samples.

Mission Profile	
Name	HAYABUSA (MUSES-C)
International Design Code	2003-019A
Objectives	Analyze asteroid samples, test new engineering technologies including autonomous navigation, sampler and reentry capsule
Launch	May 9, 2003
Place	Kagoshima Space Center (Uchinoura)
Launch Vehicle	M-V-5
Weight	510 kg
Dimensions	Core 1.0m x 1.1m x 1.6m (Hexahedron)
Orbit	Heliocentric

Table 4.1 Hayabusa Analytical Mission Profile

Mission Time-Line

1986–1987

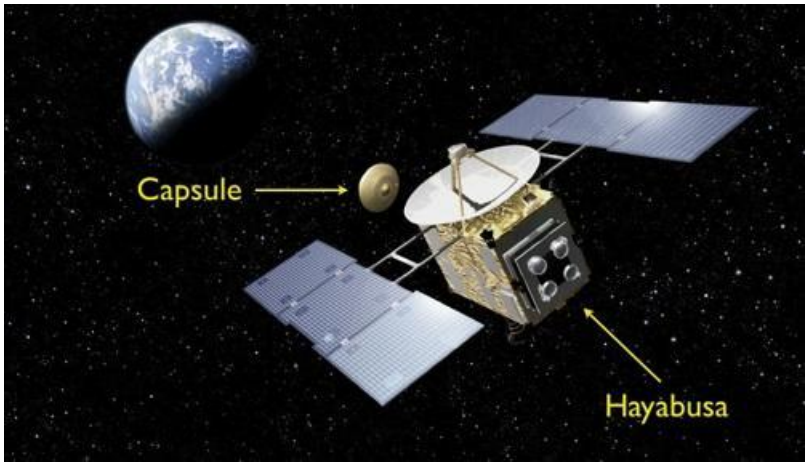

Figure 4.1 Hayabusa Initial Configuration together with the Capsule Re-Entered on the Earth

The asteroid exploration mission by the Institute of Space and Astronautical Science (ISAS) originated in 1986–1987 when the scientists investigated the feasibility of a sample return mission to Anteros and in 1995 selected the asteroid sampling as an engineering demonstration mission.

2003 May

MUSES-C was launched by M-V rocket towards a different target from the original plan, asteroid Itokawa, and the probe was named "Hayabusa".

2005 September

Hayabusa reached Itokawa using ion-thruster and swing-by maneuver.

2005 November

Hayabusa landed on the asteroid in the 19th after some problems and failed tries. It landed again in November 25, but in both cases nobody was sure the sampling operations had been carried out because of communication problems during the touchdown.

2006 April

After restoring communication and the right attitude and checking the state of the engine and batteries, Hayabusa started the return journey.

2009 March

Hayabusa was on a trajectory which would pass 20,000 km from Earth, completing the orbit transfer operation from Itokawa to Earth.

2009 June

The reentry capsule was released at 10:51 UTC on 13 June in Woomera, South Australia.

4.1.2 Geometry

In Figure 4.2 you can see the geometry of the Hayabusa capsule. From the technical design the geometry used to build the mesh is created using the CATIA software. The geometry is only a quarter of the entire capsule. This simplification is possible considering that it has a double symmetry plane. This reduction of the geometry enables a reduction in the amount of calculations for the simulations and so saves time and computational memory.

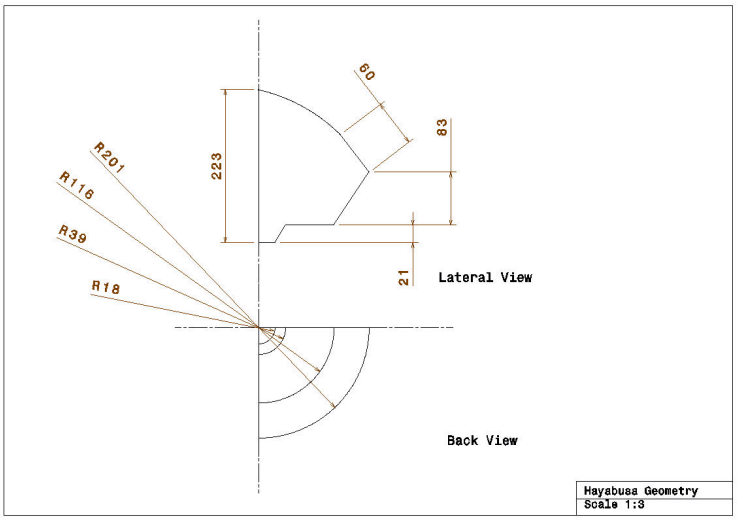

Figure 4.2 Technical Drawing of Hayabusa Capsule

A two-dimensional and a tri-dimensional geometry is created. The geometry used in the following part of the study is the two-dimensional one. In fact the capsule in its re-entry trajectory has a 0° angle of attack, so there is no need to use a tri-dimensional domain because the entire domain is symmetric. Anyway also a tri-dimensional simulation is performed to make a comparison of the results and prove that the two-dimensional simulation gives equivalent results.

4.1.3 Free Stream Conditions

The free stream conditions measured at the re-entry trajectory point analyzed, point H3, at an altitude of 78.8 km and then used as the initial condition of the simulation are the following:

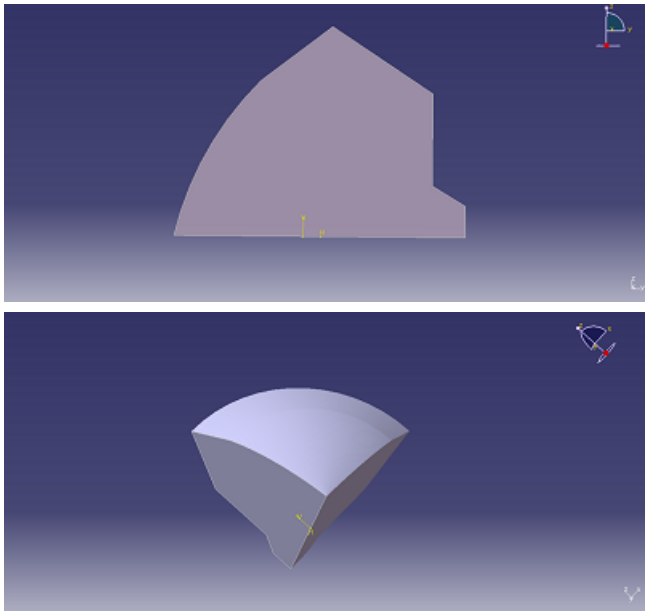

Figure 4.3 Two-Dimensional and Tri-Dimensional Hayabusa Geometry Considered

Velocity: 11705 m/s

Temperature: 199.05 K

Density: 1.908e-5 kg/m^3

4.2 Mesh

The mesh was the first big step of the work, in fact the mesh is an integral part of the numerical solution.

The mesh is a discrete representation of the domain that is involved in the problem. Essentially, it partitions space into elements (or cells or zones) over which the simulation can be performed.

The mesh is fundamental in a simulation because the rate of convergence, the solution accuracy and the simulation time depend on it. In fact during any run, the simulator checks that the mesh satisfies a fairly stringent set of validity constraints and will cease running if the constraints are not satisfied. Therefore the accuracy of the results as the outcome of the simulations depend on it.

Cells

There are two types of two-dimensional cell shapes that are commonly used. These are the triangle and the quadrilateral.

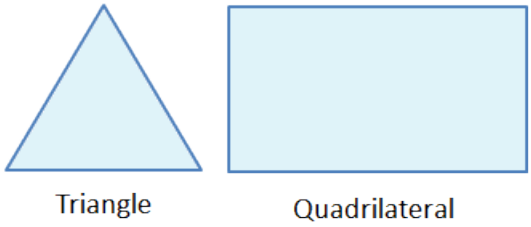

Figure 4.4 Two-Dimesional Cell Shape Used in Mesh Generation.

The basic tri-dimensional elements are the Hexahedron, Wedge, Prism, Pyramid, Tetrahedron, Tetradehral wedge.

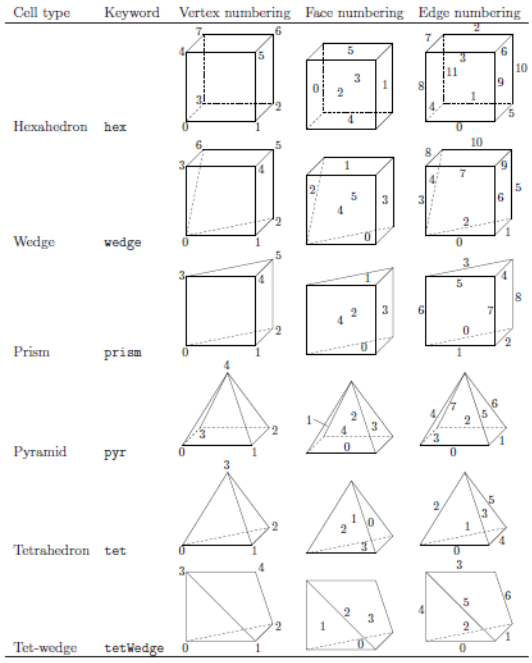

Figure 4.5 Vertex, Face and Edge Numbering for Tri-Dimensional Cell with OpenFOAM Keyword.

Grid

Structured grids are identified by regular connectivity. The possible element choices are quadri-

lateral in 2D and hexahedral in 3D. This model is highly space efficient, i.e. since the neighborhood relationships are defined by storage arrangement and also have a high level of convergence and resolution.

Other types of grid are the unstructured grid, which is identified by irregular connectivity and typically employed triangles in 2D and tetrahedral in 3D, and the hybrid grid which contains a mixture of structured portions and unstructured portions.

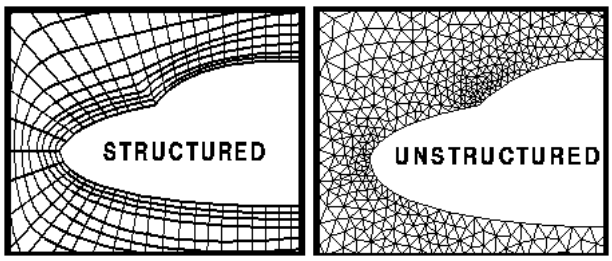

Figure 4.6 Structure and Unstructured Two-Dimensional Mesh [79]

DSMC Mesh

The fluidynamics simulators use the discretization of the space made with the mesh to solve the Navier-Stockes equations and all the other equations that rule the problem inside each element.

In the DSMC the cell are used to contain the particles that simulate the fluid, so each cell is considered as a box where collisions and possibly reactions can happen and from where the particles can enter and exit according to their velocity related to the time step.

The different use of the mesh implies that the building of the calculation domain is different for a DSMC or a CFD simulation. In particular in CFD the mesh has to be more refined where the gradients of the thermodynamic fields are higher. So it appears more refined along the boundaries and the shock layer.

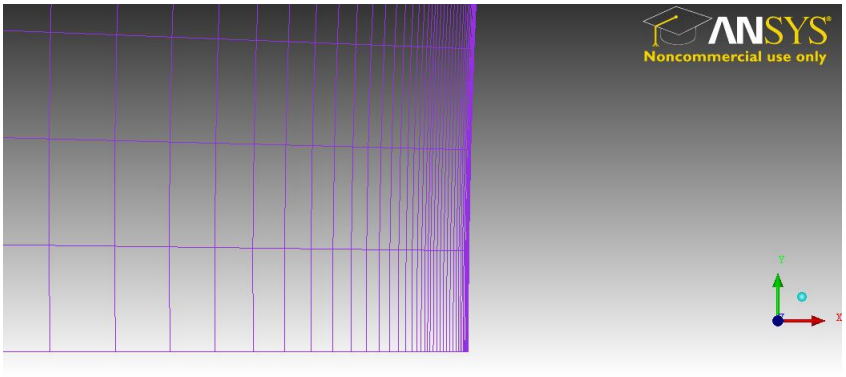

Figure 4.7 Detail of a CFD Mesh near the Right Wall of the Simulation Domain

From the other side a DSMC mesh requires a uniform size of the cells. In fact the accuracy of the results depends on the number of particles in each cell which doesn't have to be either too small or too big, and must be as uniform as possible among the cells. Moreover what is needed is also a structured mesh to make sure that once the calculation is ready it would work and the results would converge. Considering the previous observations, the building of the mesh, which is the first step of the simulation, is considerably less complex and faster in the DSMC with respect to the CFD.

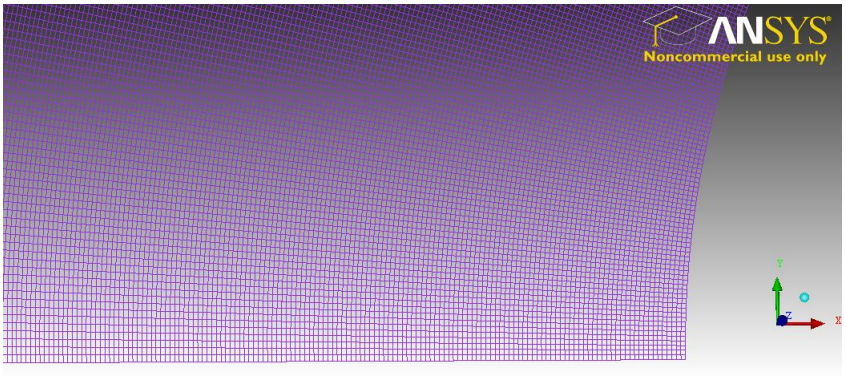

Figure 4.8 Detail of a DSMC Mesh near the Right Wall of a Simulation Domain

4.2.1 OpenFoam Mesh

In OpenFOAM there are two ways to make a mesh: to create it with the same OpenFOAM or to import it from other meshing software [75].

3D Mesh

OpenFOAM itself has two ways to create a mesh. For simple geometry you can fill the dictionary *blockMesh* where you can create the geometry, select the number of cells for each direction, that will be only hexahedron in this case, and set other initial conditions. However it is not applied to this study because here there is quite a complex geometry.

The other way to have a mesh with OpenFOAM is to use the functionality *snappyHexMesh*. What the software is going to do with this command is to insert a given geometry inside a domain box, created using the command *blockMesh* introduced before. Then it extracts the mesh from the boundary of the geometry and refines it according to a series of commands that you can select.

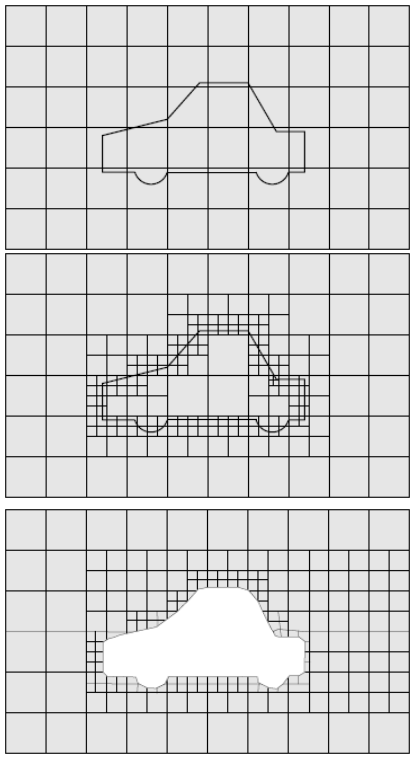

Figure 4.9 Way of Working of *SnappyHexMesh* Command

The *snappyHexMesh* utility generates 3-dimensional meshes containing hexahedra (hex) and split-hexahedra (split-hex) automatically from triangulated surface geometries, or tri-surfaces. The mesh approximately conforms to the surface by iteratively refining a starting mesh and morphing the resulting split-hex mesh to the surface. An optional phase will shrink back the resulting mesh and insert cell layers. The specification of mesh refinement level is very flexible and the surface handling is robust with a pre-specified final mesh quality. This kind of utility works only for tri-dimensional geometry.

Therefore the tri-dimensional mesh is made inside OpenFOAM with *snappyHexMesh* utility and the result is shown in Figure 4.10.

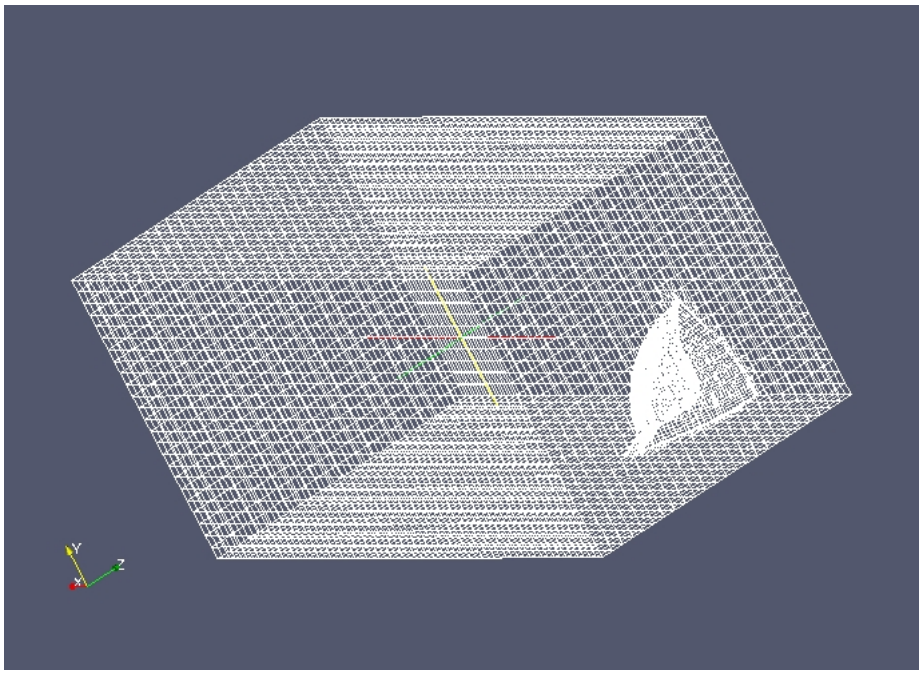

Figure 4.10 Mesh Realized with *SnappyHexMesh* Command Used for Tri-Dimensional OpenFOAM Simulation

The dimension of the domain used are chosen in a way to contain all the disturbances created by the presence of the obstacle (Haybusa) inside the stream. Therefore the dimension of the domain along the stream direction in the back of the capsule is five times the characteristic length of the capsule (a radius of about 0.18 m), while in the other directions a factor of two is used. As anticipated, a double symmetry plane is used. The cell size is a 1 mm cube and it is as uniform as possible for all the cells inside the domain.

2D Mesh

The two dimensional mesh is imported from an external meshing program called ANSYS ICEM CFD [36].

ANSYS ICEM CFD provides advanced geometry acquisition, mesh generation, and mesh optimization tools to meet the requirement for integrated mesh generation. ANSYS ICEM CFD's mesh generation tools offer the capability to parametrically create meshes from geometry in numerous formats: structured, unstructured, hybrid. The resulting structured or unstructured

meshes, topology, inter-domain connectivity and boundary conditions can easily be translated to input files formatted for a particular solver.

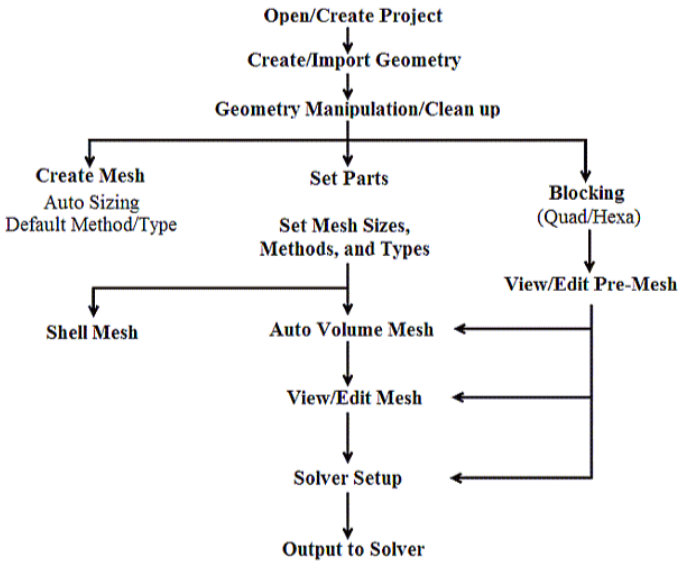

Figure 4.11 Overall Process Mesh Generation Using ANSYS ICEM CFD

- *Create/Import Geometry*: Creation of the whole domain and import of the Hayabusa geometry inside it. The dimensions of the two-dimensional domain is reduced with respect to the tri-dimensional ones.

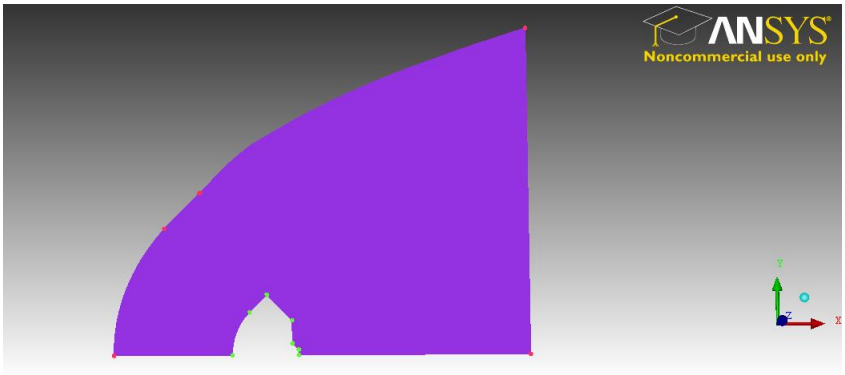

Figure 4.12 The Entire Mesh Domain

- *Geometry clean up*: The entire domain is converted from millimeters to meters because OpenFOAM uses it as a default unit of measurement.
- *Blocking*: The mesh is generated using the technique of creating blocks. It allows greater control of the mesh and to set all the parameters in the desired way. It consists in the creation of blocks which cover the entire domain and in the consequent meshing of each block. The block topology model is generated directly on the underlying CAD geometry starting with one big block. It is further refined through the splitting of the first block in more blocks to allow the creation of cells as uniform as possible at least in the interest zone, so around the shock. For this reason the blocks used are as squared as possible. In this way the increase of the size of the cell proceeding to the outside of the mesh is reduced.

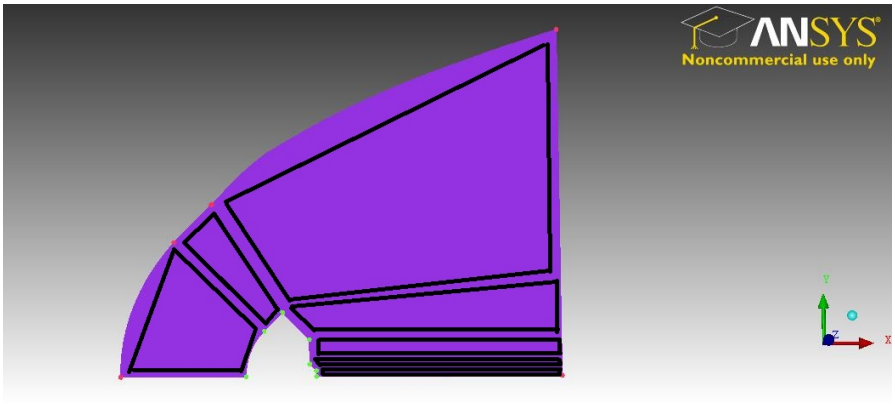

Figure 4.13 Blocks Creation Inside the Domain of the Simulation

- *Edit pre-mesh*: Before creating the mesh the parameter of the mesh like the number of cells for each side and the meshing law (linear, bi-quadratic,...) are set. The number of cells is set in a way to have the dimensions of each cell equal to $1mm$ following Bird's study (the reason for this number will be discussed later) and obviously with a uniform law.
- *View mesh*: As it is possible to see from the details reported in Figure 4.14, the mesh is quite uniform except in the back, but it is acceptable considering that this part of the domain is not so interesting for the study. In addition, a refined mesh also in that zone requires an increase in the number of blocks and in the complexity of the mesh.

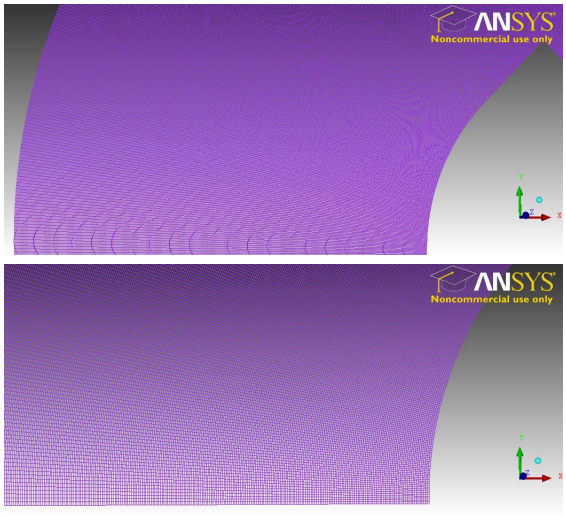

Figure 4.14 Detail of the Two-Dimensional Mesh Created Using ANSYS ICEM CFD

- *Output to solver*: The file produced is a .stl file considering that it is one of the acceptable format for OpenFOAM.

The domain used is smaller with respect to the tri-dimensional one to reduce the computational resource used in the simulation. In fact this mesh is used in OpenFOAM as an import, so more resources will be used to run the simulation inside it instead of using one created with OpenFOAM itself. Anyway it includes all the discontinuities in the stream created from the shock in front of the capsule which is the subject of this study. The cell size is the same except for the fact that this time it is 1 mm^2 instead of 1 mm^3. The mesh is structured as suitable for DSMC. Instead in the 3D case it is not because it is the *snappyHexMesh* command which creates autonomously the mesh and it is not able to create automatically a structured mesh with complex geometry.

4.2.2 Sparta Mesh

Sparta uses a Cartesian hierarchical grid mesh. Cartesian means that the faces of a grid cell, at any level of the hierarchy, are aligned with the Cartesian xyz axes. I.e. each grid cell is an axis-aligned parallelepiped or rectangular box. The hierarchy of grid cells is defined in the following manner. The entire simulation box is a single "root" grid cell at level 0 of the hierarchy. The

dimensions are specified in the input file giving a value for each Cartesian direction. It is sub-divided into a regular Nx by Ny by Nz grid of cells, all at level 1 of the hierarchy. The subdivision in the same way, is specified in the input file with the *create_ grid* command. "Regular" means all the Nx per Ny per Nz sub-divided cells within a parent cell are the same size. Any of the cells at level 1 can be further sub-divided in the same manner to create cells at level 2, and recursively for levels 3, 4, etc. Note that this manner of defining a hierarchy allows for flexible grid cell refinement in any region of the simulation domain. Anyway this is not required in this study because as already said a DSMC simulation needs a homogeneous mesh.

The flow region is the portion of the simulation domain that is "outside" any surface object. In fact in SPARTA you can import a collection of surface elements that represent the surface of one or more physical objects which will be embedded in the global simulation box.

When surface objects are defined via the *read_ surf* command, they intersect child cells. Child cells can thus become one of 3 flavors: unsplit, cut, or split. A child cell not intersected by any surface element is an unsplit cell. It can be entirely in the flow region or entirely inside a surface object. If a child cell is intersected so that it is partitioned into two contiguous volumes, one in the flow region, the other inside a surface object, then it is a cut cell. This is the usual case. Additionally, each of the two or more contiguous flow regions is a sub cell of the split cell.

In Sparta only a two-dimensional simulation is done after showing in Chapter 6 that the results of the tri-dimensional and two-dimensional cases are equivalent for Hayabusa.

The resulting mesh used for Sparta's simulation is shown in Figure 4.16. The domain considered at the beginning was the same used for the tri-dimensional mesh of OpenFOAM, but for computational memory problems explained in Appendix 1 it is reduced. The actual domain is a box of 0.6 m per 0.4 m. The cell size in this case is 5 mm^2 for reasons explained in the Paragraph 6.3, concerning computational memory.

4.3 Physics

The basic physical model used and equal for all the DSMC software was presented in Chapter 2. In the present Paragraph the additional model and laws used, for each software considered are presented. These are often required for the post process to extrapolate the data.

The physical boundary conditions under examination are those at point H3 of the Hayabusa re-entry trajectory and they are presented in Paragraph 4.1.3.

Figure 4.15 Hayabusa Geometry Positioned inside the Domain of the Simulation

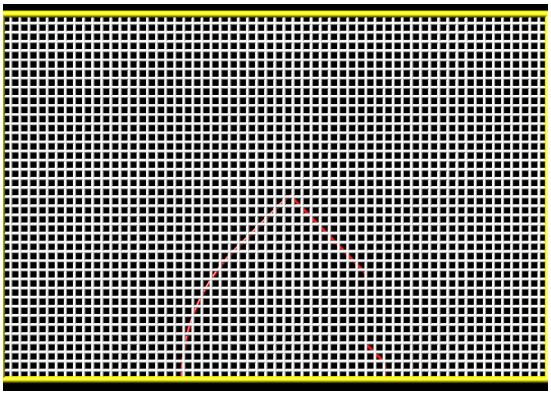

Figure 4.16 Two-Dimensional Mesh Used for Sparta Simulation

The fundamental parameters in a DSMC simulation are the cell size, the equivalent number of particles and the time step.

The linear dimensions of the cells should be small in comparison with the length of the macroscopic flow gradients normal to the streamwise directions. In order to accurately model collisions by using a statistical approach, the cell size should be of the order or smaller than the local mean free path in the direction of primary gradients [1; 22; 25]. This is because in certain regions, such as in the vicinity of the surfaces, the cell size must be small enough to adequately capture the steep macroscopic gradients and the flowfield physics near the wall. The mean free path for the Earth's atmosphere at an altitude of 78.8 km according to the U.S. Standard Atmosphere is 3.762e-3 m [77].

An additional requirement of the DSMC method is related to the minimum number of simulated particles in the cells. As mentioned earlier, the DSMC method uses a cell-based system for the sampling of the macroscopic properties and for the selection of collision partners. As the collision rate is a function of the number of particles in the cells, it is desirable that each cell has the largest possible number of particles. However, the possible number of collision partners is a function of the number of particles in each cell. In this scenario, the greater the number of particles, the greater is the number of possible collision pairs. As a result, it is necessary to determine the optimum number of particles in each cell; enough to promote statistical accuracy while maintaining realistic computational expenditure. In order to solve this conflict, Bird [26] introduced the option of subdividing the cells into an arbitrary number of sub-cells for the selection of collision pairs. This procedure improves the accuracy of the method by ensuring that collisions occur only between near neighbor particles. Thus, it is desirable that each cell has a minimum number around 20 to 30 particles [1].

Another requirement of the DSMC method is the setting of an appropriate time step. The trajectories of the particles in physical space are calculated under the assumption of the decoupling between the particle motion and the intermolecular collisions. The time step should be chosen to be sufficiently small in comparison with the local mean collision time to allow the uncoupling between the movement and collisions of a set of particles. In addition, if the time step is too large, particles can cross many cells in one time step and consequently the results may be inaccurate. On the other hand, too small a time step will result in inefficient computation [27, 28, 76]. The local mean collision time is 3.161e-7 s.

Considering the data reported before, the theoretical initial parameters for the simulation considered are:

Cell size: 0.001 m

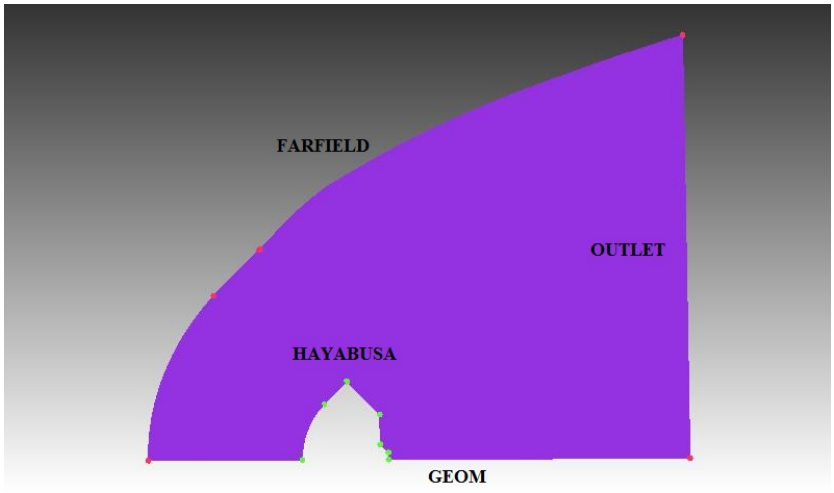

Figure 4.17 Boundaries of the Simulation Domain

Equivalent particles per cell: 20

Time-step: 1e-7 s

However these parameters are the ones that mainly rule the simulations. The success of the calculation and also the accurancy of the results depend on them. In order to examine how these parameters change the results and which are the best ones, a sensitivity study is performed at Chapter 5 varying the cell size, the number of particles per cell and the time-step.

4.3.1 OpenFOAM Physics

The inflow boundary model [75] used in OpenFOAM for the present study is *FreeStream*. The *FreeStream* boundary condition looks locally (for every face of the patch) at the mass flow rate. If the flow is going outside, the boundary will be locally *zeroGradient* (homogeneous), if it is going inside, the boundary will be locally *fixedValue*. The flow considered is a no-reacting flow composed of N2 and O2, whose number density is respectively 3.242e20 and 7.544e19.

The boundaries considered are the ones shown in Figure 4.17 and in Table 4.2.

The type *patch* is the basic patch condition that contains no geometric or topological information about the mesh, e.g. an inlet or an outlet. The type *wall* is used where a patch that coincides with a wall needs to be identifiable as such, particularly where specialist modeling is applied at wall boundaries. The type *symmetryPlane* is used for symmetry plane

Boundary	Type
HAYABUSA	wall
FARFIELD	patch
OUTLET	patch
GEOM	symmetryPlane

Table 4.2 Boundary Conditions Applied in the Simulation Domain

For all the boundaries (except for the symmetry plane) the base numerical patch condition *fixedValue* is assigned which means the value of each field considered must be specified.

Molecular Model

The molecular model used is the Variable Hard Sphere model proposed by Bird [43]. According to this model the molecular diameter is 4.17e-10 for N2 and 4.07e-10 for O2. The temperature-dependence of viscosity (ω) is set respectively for N2 and O2 at 0.74 and 0.77.

Collision Model and Energy Exchange

The model introduced by Larsen and Borgnakke [75] is used. The reference temperature considered is 273 K. The relaxation (or collision) number taken into account is 5. Two internal degrees of freedom are considered.

Properties Measurement

The DSMC technique is a particle-based method in which the macroscopic gas properties, such as mass density, velocity, pressure, and temperature are recovered from the particle movements and collisions at the microscopic level. The DSMC method uses the cell system for sampling

these macroscopic properties and then they are used for engineering purposes. One of the most simple basic properties is the number density (n) defined as the number of particles (N) within a volume (V)

$$n = \frac{N}{V} \quad (4.1)$$

and the mass density ρ is defined as the product of the molecular mass (m) and the number density,

$$\rho = nm \quad (4.2)$$

The scalar pressure P is defined as the average value of the three components in the normal component of the pressure tensor (p_{xx}, p_{yy}, p_{zz}),

$$P = \frac{1}{3}\rho(\overline{u'^2} + \overline{v'^2} + \overline{w'^2}) \quad (4.3)$$

where, u', v', and w' are the instantaneous velocity of a molecule relative to the stream velocity components in the x, y, and z directions, respectively. Considering an equilibrium gas all the three normal components of the pressure tensor are equal; however, they are different for a non-equilibrium gas.

4.3.2 Sparta Physics

Boundary Conditions

The particles are inserted into the domain from the left and top border of the domain [23]. The in-flow considered for both the no-reacting and reacting case is composed by N2 and O2, with a total number density of 3.242e20. The percentage of N2 and O2 is respectively 80 and 20. The boundary condition considered for each side of the domain is specified in Figure 4.18.

Style *o* (outflow) means the particles freely exits the simulation. Style *a* means an axi-symmetric boundary, this effectively means that the x-axis is the axis of symmetry.

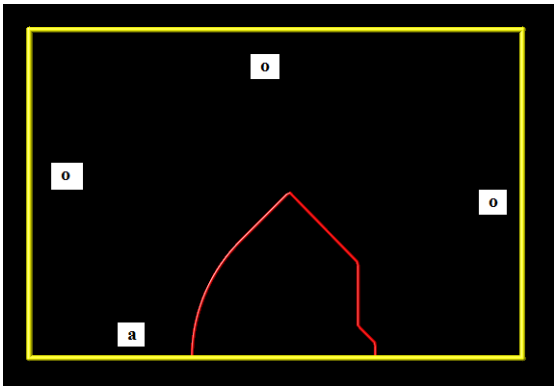

Figure 4.18 Boundary Condition Applied for Sparta Simulation

Molecular Model

The molecular model used is the Variable Soft Sphere model proposed by Moura and Matsumoto [44; 45]. According to this model the molecular diameter is 4.07e-10 for N2 and 3.96e-10 for O2. The temperature-dependence of viscosity (ω) is set respectively for N2 and O2 at 0.74 and 0.77 (only data about the free stream are reported for greater clarity).

Collision Model and Energy Exchange

The model introduced by Larsen and Borgnakke [51] is used. The reference temperature considered is 273 K. Two vibration degrees of freedom are considered.

Properties Measurement

The number density ($Nrho$) value computes the number density [23] for the grid cell volume due to particles in cell:

$$Nrho = (fnum/volume)N \quad (4.4)$$

N is the number of particles, $fnum$ is the real/simulated particle ratio, and $volume$ is the flow volume of the grid cell.

The mass density ($massrho$) value computes the mass density for the grid cell volume due to particles in each cell:

$$Massrho = fnum \cdot volume \cdot Mass \quad (4.5)$$

$Mass$ is the molecular mass.

The pressure (P) value uses the $therma\_KE$ to compute a pressure for the grid cell due to particles in the cell:

$$P = (2/3)fnum/volume \cdot thermal\_KE \quad (4.6)$$

where $thermal\_KE = Sum\_i((1/2)mass\_i \cdot Csq\_i)$ and $Csq = Cx^2 + Cy^2 + Cz^2$ and C is the thermal velocity of each particle.

4.4 Chemistry

Only Sparta can simulate chemistry reactions at the moment of the present study because in OpenFOAM they have not been implemented yet. As a consequence this Paragraph deals exclusively with Sparta.

The model used is the Total Collision Energy (TCE) model [23]. The reactions considered are listed below. For example in a reaction indicated as follow:

R1 + R2 + ... -> P1 + P2 + ...

type style C1 C2 ...

The first line is a text-based description of a single reaction. R1, R2, etc are one or more reactants. P1, P2, etc are one or more products. The number of allowed reactants and products depends on the reaction type. The type of each reaction is a single character with the following meaning. The type determines how many reactants and products can be specified in the first line.

D = dissociation = 2 reactants and 3 products;

E = exchange = 2 reactants and 2 products;

I = ionization = 2 reactants and 2 or 3 products.

A dissociation reaction means that R1 dissociates into P1 and P2 when it collides with R2. R2 is preserved in the collision, so P3 = R2 is required. An exchange reaction is a collision between R1 and R2 that results in new products P1 and P2. There is no restriction on the species involved in the reaction. An ionization reaction with 2 products is typically a collision between R1 and R2 that results in a positively charged ion and an electron. However, Sparta does not check for this, so there is no restriction on the species involved in the reaction. An ionization reaction with 3 products is typically a collision between a neutral R1 and an electron R2 which ejects an electron from the neutral species, resulting in P1 and P2. Again, Sparta does not check for this, so there is no restriction on the species involved in the reaction. R2 is preserved in the collision, so P3 = R2 is required.

The style of each reaction is a single character (upper or lower case) with the following meaning: A = Arrhenius; Q = Quantum; S = Surface. The style determines how many reaction coefficients are listed as C1, C2, etc, and how they are interpreted by Sparta [59]. For the A = Arrhenius style, there are 5 coefficients:

C1 = number of internal degrees of freedom (as defined by the TCE model);

C2 = Arrhenius activation energy ε_{act};

C3 = Arrhenius prefactor a;

C4 = Arrhenius exponent b;

C5 = overall reaction energy (positive for exothermic).

For S = Surface style, there is a single coefficient:

C1 = probability that the reaction occurs (0.0 to 1.0)

Inflow Reactions

O2 + N –> O + O + N

D A 1.0 8.197e-19 1.660e-8 -1.5 -8.197e-19

O2 + NO –> O + O + NO

D A 1.0 8.197e-19 3.321e-9 -1.5 -8.197e-19

O2 + N2 –> O + O + N2

D A 1.0 8.197e-19 3.321e-9 -1.5 -8.197e-19

O2 + O2 –> O + O + O2

D A 1.0 8.197e-19 3.321e-9 -1.5 -8.197e-19

O2 + O –> O + O + O

D A 1.0 8.197e-19 1.660e-8 -1.5 -8.197e-19

N2 + O –> N + N + O

D A 1.0 1.561e-18 4.980e-8 -1.6 -1.561e-18

N2 + O2 –> N + N + O2

D A 1.0 1.561e-18 1.162e-8 -1.6 -1.561e-18

N2 + NO –> N + N + NO

D A 1.0 1.561e-18 1.162e-8 -1.6 -1.561e-18

N2 + N2 –> N + N + N2

D A 1.0 1.561e-18 1.162e-8 -1.6 -1.561e-18

N2 + N –> N + N + N

D A 1.0 1.561e-18 4.980e-8 -1.6 -1.561e-18

NO + N2 –> N + O + N2

D A 1.0 1.043e-18 8.302e-15 0.00 -1.043e-18

NO + O2 –> N + O + O2

D A 1.0 1.043e-18 8.302e-15 0.00 -1.043e-18

NO + NO –> N + O + NO

D A 1.0 1.043e-18 8.302e-15 0.00 -1.043e-18

NO + O –> N + O + O

D A 1.0 1.043e-18 1.862e-13 0.0 -1.043e-18

NO + N –> N + O + N

D A 1.0 1.043e-18 1.862e-13 0.0 -1.043e-18

NO + O –> O2 + N

E A 0.0 2.684e-19 1.389e-17 0.0 -2.684e-19

N2 + O –> NO + N

E A 0.0 5.175e-19 1.069e-12 -1.0 -5.175e-19

O2 + N –> NO + O

E A 0.0 0.0 4.601e-15 -0.546 2.684e-19

NO + N –> N2 + O

E A 0.0 0.0 4.059e-12 -1.359 5.175e-19

O + N –> NO+ + e

I A 0.0 4.404e-19 8.766e-18 0.0 -4.404e-19

N + N –> N2+ + e

I A 0.0 9.319e-19 3.387e-17 0.0 -9.319e-19

O + O –> O2+ + e

I A 0.0 1.1128e-18 1.8580e-17 0.0 -1.1128e-18

NO+ + N –> O + N2+

E A 0.0 4.832e-19 1.1956e-16 0.0 -4.832e-19

N2+ + O –> N + NO+

E A 0.0 0.0000 1.744e-18 0.302 4.832e-19

N2 + N+ –> N + N2+

E A 0.0 1.684e-19 1.6605e-18 0.5 -1.684e-19

N2+ + N -> N2 + N+

E A 0.0 0.0000000 1.295e-18 0.5 1.684e-19

NO+ + N -> N2 + O+

E A 0.0 1.767e-19 5.6458e-17 1.08 -1.767e-19

N2 + O+ -> N + NO+

E A 0.0 0.0000000 3.9708e-18 -0.710 1.767e-19

NO+ + O -> O2 + N+

E A 0.0 1.767e-19 1.6605e-18 0.5 -1.767e-19

O2 + N+ -> O + NO+

E A 0.0 0.0000000 3.040e-18 -0.29 1.767e-19

NO+ + O -> N + O2+

E A 0.0 6.710e-19 1.1956e-17 0.29 -6.710e-19

O2+ + N -> O + NO+

E A 0.0 0.0000000 8.918e-13 -0.969 6.710e-19

NO+ + O2 -> NO + O2+

E A 0.0 4.501e-19 3.9853e-17 0.41 -4.501e-19

O2+ + NO -> O2 + NO+

E A 0.0 0.0000000 3.990e-17 0.41 4.501e-19

O2+ + N -> O2 + N+

E A 0.0 3.949e-19 1.4447e-16 0.14 -3.949e-19

O2+ + O -> O2 + O+

E A 0.0 2.485e-19 6.6422e-18 -0.09 -2.485e-19

O+ + O2 –> O + O2+

E A 0.0 0.0000000 4.993e-18 -0.004 2.485e-19

O2+ + N2 –> O2 + N2+

E A 0.0 5.619e-19 1.6439e-17 0.00 -5.619e-19

N2+ + O2 –> N2 + O2+

E A 0.0 0.0000000 4.5899e-18 -0.037 5.619e-19

O+ + N2 –> O + N2+

E A 0.0 3.148e-19 1.5111e-18 0.00 -1.148e-19

N2+ + O –> N2 + O+

E A 0.0 0.000 4.118e-11 -2.2 1.148e-19

O+ + NO –> O2 + N+

E A 0.0 3.673e-19 2.3248e-25 1.90 -3.673e-19

N+ + O2 –> NO + O+

E A 0.0 0.000 2.443e-26 2.102 3.673e-19

O + e –> O+ + e + e

I A 0.0 2.188e-18 6.4761e3 -3.78 -2.188e-18

N + e –> N+ + e + e

I A 0.0 2.322e-18 4.1513e4 -3.82 -2.322e-18

Surface Reactions

O+ –> O

E S 1.0

N+ –> N

E S 1.0

N2+ –> N2

E S 1.0

O2+ –> O2

E S 1.0

NO+ –> NO

E S 1.0

5 Sensitivity Study and Simulation Optimization

The simulations are performed using the model shown before. A DSMC requires extremely high computational resources. In fact it is sufficient to think that it has to simulate the movement of each particle in the domain, for a number even equal to millions of particles across hundreds of thousands of cells or more, considering also collisions and chemistry reactions, if they are present, for each time step. And after each iteration it has to save the position, velocity, temperature,.. of each particle to have some initial data for the next time step. In this case, following rigorously Bird's indications [1] for the domain considered, the simulation counts 240000 cells for about 173 million particles. For this reason it is clear that a super computer is needed to run this type of simulation. In this case the cluster named Bellatrix present at the EPFL is used.

Bellatrix Super Computer

Bellatrix is a Sandy Bridge based cluster available to the EPFL community. The cluster is composed of 424 compute nodes, each with 2 Sandy Bridge processors running at 2.2 GHz, with 8 cores each and 32 GB of RAM for a total of 6144 cores. Its maximum performance data are 119 TFLOPs and a total RAM of 14TB.

Bird gave some kind of rules for a correct DSMC, in particular for the setting of the principal parameters presented before, so the equivalent number of particles, the cell size and the time step. Considering that there are different DSMC software it is impossible to know first if the indications given by Bird are correct for all of them. For this reason, before considering some

results from the simulations, a sensitivity analysis is necessary where you can compare some indicative results from different simulations and establish which are correct. Different simulations mean simulations where the main parameters are changed to see how the results change according to them. The parameters are changed in a schematic way so that it is possible to obtain such a law for variations of the parameters. The data of each simulation are compared with the mean value of all the simulations to establish the most accurate [12].

This analysis is also important to understand what is the most efficient way to do these simulations, in order to find the best way to achieve accurate results but also an acceptable computational time, considering that this calculation is very long and resource consuming.

From this preliminary study efforts have been made to find the correct final time for the simulations, thus the minimum time for which the variations in the results are not significant. This is another thing to take into account to establish the most efficient way for the calculation.

The study conducted in the present Chapter uses simulations without reactions. In this way it is possible to make a comparison between the data coming from Sparta and OpenFOAM, considering the chemical reactions have not been implemented yet in this software for the DSMC solver.

5.1 OpenFOAM

Data

In the sensitivity analysis only some data given directly from the software are considered. Therefore data either coming from secondary calculations, or all the interest data which it is important to extrapolate from this study are not taken into account. The latter will be reported only for the simulation that is established to be the most efficient. The pressure, overall temperature and Mach number data for the sensitivity analysis are chosen to be analayzed. The values along the stagnation line are considered. Four hundred data points are recorded along 0.2 m that ends in the stagnation point. Therefore, considering a cell size of 0.001 m, there are two data points for each cell to have a more homogeneous set of data. Significant data considered are as follow: (a) the position where the Mach number is equal to 1 which should give the exact position of the shock. Indeed, in the conditions analyzed, it is evident the shock is diffused, there is not a precise discontinuity point, because of the rarefaction of the gas; (b) the part of the pressure slope where the gradient is higher than one. This is a feature of the shock in a rarefied gas. In

fact in a dense fluid, the increase of the pressure in the shock should be vertical, so it happens in a single point (discontinuity), as anticipated; (c) the maximum temperature and the part of the temperature slope where the temperature is higher than 95% of the maximum temperature reached along the streamline. These give an indication about the accurancy of the simulation, comparing the absolute value reached by the temperature with similar data deriving from literature, and about the thickness of the shock respectively. For each simulation the time required by the super computer to complete the calculations and the computational resources used to evaluate the most efficient simulation are recorded. In this case all the simulations used 4 nodes of Bellatrix each with 16 two Gb of RAM processor. Therefore the only discriminant factor to establish the most efficient simulation will be the time for OpenFOAM.

Parameters

Considering a fix mesh of a cell size equal to 1 mm, as suggested by Bird, which will not be changed for reasons of time, the modified parameter that are changed are the number of particles per cell, that depends on the equivalent number of particles, and the time step. For each series of simulation the variations of only one parameter are considered while the other is maintained constant at the reference value, the value proposed by Bird.

5.1.1 Particle Factor

The possible difference made by the number of particles for each cell, as said, is considered with the parameter called "*nEquivalentParticle*". Starting with Bird's indications, the parameter is set to a value that guarantees a quantity of 20 particles per cell. The study is conducted increasing and decreasing this value of a factor of 3. All the parameters considered are reported in Table 5.1. The analyzed values, found from the simulations and related to each case, are reported in the following Table 5.2. In the first column of this table is the name of the simulation, where p means that the particle factor is considered and O that OpenFOAM software is used. In the other coloumns the position where the Mach number is equal to one, the maximum overall temperature, the lenght of the part of the overall temperature and pressure slope considered as reported in the sub-paragraph "Data" are respectively indicated. In the Factor column 'ref.' indicates which reference number of particles per cell in this case is taken into consideration.

	Particles per Cell	*nEquivalentParticles*	Factor
I p O	20	1e12	ref.
II p O	7	3e12	1/3
III p O	60	3.3e11	3

Table 5.1: Parameters Chosen for the OpenFOAM Sensitivity Analysis for the Particle Factor

	Position(x) Ma=1 (m)	max T (K)	Shock Layer T (m)	Shock Layer p (m)
I p O	7.840e-2	6.613e4	4.360e-2	5.010e-2
II p O	7.840e-2	6.619e4	4.360e-2	4.910e-2
III p O	7.840e-2	6.614e4	4.360e-2	4.910e-2

Table 5.2: Values Obtained in the OpenFOAM Sensitivity Analysis for the Particle Factor

5.1.2 Time Step Factor

The sensitivity analysis about the time step, as the one before, takes as a reference value the one indicated by Bird. According to the data of this simulation the reference value is 1e-7 seconds. Two other values are considered, one bigger and one smaller, to understand how the results change with the choice of the time step. The values chosen are visible in the following Table 5.3. The analyzed values found from the simulations, related to each case, are reported in the following Table 5.4. In these tables the name of the simulation is in the first column, where t means that the time step factor is considered.

5.1.3 Mean Value and Data Confront

In the following Table 5.5 it is possible to see the mean value for each parameter considered computed over all the simulations. In the following Figure from 5.1 to 5.6 the comparison

	Time Step (s)	Factor
I t O	1e-7	ref.
II t O	2e-8	5
III t O	5e-7	1/5

Table 5.3: Parameters Chosen for the OpenFOAM Sensitivity Analysis for the Time Factor

	Position(x) Ma=1 (m)	max T (K)	Shock Layer T (m)	Shock Layer p (m)
I t O	7.840e-2	6.613e4	4.360e-2	5.010e-2
II t O	7.840e-2	6.611e4	4.410e-2	4.860e-2
III t O	7.790e-2	6.585e4	4.160e-2	4.910e-2

Table 5.4: Values Obtained in the OpenFOAM Sensitivity Analysis for the Time Factor

	Position(x) Ma=1 (m)	max T (K)	Shock Layer T (m)	Shock Layer p (m)
Mean Value	7.830e-2	6.608e4	4.330e-2	4.920e-2

Table 5.5: Mean Values among the Values Analyzed in the Sensitivity Analysis for OpenFOAM

among the values considered for each set of simulations is reported. In the following Table 5.6 and 5.7 it is possible to see the numerical comparison among the values of each simulation and the mean value of all the simulations. This is done for the particle factor (Table 5.6) and for the time step factor set of simulations (Table 5.7). In this table 'abs Diff' means the absolute difference and '% Diff' means the percentage difference with respect to the mean value.

Taking an overview of the results it is evident the variations between each case are very little, in most cases they do not reach 1 %. In fact, as can be seen from the graphs where the comparison among the simulations belonging to each factor study are made, it seems there is only one curve instead of three in the majority of cases, because they are superimposed. Therefore it is possible to say the program is robust and keeps the same results even if there are some relevant modifications in the base parameters, at least in the time step and in the number of particles. A deeper analysis of results shows that the modifications to the number of particles for each cell do not significantly affect the results. Trend variations in the results are impossible to see because the variations are negligible. It isn't possible also to see some trend in the variations of the results because there are really small variations. Therefore it is possible to conclude modifying the number of particles does not significantly vary the results obtained, at least in a range of three times more or less starting from the value indicated by Bird. In the time step analysis there are some appreciable variations, even if still little. In particular the most important data is the variation with the width of the shock which varies from +1.8% to -4% with the decreasing of the time step. Considering the assumption that a relative error higher than 5% starts to be relevant, all the simulations are valid. It would seem the most accurate result for this parameter is obtained with a time step equal to 1e-7s, the one suggested by Bird. However the larger the

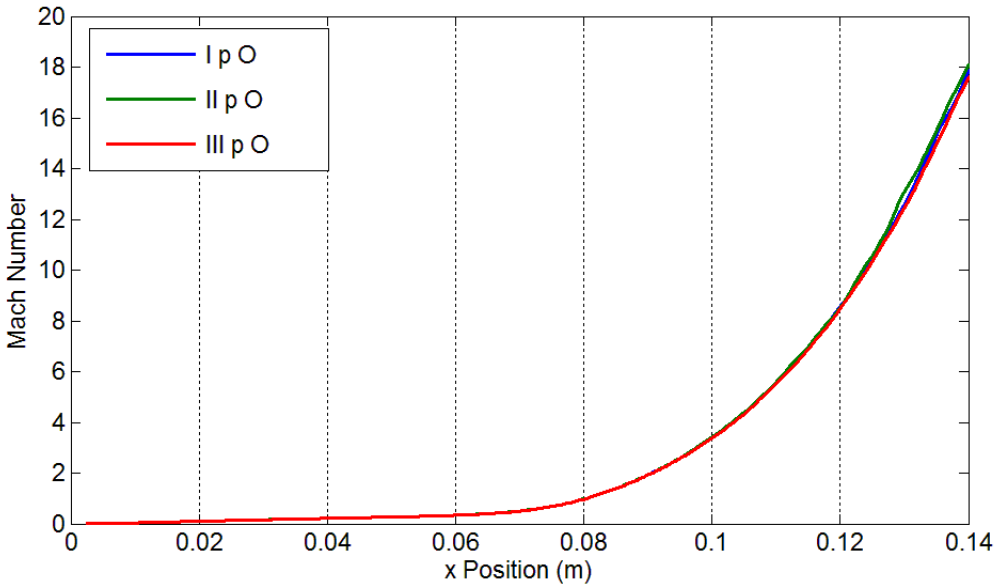

Figure 5.1: Mach Number Comparison among the Simulations Considered in the OpenFOAM Sensitivity Analysis for the Particle Factor

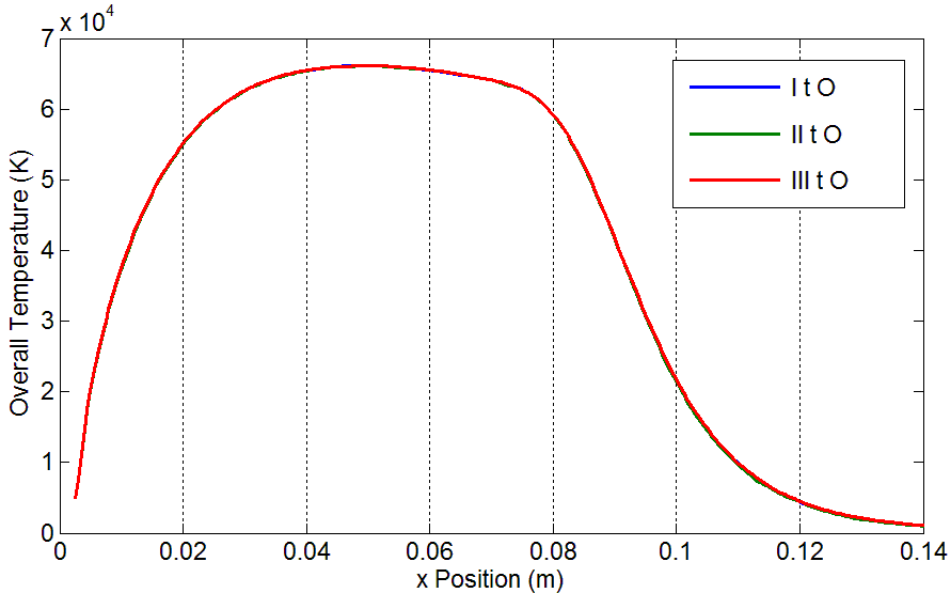

Figure 5.2: Overall Temperature Comparison among the Simulations Considered in the OpenFOAM Sensitivity Analysis for the Particle Factor

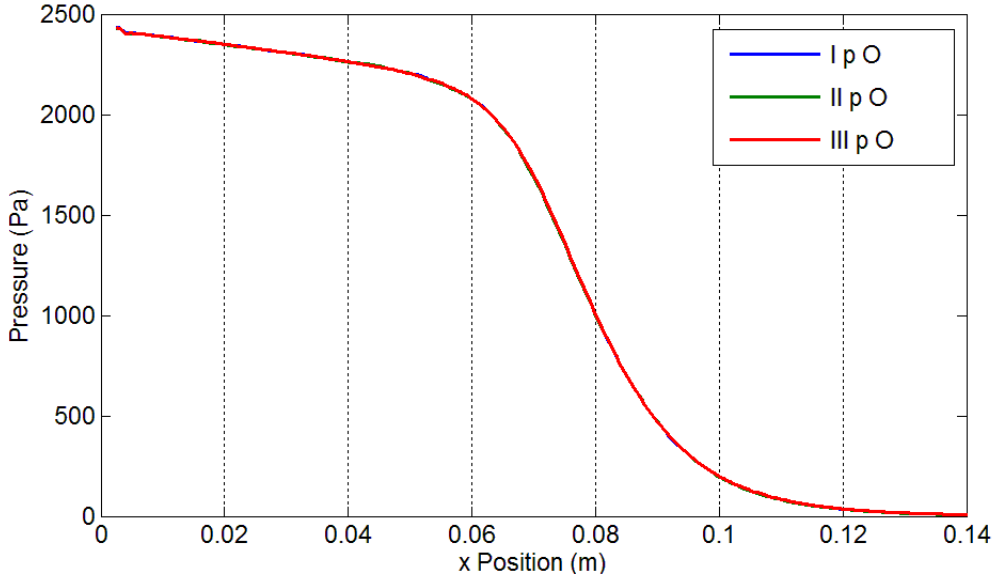

Figure 5.3: Pressure Comparison among the Simulations Considered in the OpenFOAM Sensitivity Analysis for the Particle Factor

		Position(x) Ma=1 (m)	max T (m)	Shock Layer T (m)	Shock Layer p (K)
I p O	abs Diff.	9.924e-5	-4.400e1	-2.977e-4	-8.932e-4
	% Diff.	0.035	0.067	0.682	1.782
II p O	abs Diff.	9.924e-5	-1.030e2	-2.977e-4	9.925e-5
	% Diff.	0.035	0.156	0.682	0.202
III p O	abs Diff.	9.924e-5	-5.700e1	-2.977e-4	9.925e-5
	% Diff.	0.035	0.087	0.682	0.202

Table 5.6: Comparison among the Values Analyzed in the OpenFOAM Sensitivity Analysis for the Particle Factor

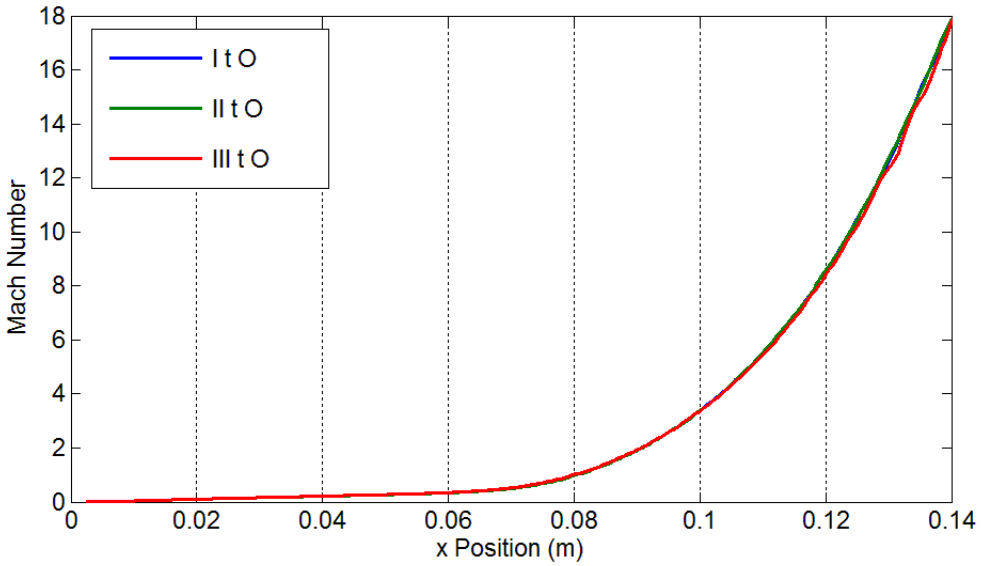

Figure 5.4: Mach Number Comparison among the Simulations Considered in the OpenFOAM Sensitivity Analysis of the Time Step Factor

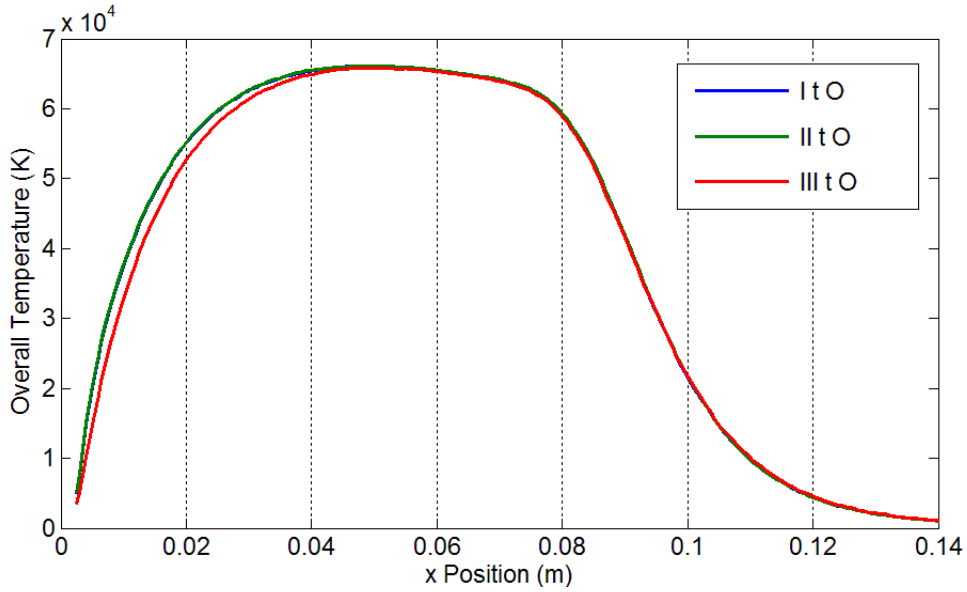

Figure 5.5: Overall Temperature Comparison among the Simulations Considered in the OpenFOAM Sensitivity Analysis for the Time Step Factor

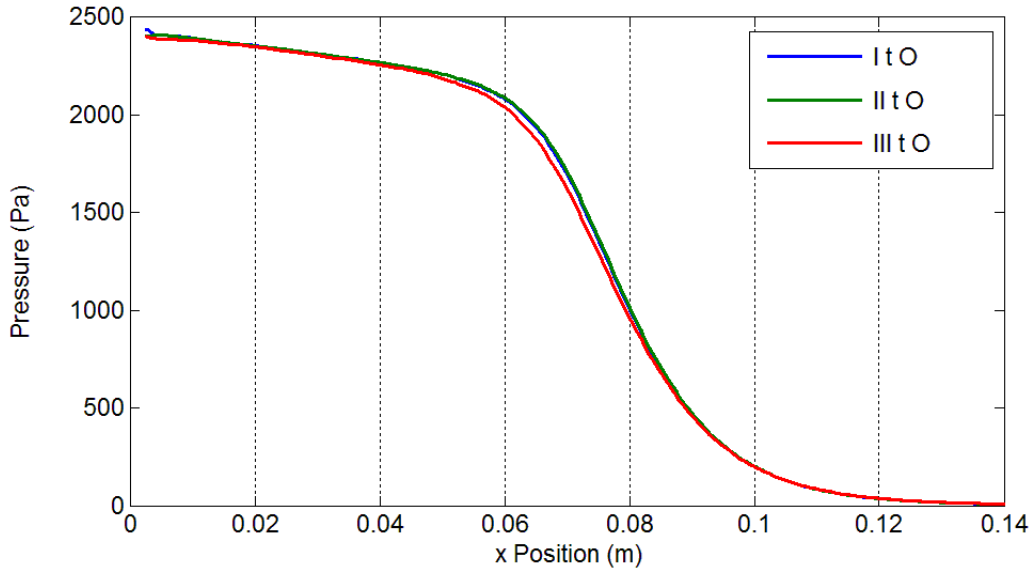

Figure 5.6: Pressure Comparison among the Simulations Considered in the OpenFOAM Sensitivity Analysis of the Time Step Factor

		Position(x) Ma=1 (m)	max T (K)	Shock Layer T (m)	Shock Layer p (m)
I t O	abs Diff.	9.930e-5	-4.400e1	-2.977e-4	-8.932e-4
	% Diff.	0.035	0.067	0.682	1.781
II t O	abs Diff.	9.930e-5	-2.800e1	-7.940e-4	5.955e-4
	% Diff.	0.035	0.042	1.798	1.220
III t O	abs Diff.	-3.970e-4	2.330e2	1.687e-3	9.930e-5
	% Diff.	0.142	0.354	4.048	0.202

Table 5.7: Comparison among the Values Analyzed in the OpenFOAM Sensitivity Analysis for the Time Step Factor

width of the shock layer is, the worst the result is. In fact, the real width of the shock layer in this case should be smaller because of the presence of the reactions. Therefore probably the decrease of the time step gives better results with regards to the temperature values.

Another appreciable variation due to the time step is in the part of the pressure slope with a gradient higher than 1. However here there is no clear trend because increasing the time step, the length of the pressure curve considered increases and then decreases again. In this case, considering also that the variations are very small, it is possible to say that there is only a random fluctuation and it is not possible to derive any sensitivity law.

It is possible to conclude that decreasing the time step an increase in the quality of some results becomes apparent. However it is necessary to do a more detailed analysis to understand if this variation is an improvement or just a process of stabilization. Moreover the increase in the quality of the results is already so small passing from a time step of 5e-7 s to 2e-8 s that decreasing the time step again will probably not produce appreciable variations to the results. In this study it is evident that the most accurate simulation, among the ones where the time step changes, is I t O.

Finally every setting tried in the OpenFOAM sensitivity analysis is established as been considering the acceptable results obtained. Therefore the discriminating factor is the resource consumption of each simulation. In this case only the time required is considered because the memory and power resources used for each simulation are the same. Therefore the setting of the quickest simulations will be chosen as the best to make the calculations and for the next chapters.

Having discovered that varying the time step and number of particles per cell parameters in the range considered here, starting from Bird's setting, does not produce sensitive variations to the results, it would be interesting to discover what is the point where the degradation of the parameters would change the results significantly. However this question will be left for a possible future study having this analysis as a starting point.

5.1.4 Computational Resources Analysis

In the following Table 5.8 it is possible to see the computational time for each simulation to achieve the final time of 0.005 s. The time is reported in hours (h) and minutes (').

In this case it is possible to see that the particle factor is very influential in the computational time, much more then the time step factor, even if also the latter changes significantly the time

	I p O	II p O	III p O	I t O	II t O	III t O
Simulation Time	21h 7'	3h 38'	27h 26'	21h 7'	24h 39'	7h 37'

Table 5.8: Simulation Time for each Simulation Considered in the OpenFOAM Sensitivity Analysis

necessary to finish the simulations. From the overall sensitivity study it is possible to conclude the most efficient simulation is the II p O, so the one with a number of 7 particles per cell and a time step of 1e-7 s. Therefore this simulation will be used for the analysis of the minimum final time and also to obtain the results necessary for the following chapter.

Certainly, increasing the time step to 5e-7 s like in the III t O simulation and maintaining the number of particles of the II p O simulation, it would decrease even more the computational time. However a further analysis will be necessary on the results to verify if they are accurate or not, which will not be done here, but left for a future study.

5.1.5 End Time Analysis

This last part of the sensitivity analysis is about establishing the minimum end time for the simulations to have steady results considering, as said before, the II p O simulation which is the most efficient has been studied. Until now an end time of 0.005 s has been used. In the following study the end time will be decreased and the same parameters of the previous study will be checked. Therefore the point where Mach equals 1, the maximum temperature and the length of the considered part of the pressure and temperature slope. The aim is to discover the point from which the variations in the results are sensitive, so higher than the 5% with respect to the 0.005 s results. The end time should also be increase to discover if the results at 0.005 s are good or can be improved. This verification will be omitted if the variations in the parameters analyzed from 0.005 s to the next inferior steps are almost zero, which means an asymptote in the solution has already been achieved.

From the data reported in the previous Table 5.9 it is clear that at 0.005 s the results of the simulation achieve an asymptote. In fact each data considered varies less than 2% between 0.005 s and 0.002 s. Therefore it is not necessary to consider data from a time above 0.005 s to see if this is a sufficient end time or if the solution will improve again increasing the end time.

Besides it is possible to see that the variation in the width of the shock layer becomes significant at 0.001 s, and at 0.0008 s, there is more than 5% difference, which is the acceptable limit fixed

Time (s)	Position(x) Ma=1 (m)	max T (K)	Shock Layer T (m)	Shock Layer p (m)
0,005	7.840e-2	6.613e4	4.370e-2	0.0501
	/	/	/	/
0,004	7.840e-2	6.613e4	4.370e-2	5.110e-2
	0%	0.011%	0%	1.982%
0,003	7.790e-2	6.619e4	4.320e-2	5.010e-2
	0.181%	0.082%	1.140%	0%
0,002	7.740e-2	6.624e4	4.320e-2	5.110e-2
	0.352%	0.160%	1.141%	1.982%
0,001	7.590e-2	6.636e4	4.230e-2	5.110e-2
	0.890%	0.351%	3.412%	1.980%
0,0008	7.430e-2	6.670e4	4.110e-2	5.110e-2
	1.451%	0.872%	5.960%	1.980%
0,0006	7.310e-2	6.681e4	3.970e-2	5.130e-2
	1.902%	1.031%	8.980%	2.682%

Table 5.9: Variation in the Values Considered in the OpenFOAM Sensitivity Analysis Decreasing the End Time in the II p O Simulation

for this analysis. The other parameters considered do not change significantly until 0.0006 s. Taking these into consideration an end time of 0.0006 s also is acceptable. However it is not possible to tolerate such change in the width of the shock layer. The conclusion is that the minimum end time for such a simulation is 0.001s. From now all the results considered will be taken at a time of 0.001 s.

In Appendix 2 the results of this analysis are shown for an end time which vary from 0.005 s to 0.001 s and it is evident the steady state achieved by the simulation.

5.2 Sparta

Data

In Sparta the data considered for the sensitivity analysis are only data given directly from the simulations as for OpenFOAM. They are the same considered in the previous sensitivity study because they are very indicative of the phenomena studied but also because in this way it is possible to make a comparison with the other software.

In Sparta the sampling for the Mach number, temperature and pressure is possible only with the extrapolation of a datum for each cell because of the default setting. The data are taken along the stagnation line as before, for a sample line of 0,2 m. The number of data points depends on the number of cells along this line, which in turn depends on the size of the cell, which is going to change as specified later.

Also in this case the computational time, memory and power are recorded, which at this time are different from one simulation to the other, to determine the most efficient one. Between the computational memory and power, only the RAM is taken into account because it is the most influential parameter, considering the huge quantity of data that the simulations have to deal with at each time step.

Parameters

The sensitivity analysis for Sparta takes into consideration the time step and number of particles per cell as for OpenFOAM, but also the cell size. In fact, the creation of the mesh is implemented in the same program, as described before, so it is much easier to change it.

5.2.1 Particle Factor

The problem analyzed is the same as the OpenFOAM simulation, so the parameters suggested by Bird's research are the same. The number of particles suggested by Bird is 20/30 per cell. Starting from this number as the reference value, as for the OpenFOAM study, a correct sensitivity analysis should have a simulation with both a higher and a lower number of particles, considering the same factor in both cases. However, a problem arose with Sparta to run a simulation with a high number of particles, because of memory problems which will be analyzed in Appendix 1. Therefore in the Sparta case the sensitivity study is useful not only to understand what is the most efficient simulation, but also to understand what simulations are able to run with the computer available in the laboratory. For this reason the standard number of particles per cell was drastically reduced and also the standard cell size was reduced. Besides the same increasing factor was not used for each case. An attempt is made to increase and decrease the factor step by step. This is done to verify the limits in the particle and cell size factors to achieve good results from the simulations with an acceptable number of resources. The particle factor is analyzed using a reference value of 1 particle per cell. Then the other cases investigated, have

	Particles per Cell	*nEquivalentParticles*	Factor
I p S	1	1e16	ref.
II p S	10	1e15	10
III p S	50	5e14	50
IV p S	0.1	1e17	1/10

Table 5.10: Parameter Chosen for the Sparta Sensitivity Analysis for the Particle Factor

	Position(x) Ma=1 (m)	max T (K)	Shock Layer T (m)	Shock Layer p (m)
I p S	3.550e-2	7.632e4	1.000e-2	5.500e-2
II p S	3.550e-2	7.329e4	2.000e-2	4.000e-2
III p S	/	/	/	/
IV p S	2.650e-2	1.046e5	2.000e-3	3.500e-2

Table 5.11: Values Obtained in the Sparta Sensitivity Analysis for the Particle Factor

a higher number of particles, in two cases, respectively of a factor of 10 and 50 with respect to the reference value. Instead, one has a lower number of particles by a factor of ten as reported in Table 5.10.

The values considered related to each case are reported in the following Table 5.11.

In case III p S, as can be seen, there are no results because the simulation wasn't able to run due to memory problem. This limit will be analyzed in Paragraph 5.2.5.

5.2.2 Time Step Factor

The correct time step according to Bird is 1e-7s, as said before. This is considered the reference value. The variations in this factor are reported in the following Table 5.12. The values considered related to each case are reported in the following Table 5.13.

5.2.3 Cell Size Factor

It has already been specified that the reference value for the cell size is 1mm, but for reasons of memory, which are explained in Paragraph 5.2.1, the reference cell size value was increased

	Time Step (s)	Factor
I t S	1e-7	ref.
II t S	1e-8	1/10
III t S	1e-6	10

Table 5.12: Parameters Chosen for the Sparta Sensitivity Analysis for the Time Factor

	Position(x) Ma=1 (m)	max T (K)	Shock Layer T (m)	Shock Layer p (m)
I t S	3.550e-2	7.632e4	1.000e-2	5.500e-2
II t S	3.550e-2	7.331e4	1.500e-2	1.500e-2
III t S	3.550e-2	7.153e4	2.000e-2	3.500e-2

Table 5.13: Values Obtained in the Sparta Sensitivity Analysis for the Time Step Factor

until 0.005 m. Starting from this dimension, in the analysis a bigger and a littler cell size are examined, as reported in Table 5.14. For the other parameters in this case, as before, the reference values are considered. Here there is a time step of 1e-7 s and a number of particles per cell equal to 1.

In the Table 5.15 it is possible to read the absolute results for each simulations.

5.2.4 Mean Value and Data Comparison

In the following graphs represented from Figure 5.7 to Figure 5.15 it is possible to see the comparison among the values considered for each set of simulations as in the OpenFOAM study. In Table 5.17, 5.18, 5.19 the numerical results of the sensitivity analysis are reported with regard to the particles per cell, time step and cell size factor compared to the mean value of all the simulations. These latter values are reported in Table 5.16. As it is possible to see the data of the IV p S simulation are really not precise because of the big fluctuations in the curves and also

	Size Cell (m)	Factor
I s S	0.005	ref
II s S	0.001	1/5
III s S	0.01	2

Table 5.14: Parameters Chosen for the Sparta Sensitivity Analysis for the Cell Size Factor

	Position(x) Ma=1 (m)	max T (K)	Shock Layer T (m)	Shock Layer p (m)
I s S	3.550e-2	7.632e4	1.000e-2	5.500e-2
II s S	3.350e-2	6.991e4	1.200e-2	4.000e-2
III s S	3.300e-2	6.619e4	2.000e-2	4.000e-2

Table 5.15: Values Obtained in the Sparta Sensitivity Analysis for the Cell Size Factor

	Position(x) Ma=1 (m)	max T (K)	Shock Layer T (m)	Shock Layer p (m)
Mean Value	3.500e-2	7.213e4	1.700e-2	3.700e-2

Table 5.16: Mean Values among the Values Analyzed in the Sensitivity Analysis for Sparta

because of the very different absolute value in the pressure and temperature. This is probably due to the very low number of particles per cell. In fact, in this simulation there are 0.1 particles per cell. This is way the mean value of all the simulations is calculated without counting the IV p S simulation.

Sparta sensitivity analysis gives a complete knowledge about how the main parameters change the results. It is possible to see immediately from the graphs the worst quality and also the bigger fluctuation in the majority of the results compared to those using OpenFOAM.

The absence of the results is evident in the III p S simulation, that is the one with a number of particles per cell equal to 60. Instead, the other results are all present, also when the variations of the parameters considered are consistent. As anticipated before, this is due to a problem of memory. This means the most sensitive parameter for Sparta is by far the number of particles per cell. This is confirmed also from the computational time which is reported in Table 5.20. In fact the time for the I p S simulation is about one hour. The II p S takes 30 hours so 30 times the time of the simulation with all the same parameters except for the number of particles per cell, that is 10 times higher. Such a kind of difference and also such a computational time is absent in all the set of the remaining simulations. It is clear that with the computational resources available in the laboratory it was not possible to run a simulation with a number of particles per cell equal to 60. However this kind of subject will be examined in depth in Appendix 1.

Before analyzing parameter per parameter, it is possible to see that there are big fluctuations in the absolute value of the shock layer width, represented by the data on the temperature slope. In addition the pressure values also vary a lot. These big fluctuations are due both to a not completely precise setting of the principal simulation parameters and to the low number of data points. In fact, with a quite big cell size, so few data points, all the shock layer phenomena,

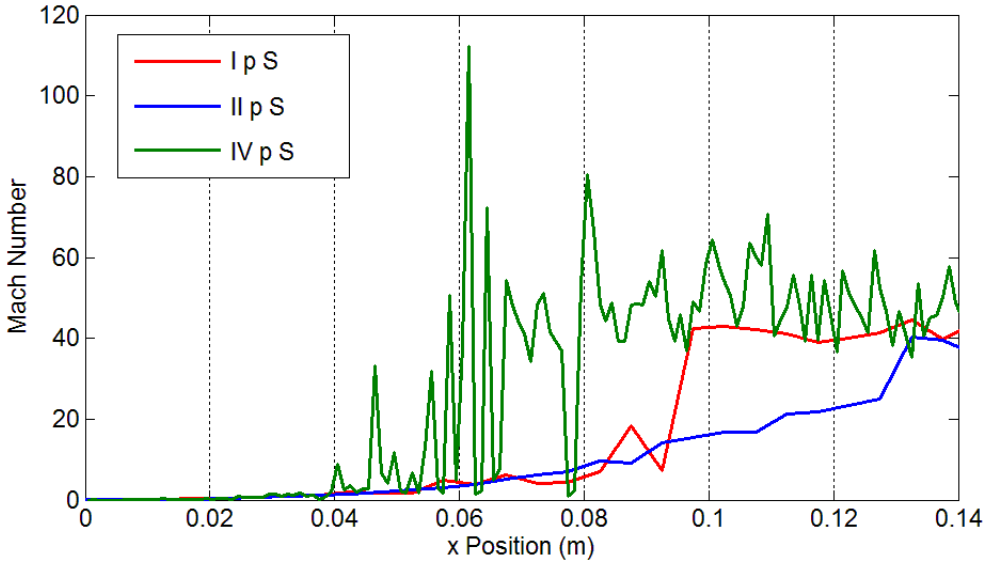

Figure 5.7: Mach Number Comparison among the Simulations Considered in the Sparta Sensitivity Analysis for the Particle Factor

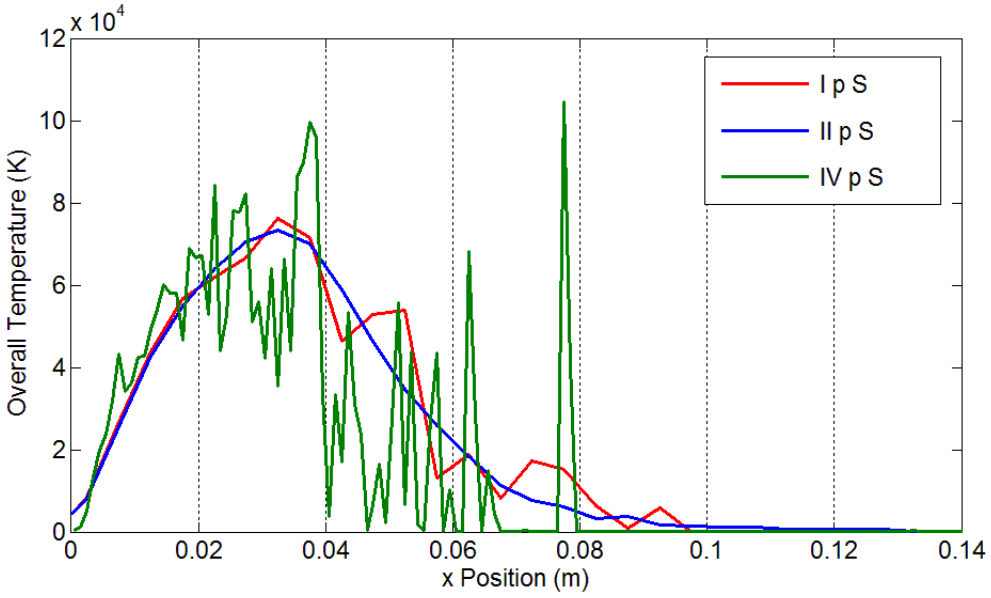

Figure 5.8: Overall Temperature Comparison among the Simulations Considered in the Sparta Sensitivity Analysis of the Particle Factor

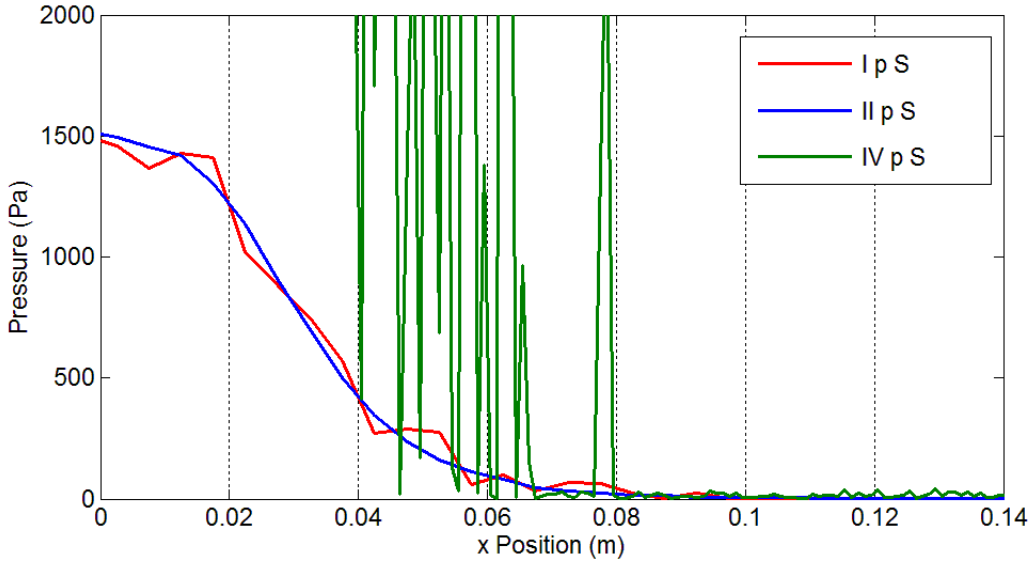

Figure 5.9: Pressure Comparison among the Simulations Considered in the Sparta Sensitivity Analysis for the Particle Factor

		Position(x) Ma=1 (m)	max T (K)	Shock Layer T (m)	Shock Layer p (m)
I p S	abs Diff.	5.000e-4	-4.194e3	7.000e-3	-1.800e-3
	% Diff.	0.211	5.503	70.020	21.211
II p S	abs Diff.	5.000e-4	-1.155e3	-7.000e-3	-3.000e-3
	% Diff.	0.211	1.584	15.003	4.292
III p S	abs Diff.	/	/	/	/
	% Diff.	/	/	/	/
IV p S	abs Diff.	-8.500e-3	-3.251e4	1.500e-3	2.000e-3
	% Diff.	3.721	31.112	750.653	3.081

Table 5.17: Comparison among the Values Analyzed in the Sparta Sensitivity Analysis for the Particle Factor

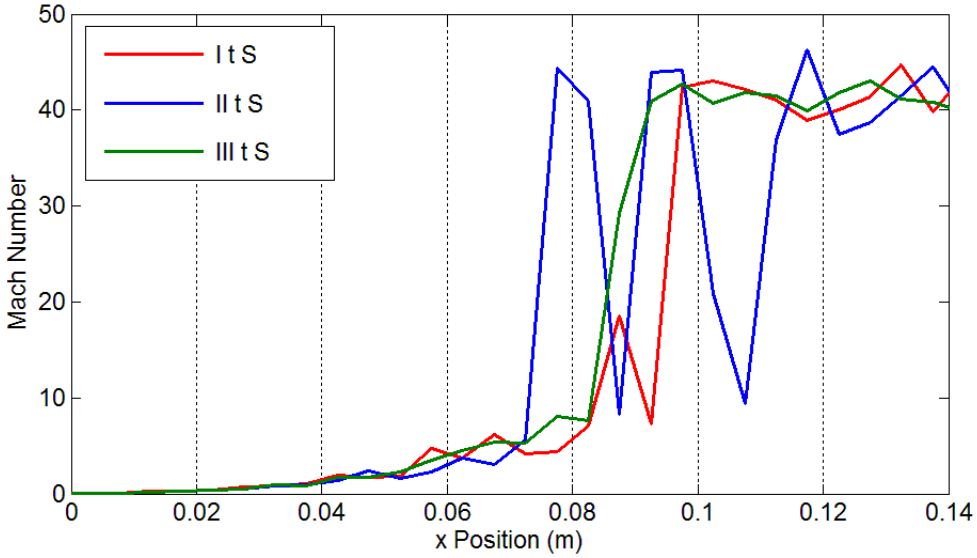

Figure 5.10: Mach Number Comparison among the Simulations Considered in the Sparta Sensitivity Analysis for the Time Step Factor

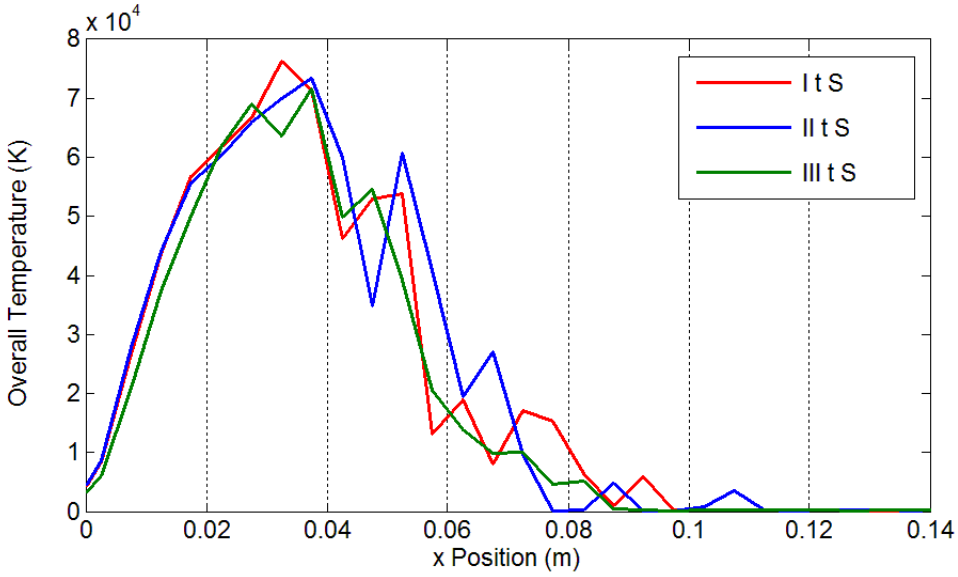

Figure 5.11: Overall Temperature Comparison among the Simulations Considered in the Sparta Sensitivity Analysis for the Time Step Factor

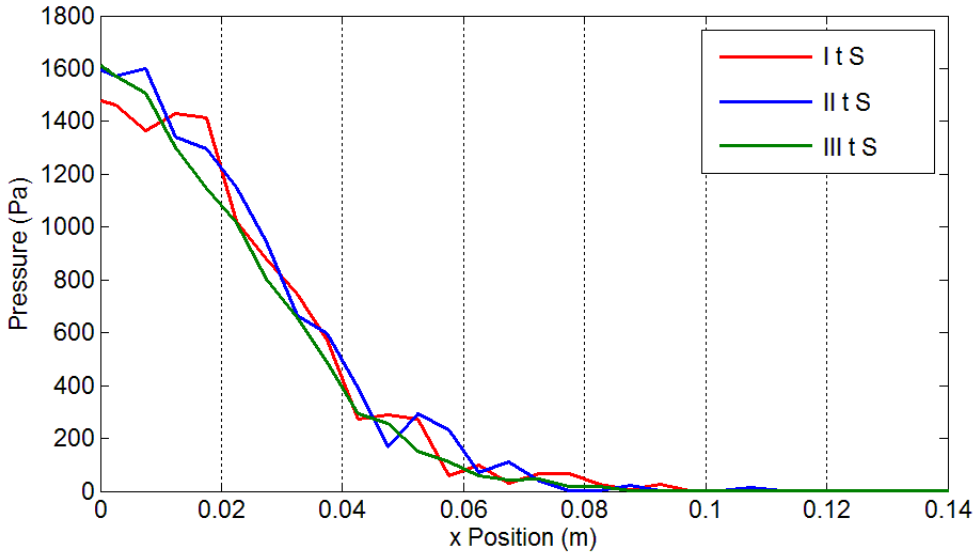

Figure 5.12: Pressure Comparison among the Simulations Considered in the Sparta Sensitivity Analysis for the Time Step Factor

		Position(x) Ma=1 (m)	max T (K)	Shock Layer T (m)	Shock Layer p (m)
I t S	abs Diff.	5.000e-4	-4.194e3	7.000e-3	1.800e-2
	% Diff.	0.211	5.502	70.033	21.225
II t S	abs Diff.	5.000e-4	-1.182e3	2.000e-3	2.200e-2
	% Diff.	0.211	1.610	13.301	48.902
III t S	abs Diff.	5.000e-4	5.960e2	-3.000e-3	2.000e-3
	% Diff.	0.211	0.833	15.001	3.083

Table 5.18: Comparison among the Values Analyzed in the Sparta Sensitivity Analysis for the Time Step Factor

		Position(x) Ma=1 (m)	max T (K)	Shock Layer T (m)	Shock Layer p (m)
I s S	abs Diff.	5.000e-4	-4.195e3	7.000e-3	-1.800e-2
	% Diff.	0.211	5.50	70	21.2
II s S	abs Diff.	-1.500e-3	2.222e3	5.000e-3	-1.000e-3
	% Diff.	0,637	3,18	41,7	1,47
III s S	abs Diff.	-2.000e-3	5.937e3	-3.000e-3	-3.000e-3
	% Diff.	0.851	8.97	15	4.29

Table 5.19: Comparison among the Values Analyzed in the Sparta Sensitivity Analysis for the Cell Size Factor

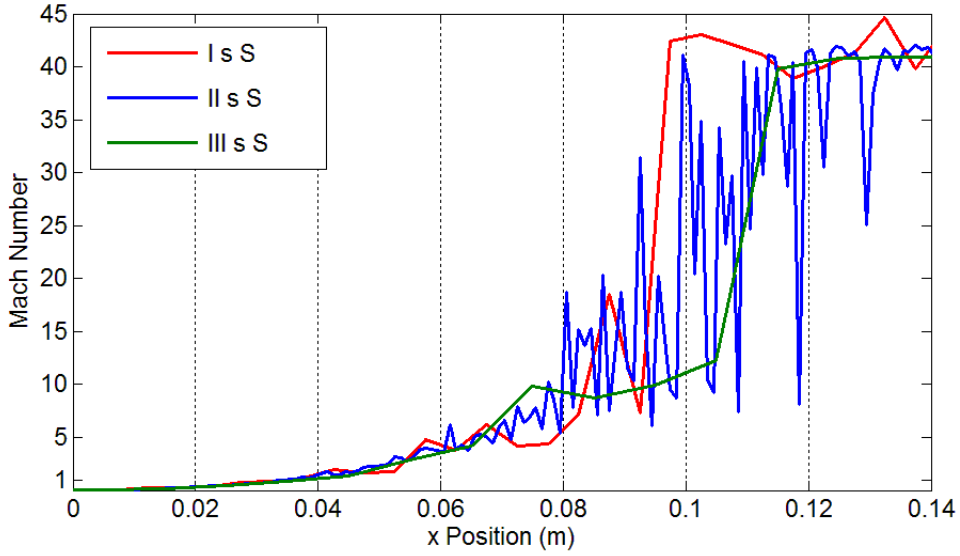

Figure 5.13: Mach Number Comparison among the Simulations Considered in the Sparta Sensitivity Analysis for the Cell Size Factor

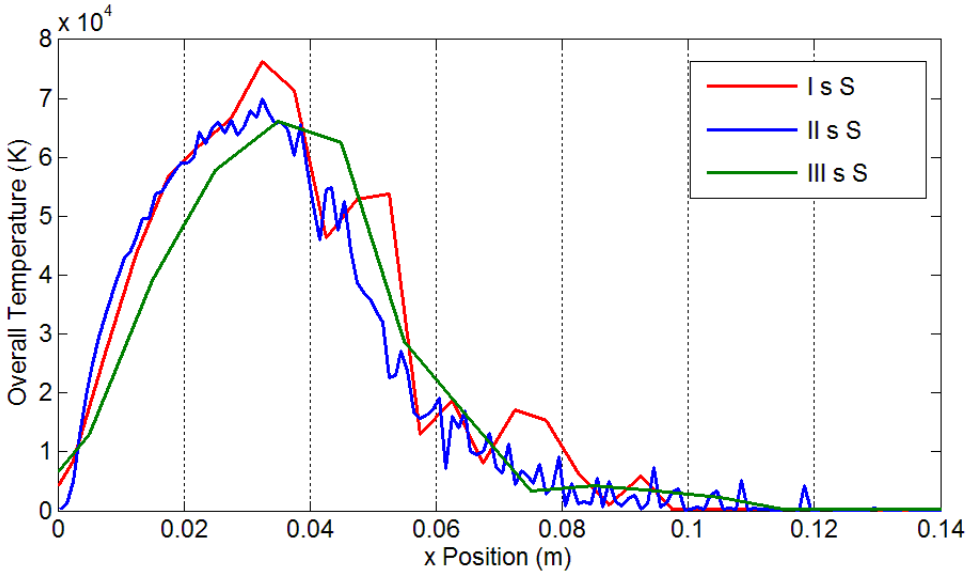

Figure 5.14: Overall Temperature Comparison among the Simulations Considered in the Sparta Sensitivity Analysis for the Cell Size Factor

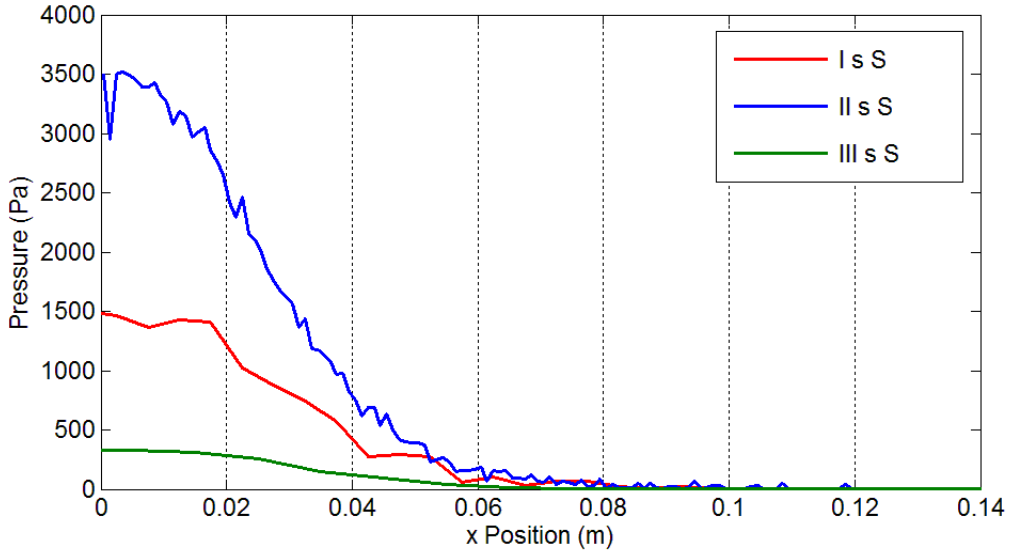

Figure 5.15: Pressure Comparison among the Simulations Considered in the Sparta Sensitivity Analysis for the Cell Size Factor

which imply big variations in a small area, take place only in a few number of cells. Therefore also variations higher than 5% must be accepted in these data. For this reason, in the following Sparta sensitivity analysis, the data obtained from the pressure and temperature slopes are not taken too much into consideration. More attention will be paid in the quality of the curves considered and in the absence of fluctuations.

an in depth examination of each factor reveals that the time step factor does not make a big difference to the absolute results. Analyzing the quality of the curves, it is possible to see that fluctuations are present in all the three simulations, but in the III t S they are a little less wide. According to this study it is not possible to derive a law about how the results vary with the time step because there is not an objective trend passing through the different time steps. In fact the fluctuations in I and II t S have almost the same magnitude and in III t S they are just a little less wide.

The number of particles per cell, as said, is the most sensitive element for the Sparta simulations. The higher the number of particles per cell, the better the results are. That is not so visible in the absolute numbers reported in Table 5.17, but it is clear from the quality of the curves. In fact the data from I p S and II p S are quite similar in the absolute value, but the graphs of the II p S simulation are smoother and more homogeneous with respect to the I p S ones. The difference is much more evident also in the IV p S. However if an attempt is made to increase the number of particles per cell again a limit will be encountered due to the lack of computational power. However considering the results and the quality of the curves, it is possible to say that

a number of particles per cell equal to 10 is enough to obtain excellent results. Besides, if the main interest is only in the absolute values of the results and an interpolation method is used to obtain graphs from them, also a simulation with 1 particle per cell produce acceptable results.

The cell size, like the time step, does not really change so much the absolute value of the results analyzed, as it is possible to see from Table 5.19. On analyzing the graphs it is evident that the smoothest is the one with the bigger cell size and the one where the fluctuations are the biggest is the one with the cell size equal to 0.001 m, that is the smallest cell. In this case the law is evident, that is, decreasing the cell size, at least in the range analyzed, the quality of the curves decreases even if the number of data points increases. However, the absolute value of the pressure, which is not included in the parameters chosen for this analysis, but is equally important, is very different for the three simulations, as can be seen from the comparison of the pressure data. In fact it is possible to notice the values of the pressure at the surface are completely different among the set of simulations. The one correct, or at least, aligned with the value of the other simulation, is only the one of the I s S simulation. Therefore, even if the best curve seems to be the one with a cell size of 0.01 m, the only acceptable value for the cell size from this analysis is 0.005 m, so the one used in the I s S. To sum up it is possible to conclude that the best setting is when the highest number of particles per cell is present, but 10 particles per cell is already more than enough. The best time among the ones taken into consideration seems to be 1e-6 s. However, since it is impossible to derive a proper law of how the results vary with the time step and considering that the quality of the results vary very little, it is possible to affirm a best time step does not exist among those considered. Terefore the choice for the best one will depend only on the computational time and resources analysis.

Increasing the cell size improves the quality of the curve, but the variations of the size could produce inaccurate results. From this sensitivity study the correct value of the cell size is the one in the I s S simulation, so 0.005 m, That is 5 times bigger then the one deriving from Bird's study.

According to these final considerations, the best simulation is the one with 10 particles per cell and a cell size of 0.005 m, where the time step is irrelevant in the range analyzed, exactly as found in the II p S simulation. The time step used in II p S simulation is 1e-7s. From the analysis in the next paragraph it will be possible to understand if this is the optimal or not.

5.2.5 Computational Resources Analysis

In the following Table 5.20, 5.21, 5.22 it is possible to see the running time and RAM used for each set of simulations.

	Simulation Time	RAM (Gb)
I p S	1h	64
II p S	30h 23'	256
III p S	/	>4096
IV p S	1h 15'	64

Table 5.20: Computational Time and Resources Used by the Simulations Performed for the Sparta Sensitivity Analysis for the Particle Factor

	Simulation Time	RAM (Gb)
I t S	1h	64
II t S	1h 5'	64
III t S	58'	64

Table 5.21: Computational Time and Resources Used by the Simulations Performed for the Sparta Sensitivity Analysis for the Time Step Factor

	Simulation Time	RAM (Gb)
I s S	1h 3'	64
II s S	18h	64
III s S	52'	64

Table 5.22: Computational Time and Resources Used by the Simulations Performed for the Sparta Sensitivity Analysis for the Cell Size Factor

Analyzing the results of the set of simulations regarding the time step factor, the computational resources used, including the time, are almost equal for all three simulations. To be precise the most efficient is the one with the bigger time step, but the difference with the others is really minimal. Therefore this is confirmation that the II p S simulation can be considered optimal and in the rest of the study this one will be used, avoiding running another simulation where the particle and cell factor will be maintained the same as the II p S and the time step will be set equal to 1e-6 s. In fact, in this case, a further verification of the results will be needed considering this is not a simulation run during the sensitivity analysis.

The set of simulations regarding the cell size factor uses all the same RAM, but the time taken increases a lot with the decreasing of the cell size, mainly passing from 0.005 m to 0.001 m. This is not surprising considering that a DSMC uses each cell as a computational domain, so the number of computational domains taken into consideration multiplies.

The computational time and also the resources vary considerably with the number of particles per cell. It varies from 1h to infinite in the simulations analyzed. If the computational time and the RAM are both considered at the same time, it is possible to make a multiplication of the two factors considering the time in minutes and the RAM in Gb. In the case of the time step and of the cell size factor, only the computational time is the discriminant factor because the computational memory is the same for all the simulations. Instead, in the first case this kind of number, which can be called 'Resources Number' increases by about 130 from I p S to II p S simulation. This gives an idea of the sensitivity of a DSMC to the particles per cell factor.

From the computational time and resources analysis it is possible to draw the following conclusions. If excellent results are the main objectives, as said in the previous paragraph, time will not be important, and the number of particles per cell used will be equal to 10. However if the main aim is discover the most efficient simulation, the choice will be the one with a number of particles per cell equal to 1, because the absolute results of this one are very close to the one with 10 particles per cell, even if there are a lot of fluctuations. However this aspect could be correct with an interpolation of the data. From now on in this study the II p S simulation will be considered because the aim is to have the best results possible. Nevertheless the I p S simulation will be considered to make preliminary tests.

5.2.6 End Time Analysis

The study of the minimum end time to obtain accurate results is conducted using a simulation with a number of particles per cell equal to 1, so the I p S simulation, to obtain results faster.

Time (s)	Position(x) Ma=1 (m)	max T (K)	Shock Layer T (m)	Shock Layer p (m)
0,005	3.550e-2	7.329e4	2.000e-2	4.000e-2
	/	/	/	/
0,004	3.500e-2	7.329e4	2.000e-2	4.000e-2
	0.123%	0%	0%	0%
0,003	3.500e-2	7.329e4	2.000e-2	4.000e-2
	0.123%	0%	0%	0%
0,002	3.300e-2	7.336e4	2.000e-2	4.000e-2
	1.09%	0.195%	0%	0%
0,001	2.600e-2	7.336e4	2.000e-2	3.500e-2
	4.85%	0.195%	0%	7.01%
0,0008	1.600e-2	7.402e4	2.000e-2	3.500e-2
	8.84%	1.02%	0%	7.01%
0,0006	1.000e-3	7.549e4	1.500e-2	3.000e-2
	14.2%	3.19%	21.1%	14.0%

Table 5.23: Variation in the Values Considered in the Sparta Sensitivity Analysis Decreasing the End Time in the I p S Simulation

Until now an end time 0.005 s has been used, as in the OpenFOAM simulations. The study is conducted exactly as in the previous case. The results are reported in the next Table 5.23.

In the last three steps, that is from 0.003 s to 0.005 s there are no sensitive variations, so it is correct to say the results reached an asymptote and it is not useful to consider an end time bigger than 0.005 s. The variations become more relevant for an end time lower than 0.003 s and are no longer acceptable after 0.001 s as in the OpenFOAM study, because the variations in the position of Mach number equal to 1 and in the length of the pressure slope considered are too high (over 5%). Even if it has been said the data obtained from the pressure and temperature slopes are not so reliable in Sparta simulations, such an error in the position of Mach number equal to one is not tolerable. Therefore the minimum end time to have steady results and the one that will be considered from now on is 0.001 s.

6 Results

The aim of this study, as presented in Chapter 1, is to validate and set up a program able to perform simulations at high altitude for atmosphere entry in order to collect data useful for the building of a thermal protection system. With regard to this target, in this chapter a comparison between the results of OpenFOAM and Sparta is made, at least for the no-reactions case, to establish which is the best DSMC software to be used. Then a comparison between these data and the theoretical ones evaluated with the perfect gas approximation is done and, only for the case with chemical reactions, the comparison is done with the experimental data measured by the Hayabusa capsule. The objective is to determine if the results given by the software are correct and so to validate the program. Finally an extrapolation of the data needed to start the sizing of a thermal shield is done. Before doing this a comparison between two-dimensional and three-dimensional simulation results is made to show the equivalence of the two and to justify the use of the two-dimensional domain in the rest of this study.

6.1 2D and 3D Simulations Comparison

In the following paragraph the data coming from the two-dimensional and three-dimensional simulations are shown (see also Appendix 2) and compared. The parameters examined are the same as the sensitivity analysis, that is the Mach number, overall temperature and pressure. Only the OpenFOAM simulations are considered in the present paragraph.

As it is possible to see from Figure 6.1 to 6.3 the graphs are almost perfectly superimposed. Therefore it is evident the two-dimensional and three-dimensional simulations are equivalent in the case studied.

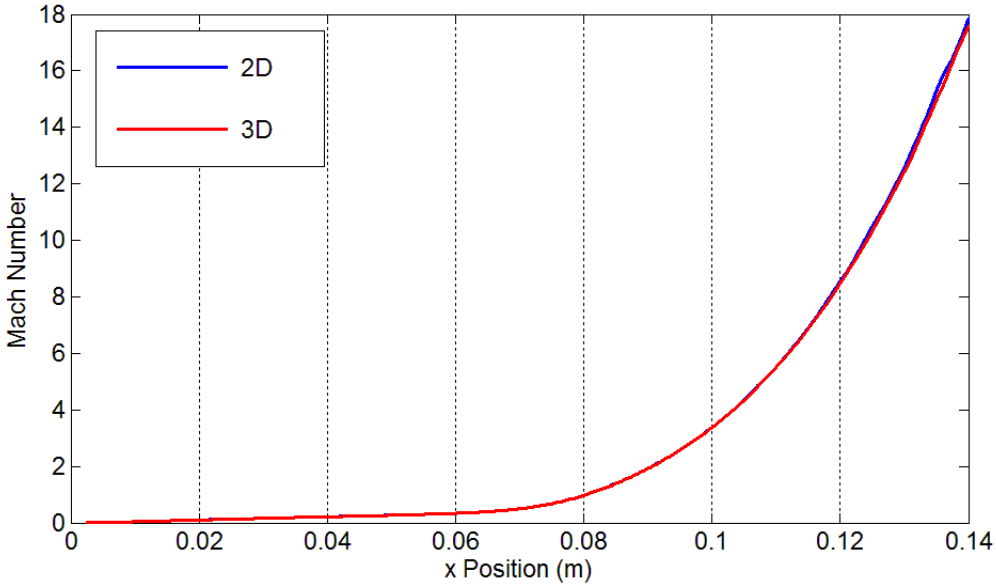

Figure 6.1 Comparison between the Mach Number Obtained from the Two-Dimensional and Three-Dimensional Simulations

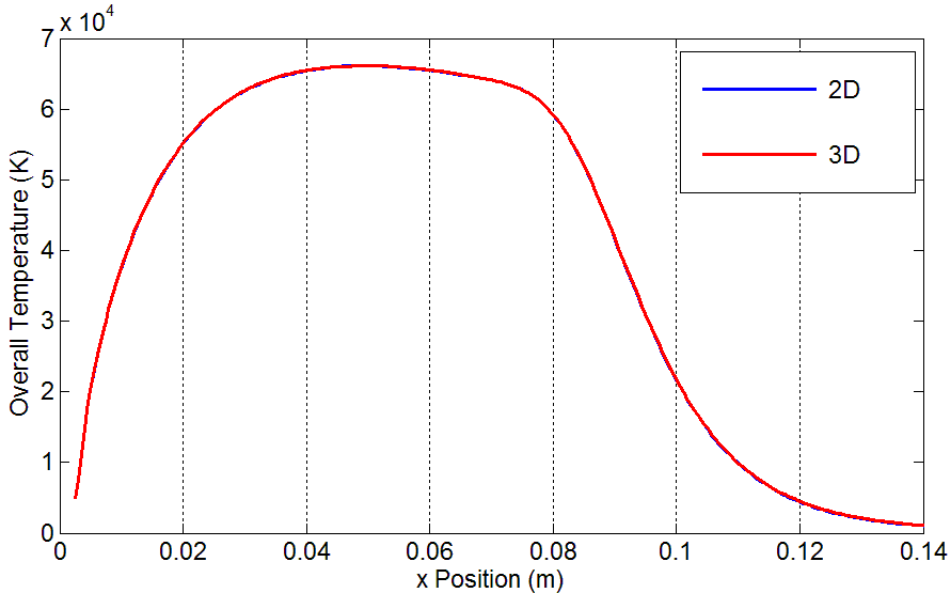

Figure 6.2 Comparison between the Overall Temperature Obtained from the Two-Dimensional and Three-Dimensional Simulations

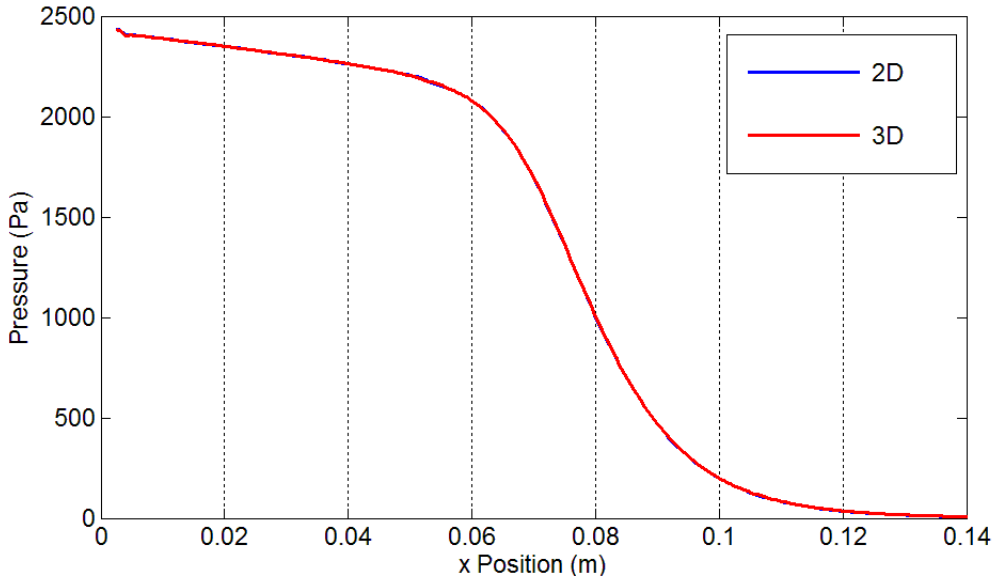

Figure 6.3 Comparison between the Pressure Obtained from the Two-Dimensional and Three-Dimensional Simulations

6.2 OpenFOAM and Sparta Comparison

In the following pages the data of OpenFOAM and Sparta best simulations respectively, as chosen in Chapter 6, are presented. The data chosen are the ones which could be interesting for a future study on the thermal shield, that is the Mach number, pressure, overall temperature and secondary temperatures. They are shown from Figure 6.4 to 6.12.

As it is possible to see there is a difference in the secondary temperatures between the two software. In fact it is important to know that five kinds of different temperatures exist and the analysis of these can be performed using different models. The meaning of the five temperatures and why it is important to take into consideration different kinds of temperatures instead of only the overall one, will be treated in the following Paragraph 6.4. For the moment it is important to know that different kinds of temperature exist and they are different according to what physical model is used or, also, to what names are given to these temperatures.

The comparison between the two software can be done only with the same data plotted that is the Mach number, pressure and temperatures. Considering the unreal conditions of this experiment there are no referent experimental data. The comparison between the two software can be done only on the quality of the curves and with respect to the theoretical data. The latter will be

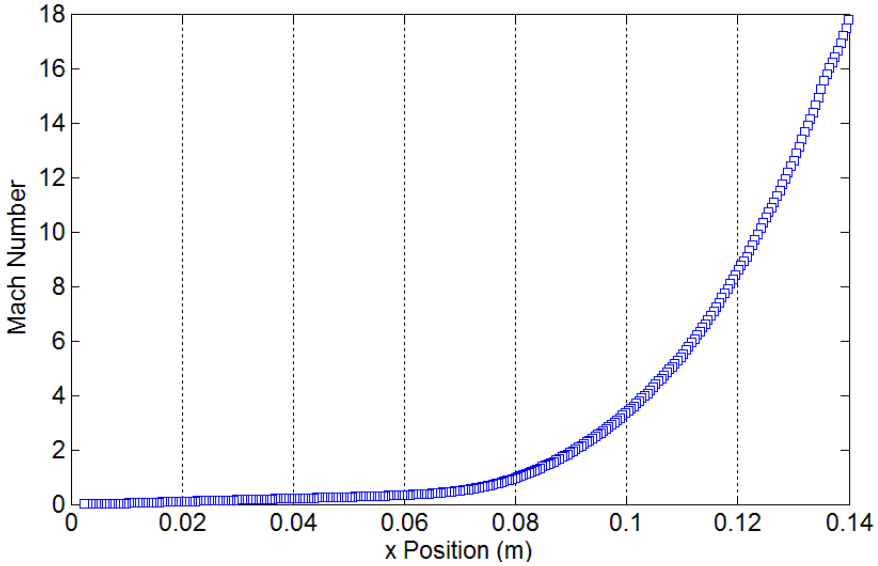

Figure 6.4: Mach Number Evaluated from OpenFOAM Best Simulation

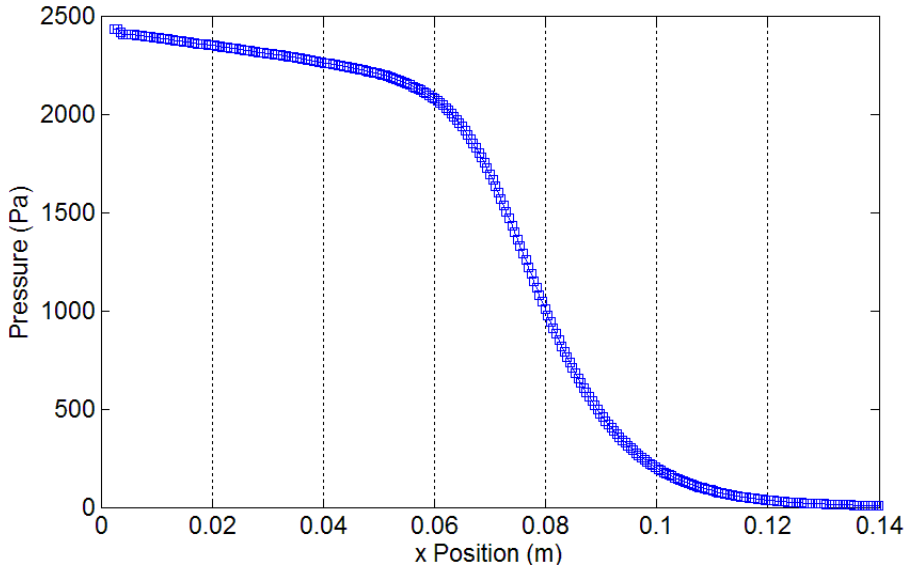

Figure 6.5: Pressure Evaluated from OpenFOAM Best Simulation

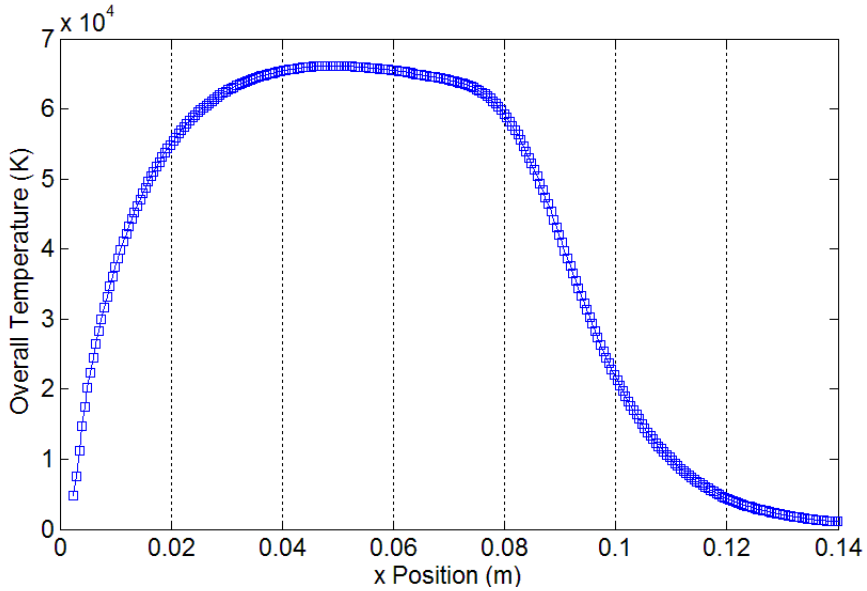

Figure 6.6: Overall Temperature Evaluated from OpenFOAM Best Simulation

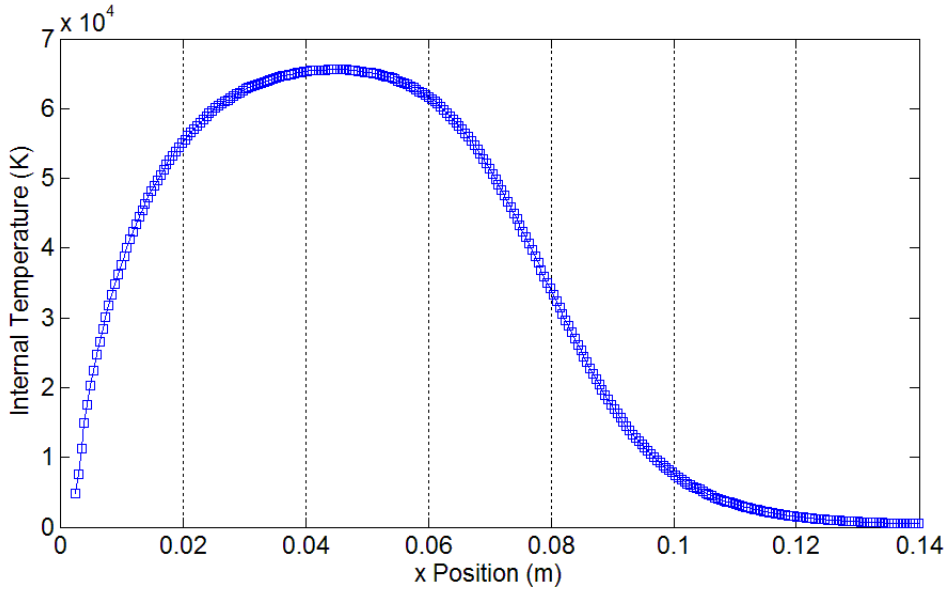

Figure 6.7: Internal Temperature Evaluated from OpenFOAM best Simulation

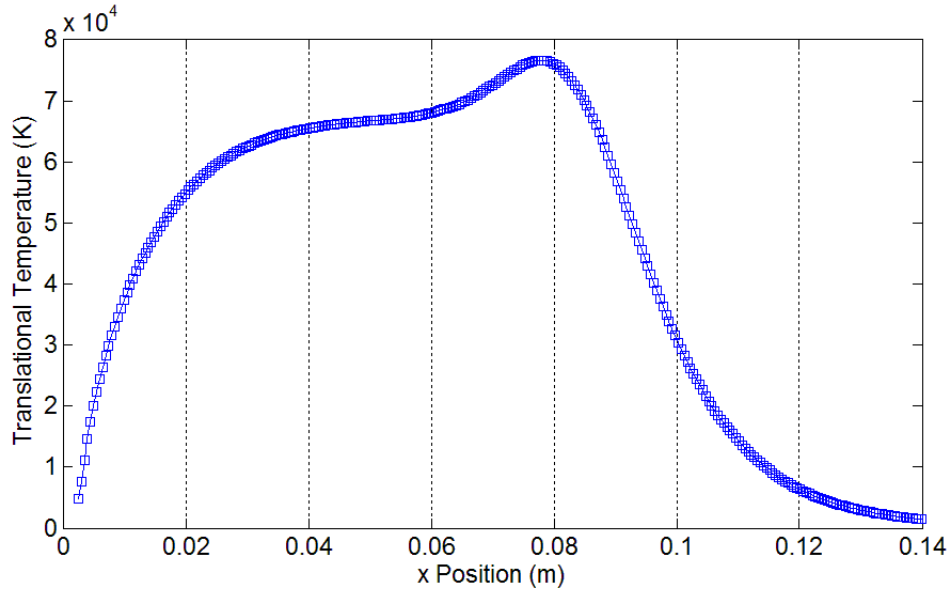

Figure 6.8: Translation Temperature Evaluated from OpenFOAM Best Simulation

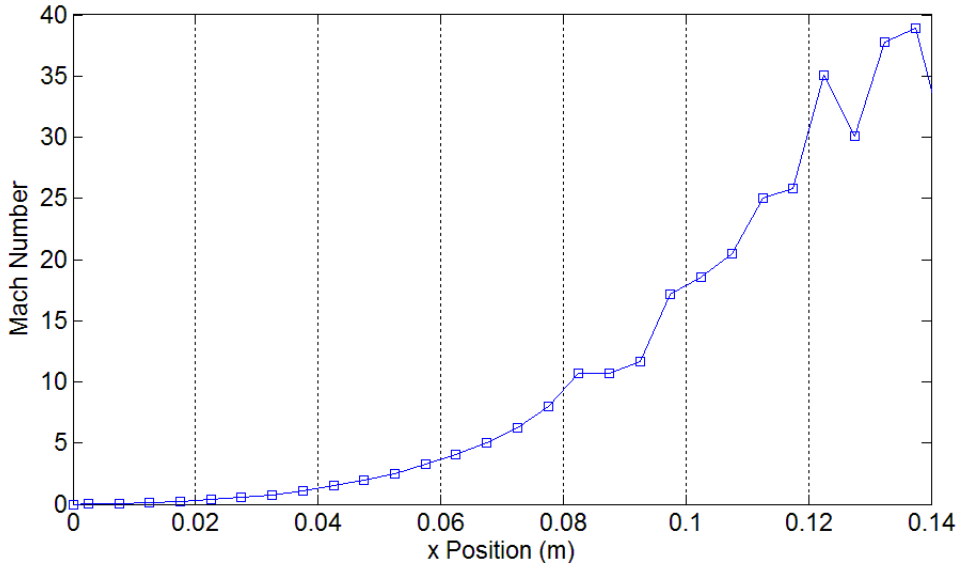

Figure 6.9: Mach Number Evaluated from Sparta Best Simulation

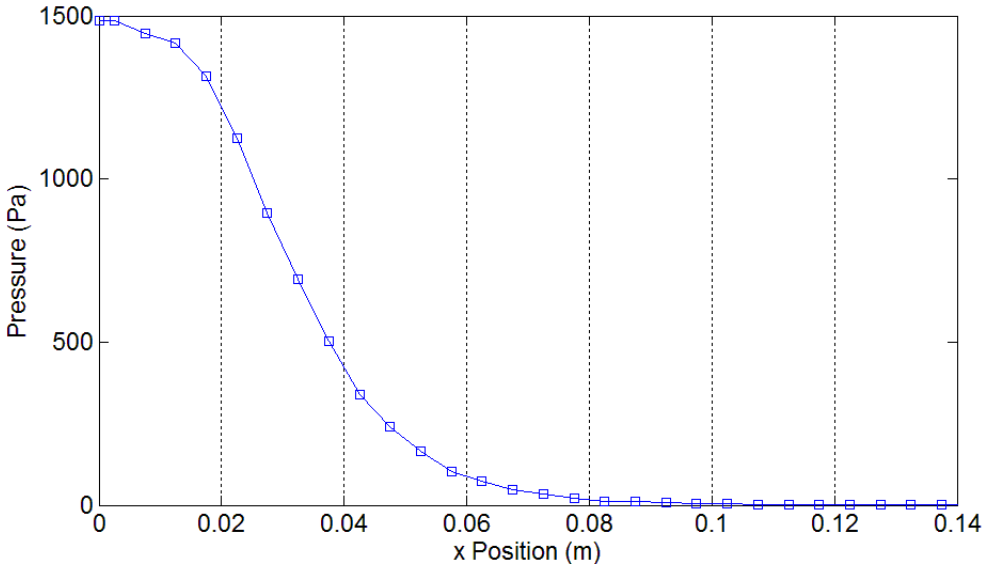

Figure 6.10: Pressure Evaluated from Sparta Best Simulation

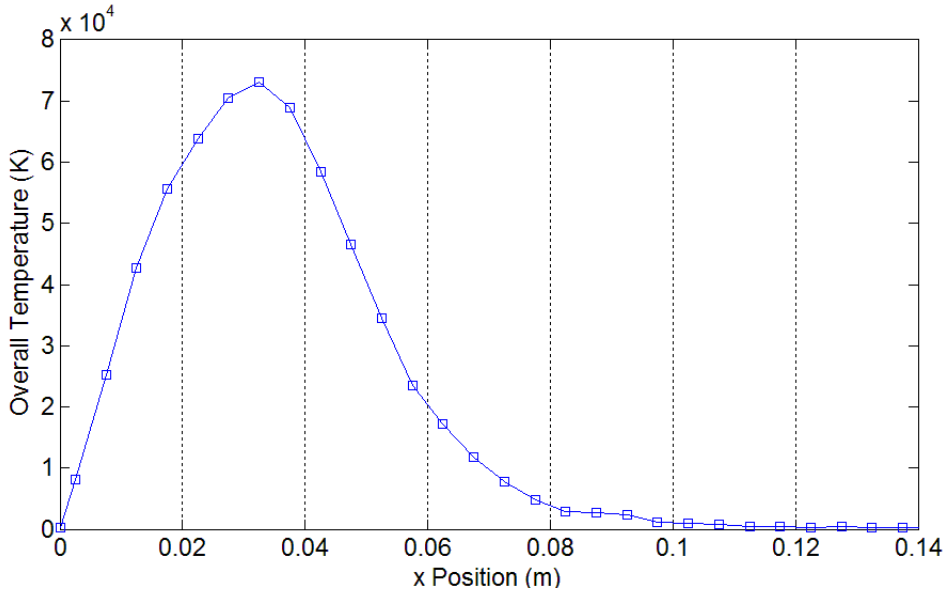

Figure 6.11: Overall Temperature Evaluated from Sparta Best Simulation

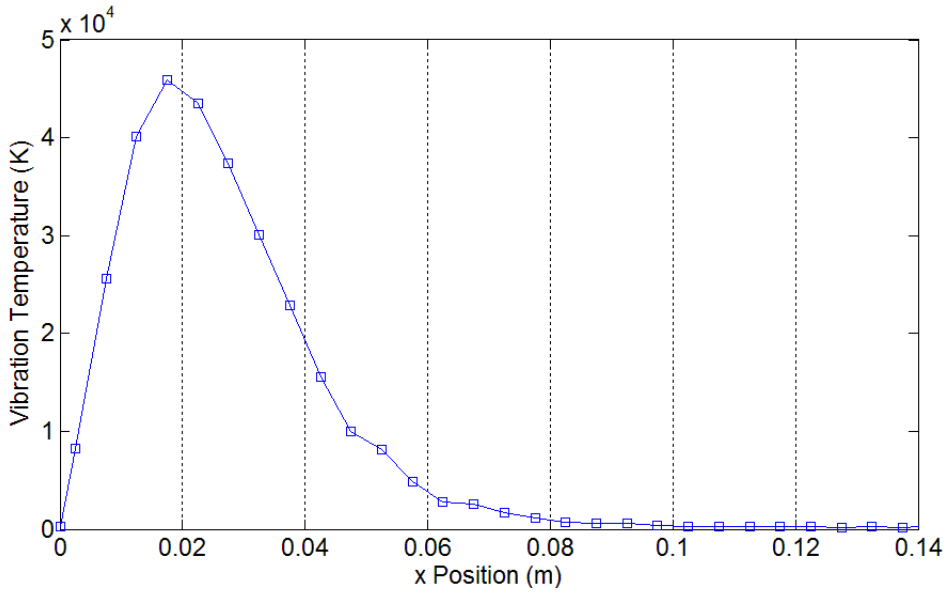

Figure 6.12: Vibration Temperature Evaluated from Sparta Best Simulation

done in the next Paragraph 6.3. Figure from 6.13 to 6.16 show the comparison between the two software and in Table 6.1 the same comparison is shown considering the absolute values. The values taken into consideration in Table 6.1 are the same as the sensitivity analysis plus the maximum pressure and maximum internal temperature (rotation temperature for Sparta).

It is possible to see immediately that the results in their absolute values do not match, even if the shape of the curves are almost the same. Therefore it is possible to say there is no difference in the physical meaning parameters evaluated, but probably the difference is in the way of evaluation of each parameter. The way of evaluation does not mean the formula used, because that is reported in the documentation and it is the same for both software, but in the way of moving and colliding particles, applying boundary conditions,... so in how is structured the DSMC solver is structured. Actually, as can be seen, the overall temperature curve of the two software is quite different, so probably it is not the same parameter which is being evaluated. Anyway this subject will be examined more in depth later.

To establish what are the correct results, some accurate reference data are necessary, for comparison, as is reported in the introduction of this paragraph. However, analyzing the graphs it is possible to make some important observations. For the moment the comparison between the two overall temperatures is not considered, instead, the pressure parameter will be discussed in parallel. From the rest of the data it is possible to see that the part of the OpenFOAM curves characterized by a negative gradient starts farther from the surface with respect to the Sparta one. This difference is about 0.4 m. This means that the border of the shock layer is farther

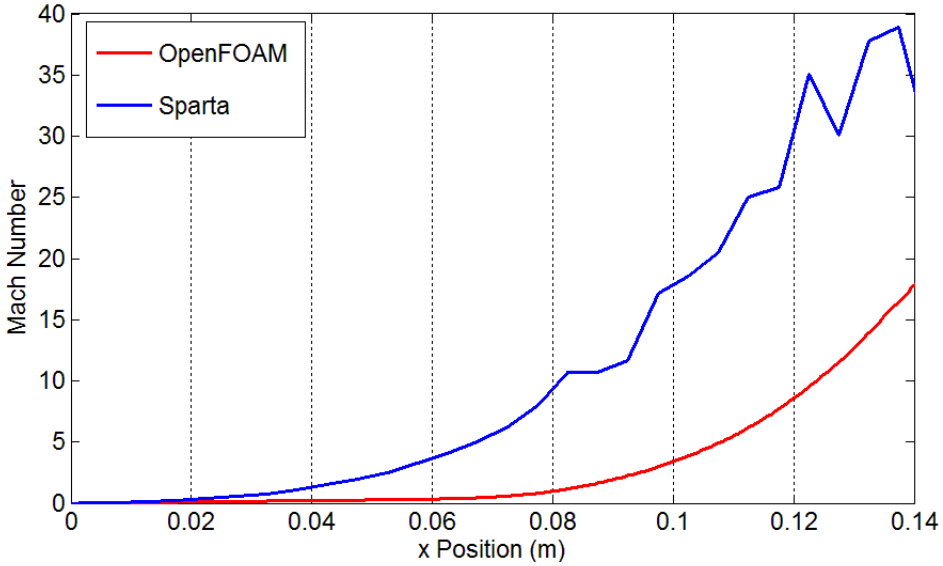

Figure 6.13: OpenFOAM and Sparta Mach Number Comparison

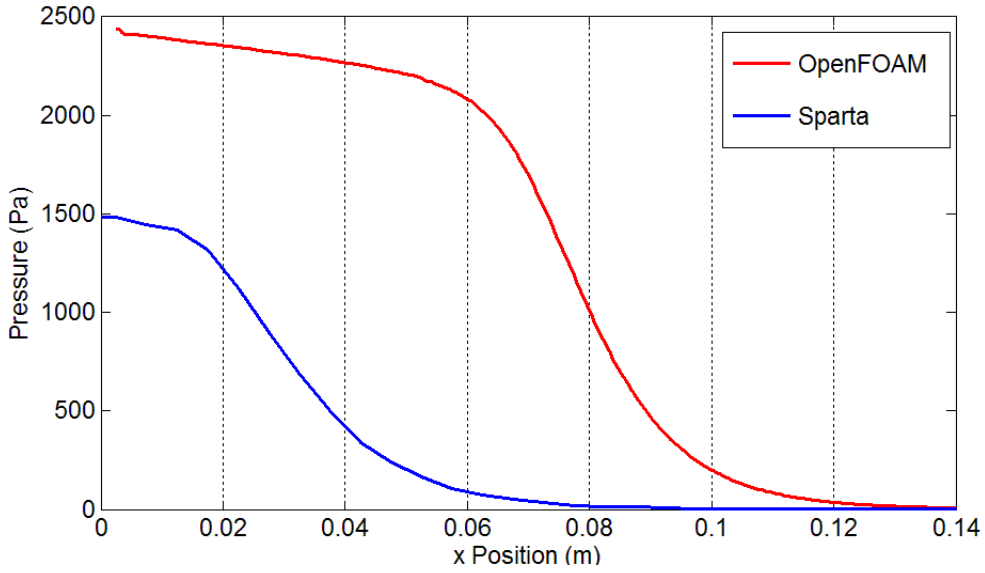

Figure 6.14: OpenFOAM and Sparta Pressure Comparison

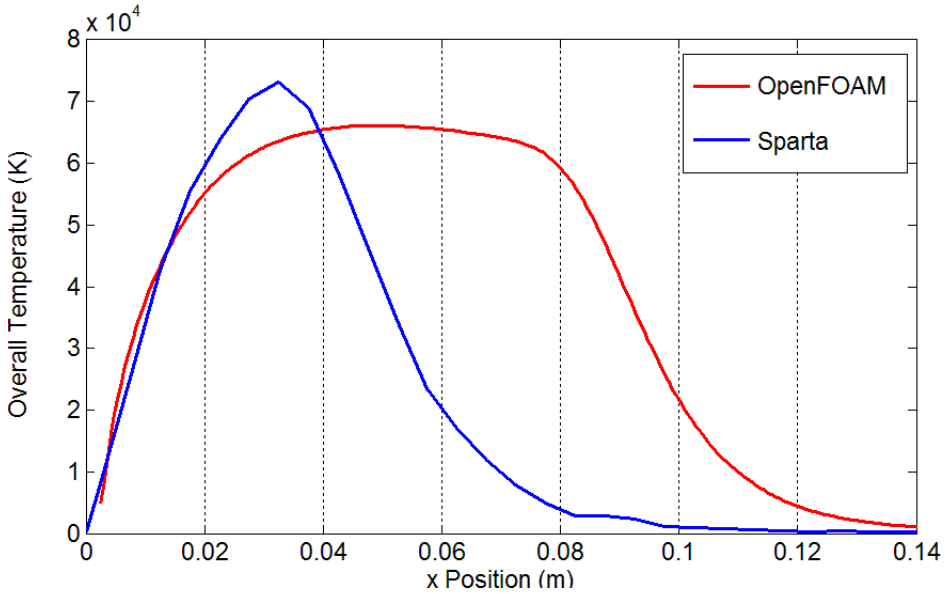

Figure 6.15: OpenFOAM and Sparta Overall Temperature Comparison

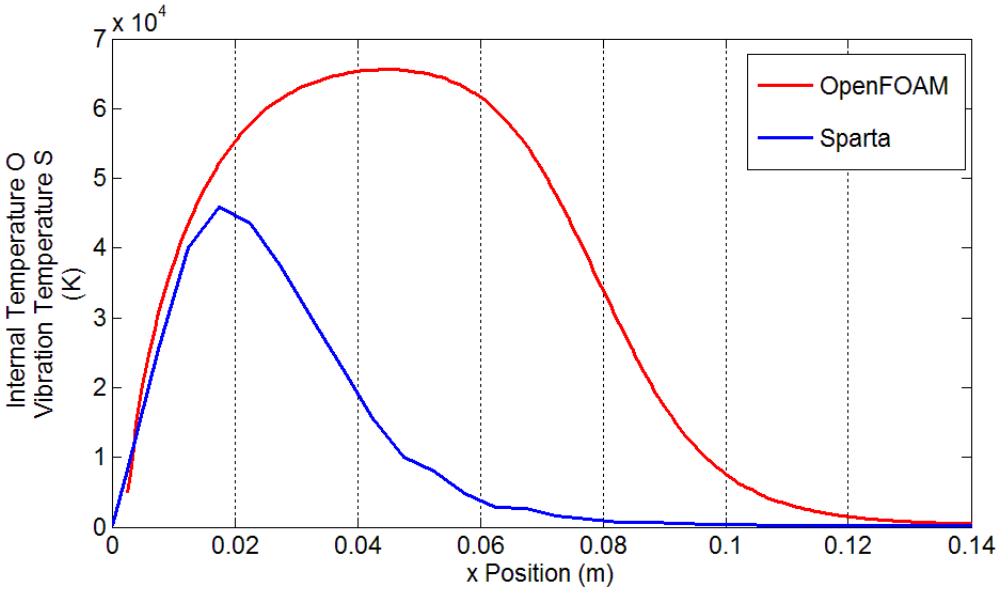

Figure 6.16: OpenFOAM Internal Temperature and Sparta Vibration Temperature Comparison

	OpenFOAM	Sparta
Position(x) Ma=1 (m)	7.840e-2	3.550e-2
max Overall T (K)	6.613e4	7.329e4
Shock Layer T (m)	4.366e-2	2.000e-2
max p (Pa)	2.439e3	1.484e3
Shock Layer p (m)	5.012e-2	4.000e-2
max Int T/Rot T (K)	6.561e4	4.587e4

Table 6.1: OpenFOAM and Sparta Relevant Data Comparison using Absolute Values

from the surface according to OpenFOAM data with respect to Sparta ones. The Mach number graph can be considered proof of this data where the position of Mach number equal to one is 0.07804 m for OpenFOAM and 0.0355 m for Sparta, so the difference is about 0.4 m.

The part of the curve with a positive gradient for all the different temperatures has almost the same inclination and position. For the pressure, the analysis is equivalent except for the fact that the gradient is always negative and there is a difference in the starting initial value. In fact, the initial gradient of the pressure slope is the same for both the curves, but it becomes higher than -1 in a position closer to the capsule surface in the Sparta case with respect to the OpenFOAM one, with a difference of about 0,4 m. This means that the width of the shock is larger in OpenFOAM with respect to Sparta. Considering the point H3 is in the transition regime, at the limit of the continuous one, it seems that Sparta data are more accurate. However it is impossible to affirm this because there are no reference data.

Another remarkable observation is that OpenFOAM absolute values of the pressure and internal temperature are higher then the Sparta ones. This observation is useful to analyze the Sparta overall temperature. In fact, from the comparison of the two overall temperatures it is clear that the shape of the two curves are different. From the OpenFOAM documentation, but also analyzing the shape of the OpenFOAM internal temperature and comparing it with some other temperature slopes deriving from literature, it is clear that what OpenFOAM refers to as internal temperature is a vibration / electron / electronic temperature in a Two-temperature model. The documentation about Sparta is not so clear about the temperature model used. However if an attempt is made to compare the Sparta overall temperature with the OpenFOAM transitional

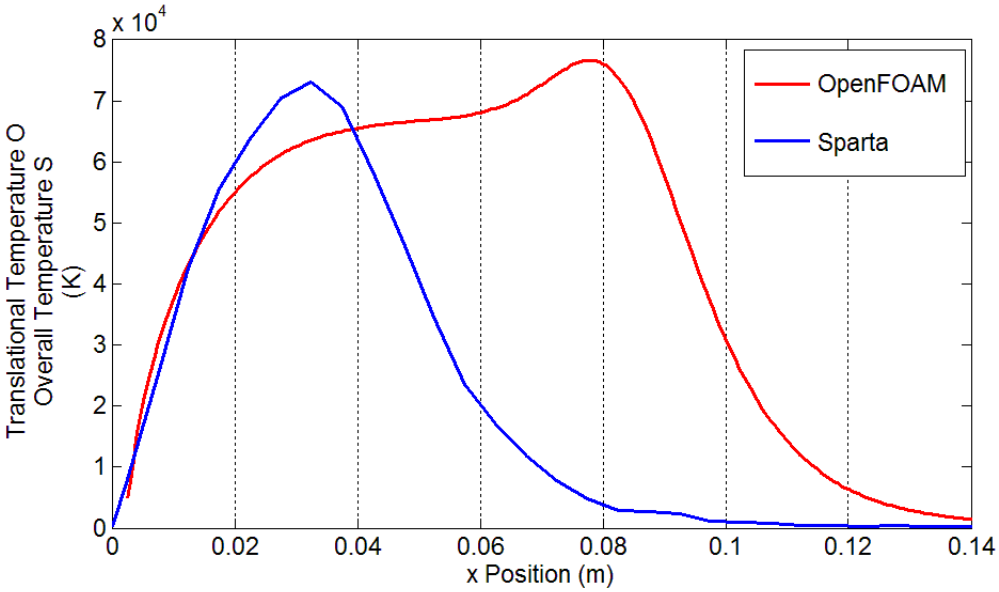

Figure 6.17: OpenFOAM Translation Temperature and Sparta Overall Temperature Comparison

temperature (Figure 6.17) it is evident the slopes here are comparable. In addition the part of the OpenFOAM curve with a negative gradient starts farther from the surface with respect to the Sparta one by 0.4 m, like the difference noticed in the rest of the graphs between OpenFOAM and Sparta simulations. Furthermore the characteristic of the pressure and internal temperature, That is that the OpenFOAM resulting data have higher absolute values with respect to Sparta ones, is evident here too. Instead if a comparison is made of both overall temperatures, besides having different shapes, the Sparta absolute value is higher than the OpenFOAM one, while the difference in the position of the part of the slope with a negative gradient, noticed also in the other graphs analyzed, is respected.

Therefore probably the overall temperature in Sparta is the vibration / electron / electronic temperature in the Two-temperature model. Anyway this topic will be discussed in further detail and deepened in the next Paragraph 6.4.

Analyzing the graphs of each software it is possible to note the OpenFOAM plots have more data points with respect to the Sparta ones, so the curves are more accurate and smoother. In fact in Sparta it is possible to dump only a datum for each cell, but , as is presented in the sensitivity analysis, it is possible to increase the number of data points decreasing the cell size. Therefore in principle it is possible to have as many data points as required. The setting of the data points depends directly on the cell size, so if a certain number of data is required, probably it is impossible to obtain the most efficient parameter setting or the best results, as discussed in the sensitivity study. For this reason it is possible to say that OpenFOAM can offer a better

quality of results between the two DSMC software analyzed.

Besides, OpenFOAM has a very flexible way of sampling data from the simulation which allows for as many data points as required and along whatever curve desired inside the domain without making any variations to the simulation parameters. In fact sampling is an operation done after the end of the simulation. For this reason it is possible to say that OpenFOAM has the most efficient and correct sampling data system too.

In the next Paragraph 6.3 an attempt will be made to verify which results are correct, OpenFOAM or Sparta.

6.3 Simulation and Theoretical Data Comparison

In the simulation without reactions it is possible to make a comparison with the theoretical data obtained considering the perfect gas approximation. In fact an ideal gas is a theoretical gas composed of many randomly moving point particles that do not interact except when they collide elastically, which is the same principle of a DSMC without chemical reactions.

Perfect gas means a gas which has the following properties:

- The particles of the gas are all equal and indistinguishable points
- The particles of the gas are in continuous movement according to straight trajectory regulated by random laws
- The particles of the gas have their own volume, negligible with respect to the volume available for the gas
- The particles of the gas have no interactions with each others
- The collisions between the particles of the gas are elastic, so no loss of energy is expected.

A gas behaves more like an ideal gas at higher temperatures and lower pressures, as the potential energy due to intermolecular forces becomes less significant compared with the particle's kinetic energy, and the size of the molecules becomes less significant compared to the empty space between them. The ideal gas model tends to fail at lower temperatures or higher pressures, when intermolecular forces and molecular size become important. It also fails for most heavy

gases, such as many refrigerants, and for gases with strong intermolecular forces, notably water vapor. At high pressures, the volume of a real gas is often considerably greater than that of an ideal gas. At low temperatures, the pressure of a real gas is often considerably less than that of an ideal gas.

Considering all the properties of a perfect gas, the one concerning the volume is not properly respected while the others are all matching with the case studied. In fact, even if the density considered is very low, it becomes higher in front of the capsule because of the collisions of the particles with the surface. As a consequence, the pressure is quite high in this area. Therefore theoretical results which do not match perfectly with simulation data can be expected because some hypothesis are not respected, even if not such a big difference is expected in the case of correct simulations. However the use of the theoretical results as the validation data for the simulation without reactions is definitely not possible. The confrontation is done all the same to discover what is the difference between the results found.

Shock Layer Relationships

A shock is a narrow layer of strong variation in the pressure, temperature, density and velocity of the fluid [25]. There are many types of shock. The relations which will be considered are for normal, stationary and adiabatic shock. In the case studied the shock considered is normal because the velocity of the fluid is perpendicular to the shock layer as it is possible to see from previous images. It is stationary because the velocity of the fluid which invests the capsule is maintained constant in this simulation. However it is not really adiabatic. This is another other source of error with respect to the theoretical condition.

Using the balance of mass, momentum and energy in a extremely thin control volume across the shock and also the ideal gas laws, it is possible to obtain the Prandlt relation for a normal shock (1.1):

$$V_1 V_2 = \frac{2}{\gamma + 1} a_0^2 \quad (6.1)$$

where V_1 is the velocity of the fluid before the shock, V_2 is the velocity of the fluid after the shock, γ is the ratio between the specific heats at constant pressure and at constant volume of the fluid considered and $a_0$is the sound critical velocity.

	Theoretical	OpenFOAM	Sparta
Pressure (Pa)	2.165e3	2.440e3	1.484e3
Overall T (K)	6.807e4	6.613e4	7.329e4

Table 6.2: Pressure and Overall Temperature Values after the Shock in the Theoretical Case and in the Sparta and OpenFOAM Simulation

Introducing the Mach number it is possible to derive the following relationship which links the latter before and after the shock:

$$M_2^2 = \frac{(\gamma - 1)M_1^2 + 2}{2\gamma M_1^2 - (\gamma - 1)} \quad (6.2)$$

where M_1 is the Mach number before the shock, M_2 is the Mach number after the shock.

Using this relationship (6.2) inside the mass, momentum and energy conservation equation, it is possible to obtain the following relations [82] which link the temperature, pressure and velocity upstream to the ones after the shock:

$$\frac{p_2}{p_1} = \frac{2\gamma}{\gamma + 1} M_1^2 - \frac{\gamma - 1}{\gamma + 1} \quad (6.3)$$

$$\frac{T_2}{T_1} = \frac{(2\gamma M_1^2 - \gamma + 1)(M_1^2(\gamma - 1) + 2)}{M_1^2(\gamma + 1)^2} \quad (6.4)$$

where p and T are respectively the pressure and temperature. The pedix 1 indicates the value before the shock and the pedix 2 the value just after the shock.

The results obtained from the shock layer relations, using as upstream values the ones present at the point considered, H3, are the following visible in Table 6.2 under the heading "Theoretical". The comparison with the simulation data is visible in the same Table 6.2.

As it is possible to see, the data from both simulations do not perfectly match the theory ones, as expected. However they are in the same order of magnitude and the difference is not so big

except in the case of Sparta pressure. Anyway the absolute value of this parameter has already been found to be uncertain in previous analysis. Therefore it possible to conclude without any doubts that absolute pressure values are not reliable in Sparta. Moreover the theoretical pressure is referred to the value at the shock, but the simulation datum considered is the value of the pressure just before the capsule surface. In such rarefied conditions it is difficult to evaluate the end of the shock to establish what pressure value to take into account, because the shock layer is wider with respect to the one in continuous regime. In fact the increasing part of the pressure slope is not vertical as in dense fluids. Nevertheless it is possible to see from the Figure 6.14 that the pressure slope continues to increase until it reaches the surface of the capsule, where certainly the discontinuity zone constituted by the shock layer is already finished. Therefore the pressure values taken into account deriving from the DSMC are overestimated. This means the Sparta error is higher, instead the OpenFOAM value matches the theoretical data better. For the rest of the present analysis the Sparta pressure data will not be considered.

On the other hand it is possible to conclude that the results obtained by the simulations in the case of absence of reactions can be trusted. Therefore, if it is not possible to entirely validate the software in the case without reactions, at least the results match what is expected.

Considering the comparison between Sparta and OpenFOAM, the results which match more with the theory are the ones of OpenFOAM. However, as said before, this comparison is not expected to match the theoretical data because the hypothesis adopted in the theory have not been completely respected in the simulation. As a consequence it is impossible to say if the greater divergence of the Sparta results from the theoretical data with respect to the one of OpenFOAM is a worst or better result. Therefore this cannot be used as proof to establish what the best results are. The only possible validation criteria is the comparison with experimental data which can be done exclusively for Sparta simulations considering that it is the only software which implements chemical reactions for the moment, between the two considered.

6.4 Extrapolation of Useful Results

In the following paragraphs attention is focused on the simulation with chemical reactions. As has been explained before only Sparta has implemented chemical reactions inside the DSMC code, while OpenFOAM not yet. Therefore from this moment the subject of the study will be the Sparta simulations with chemical reactions. The parameter setting for the simulation analyzed is the one discovered to perform best in the sensitivity analysis . A variation is done in the number of particles per cell used. In fact a simulation with 10 particles per cell, as established

from the sensitivity study to be the best setting, is not able to run with the resources available at EPFL, for problems which will be analyzed in Appendix 1. For this reason in the simulation for the following analysis the particle parameter uses is 1 particle per cell in the simulation used for the following analysis.

The data useful to start the design of a thermal shield which could be extrapolated from such a simulation are presented in the following paragraph. They are the Mach number, pressure, mass fraction, overall temperature, translation / rotation temperature and vibration / electron / electronic temperature. All of these are considered along the stagnation line as said in the previous paragraphs.

The Mach number curve is important because, even if it cannot give the exact position of the shock, considering the actual one is diffuse as a consequence of the rarefaction of the fluid, it provides an estimation of that zone. The pressure, overall temperature and mass fraction are useful to evaluate the convective heat transfer coefficient. The overall temperature is used to evaluate the convective heat flux. The remaining types of temperature are used to evaluate the radiate heat flux.

Shock Position

Figure 6.18 shows the Mach number over the x position.

The mach equal to one is at 0.0255 m. The strong variation diffuse zone, created by the shock layer in a rarefied gas, is in its proximity.

Convective Heat Flux

In a re-entry like in an entry journey towards a planet, a capsule is exposed to a severe heating environment, as a consequences of the excitation to very high temperatures of the gas in front of the spacecraft. This is caused by the large amount of energy which has to be received by the capsule. It is due to the large dissipation of kinetic energy in the interaction with the gaseous atmosphere. Energy is transferred to the vehicle surface via two mechanisms [7]; (1) interactions of particles with the surface (convective heating), and (2) absorption of electromagnetic radiation emitted by the shock layer (radiate heating). It is fundamental to know these heat fluxes to

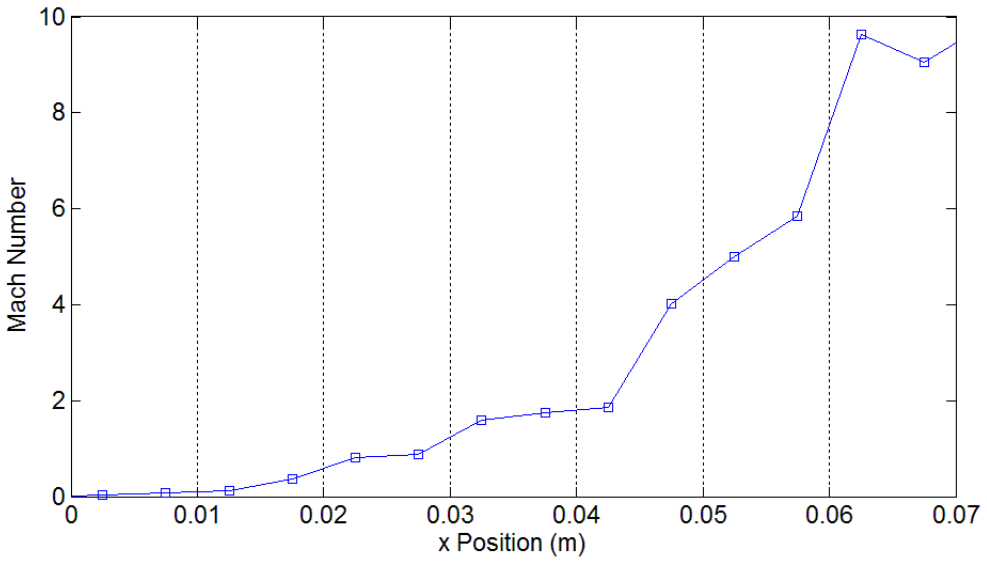

Figure 6.18: Mach Number Evaluated using Sparta Simulation with Chemical Reactions

project an effective thermal shield. In this paragraphs convective heating is examined, while radiate heating will be dealt with in the next paragraph.

Convection is the dominant form of heat transfer in liquids and gases. It consists in the transfer of heat from one place to another by the movement of fluids. The total heat transfer is due to the superposition of energy transport by random motion of the molecules and by the bulk motion of the fluid in the presence of a temperature gradient.

As presented in Chapter 1, the most problematic point is the stagnation point, and it is at this exact point that the sizing of the thermal shield is calculated. The design is based on the stagnation point because in this point the surface of the capsule encounter the worst conditions. The reason of this is that during the mission the attitude could change due to some unexpected events and different points of the spacecraft surface could become the stagnation point. Therefore the heat flux is calculated for this point.

The convective heat flux is evaluated using the Fourier law (6.5).

$$\frac{\partial q}{\partial t} = -\sigma_{\mu\nu} \nabla T \quad (6.5)$$

In the case of convective heat flux the tensor which appears in the formula ($\sigma_{\mu\nu}$) is the convective heat tensor and q is the heat flux per square meter. In the conduction of this preliminary study

some approximation are done. Considering an isotropic field, the tensor reduces to the constant k, the convective heat transfer coefficient. The temperature is taken to vary linearly in the domain considered, which is the stagnation line. The Fourier law in this case becomes (6.6):

$$\frac{\partial q}{\partial t} = -k\frac{(T - T_s)}{\triangle x} \quad (6.6)$$

In (6.6) T is the air temperature. For this value the last value of the overall temperature calculated from Sparta before the capsule surface is taken into consideration. T_s is the temperature of the capsule surface and k is the convective transmission coefficient. The latter is evaluated using the Nasa software CEA (Chemical Equilibrium with Applications).

Convective Heat Transfer Coefficient

The convective transmission coefficient depends on what kind of fluid is being dealt with and on the pressure and temperature too. In this case the fluid is a mixture of species, so it is impossible to derive it from any reference tables.

A specific program developed by NASA to evaluate the convective transmission coefficient, CEA software, is used.

CEA is a program which calculates chemical equilibrium product concentrations from any set of reactants and determines thermodynamic and transport properties for the product mixture, in addition to many other functions. It is in wide use by the aerodynamics and thermodynamics community.

CEA needs the overall temperature (Figure 6.19), pressure (Figure 6.20) and the mass fraction for each species present at the point where the convective transmission coefficient must be evaluated. The point taken into consideration is the last data point before the capsule surface, along the stagnation line. The values used are provided by the Sparta simulation and are reported in the following Table 6.3.

As presented in the previous chapter, there is some uncertainty in the meaning of the Sparta overall temperature. This aspect will be examined more closely in Paragraph 6.5. However, even if the Sparta overall temperature is not the temperature considered in the One-temperature model (see next sub-paragraph), the temperature in proximity of the capsule surface, which is

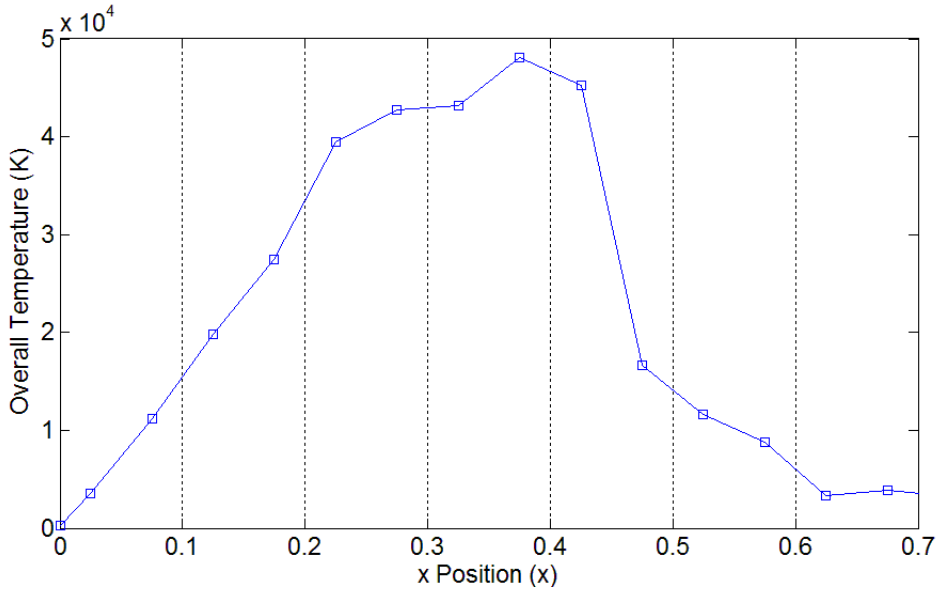

Figure 6.19: Overall Temperature Evaluated using to Sparta Simulation with Chemical Reactions

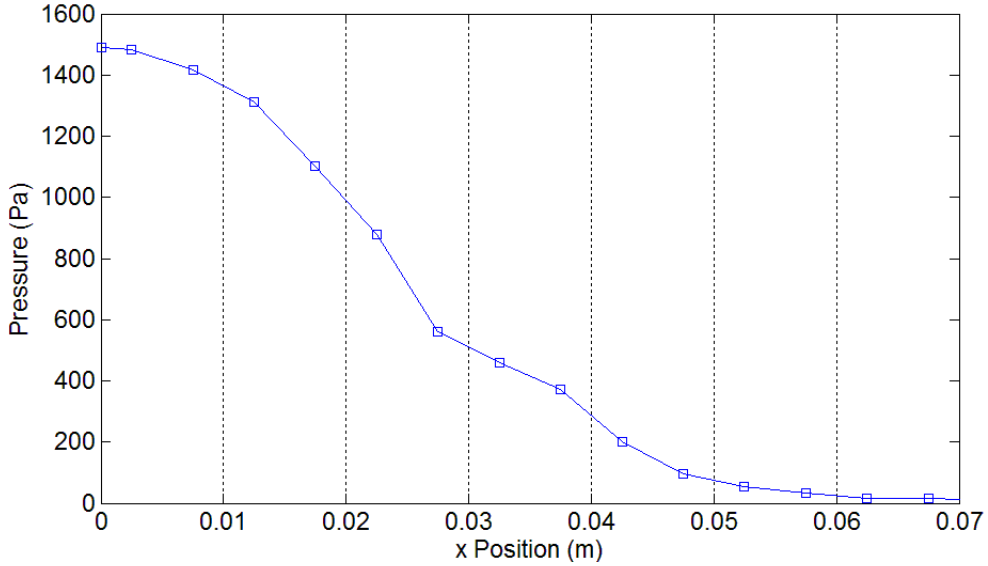

Figure 6.20: Pressure Evaluated using to Sparta Simulation with Chemical Reactions

Pressure (Pa)		1.569e3
Temperature (K)		3.495e3
Mass Fraction	N2	2.670e-1
	O2	1.000e-3
	N	4.899e-1
	O	2.066e-1
	NO	1.070e-2
	N2+	2.700e-3
	O2+	1.000e-3
	N+	1.060e-2
	O+	9.000e-3
	NO+	0.0015

Table 6.3: Pressure, Temperature and Mass Fraction just beyond Hayabusa's Surface used to Evaluate the Convective Heat Transfer Coefficient

the point taken into consideration, is similar for all kinds of temperatures, as visible from the temperature graphs. Therefore this kind of uncertainty will not produce any errors.

The convective transmission coefficient evaluated from CEA is the following:

$$k = 0.92022 \quad (6.7)$$

The resulting convective heat flux is the following:

$$\dot{q} = 5.751 MW/m^2 \quad (6.8)$$

Probably this result is not completely correct because of the surface temperature. In fact T_s is first set at a value of 300 K, the same value used in the simulation as a boundary condition. A temperature of 300 K is an expected temperature for the internal layer of a spacecraft, but not for the most external. The most external surface of a capsule is the thermal shield. This is built to reach a much higher temperature than 300 K. Its behavior is very complex, because of the large quantity of surface reactions which happen during the re-entry voyage, the variation in the composition of the material, its consumption, without calculating the modification in the gas composition due to the surface reaction. For this reason, it is difficult to have a precise external

temperature. In addition the correct convective heat flux should consider the change in the composition in the gas mixture in front of the capsule. In fact, what is usually done, is to take the results of the CFD simulation or DSMC in this case, and put them as the boundary condition of other software which are able to evaluate the heat transfer across the shield considering its chemical composition and the ablation of the material. This kind of evaluation will not be done for this study. Nevertheless, it is possible to estimate an external temperature of the capsule at re-entry into the Earth's atmosphere for the conditions considered here, of about 2000 K. From this data it is possible to evaluate a preliminary convective heat flux, more correct than the previous one.

The new convective heat flux evaluation is done launching a new simulation, identical to the previous one, where this initial condition is changed. The overall temperature results together with the previous ones are shown in Figure 6.21. As it is possible to see, the results evaluated are different with respect to the previous ones. In fact, the overall temperature for the simulation where the surface temperature is 2000 K (the blue one in Figure 6.21) is always higher than the other one in proximity of the capsule surface. The convective heat flux coefficient is estimated again using the new data regarding the temperature, but in this case the variation is irrelevant. With to this data it is possible to evaluate the new convective heat flux (6.9).

$$\dot{q} = 7.379 MW/m^2 \quad (6.9)$$

A comparison between the heat flux from the cases with (considering a surface temperature of 300 K (6.8)) and without reactions is made, to show the drastically decrease of the latter (6.10).

$$\dot{q'} = 4.543 MW/m^2 \quad (6.10)$$

The variation in the heat transfer is due to the different value of the overall temperature measured out of the capsule surface, in fact the convective transmission coefficient in maintained constant. The reason is that the simulation without reactions produces sensitive higher results in the values of temperature and in the shock layer thickness with respect to the one with reactions, as expected, because of the presence of endothermic reactions. This comparison between the two cases is shown from Figure 6.22 to 6.24. The quality of the graphs in the case without reactions is higher because a simulation with 10 particles per cell is used (II p S). This data can also be considered a reliability proof of the results produced by the Sparta simulations.

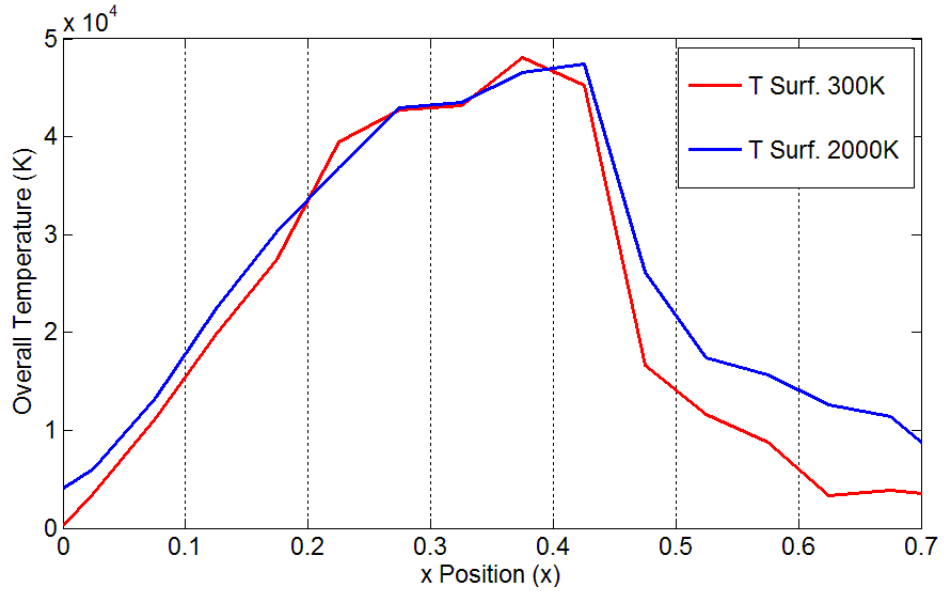

Figure 6.21: Overall Temperature in the Case of a Capsule Surface Temperature of 300K (TSurf. 300K) and 2000K (TSurf. 2000K)

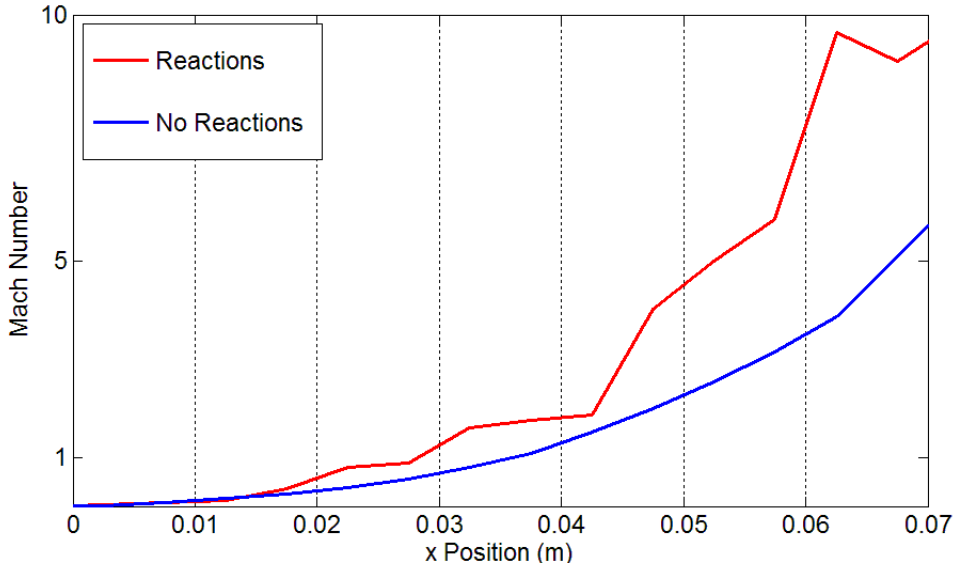

Figure 6.22 Comparison between Mach Number Deriving Sparta Simulations with and without Reactions

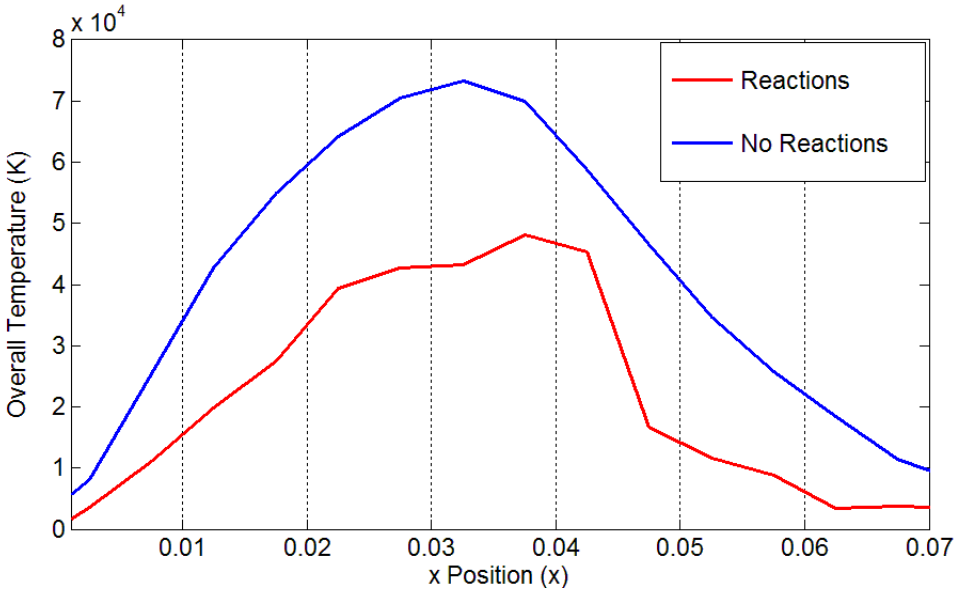

Figure 6.23 Comparison between Overall Temperature Deriving Sparta Simulations with and without Reactions

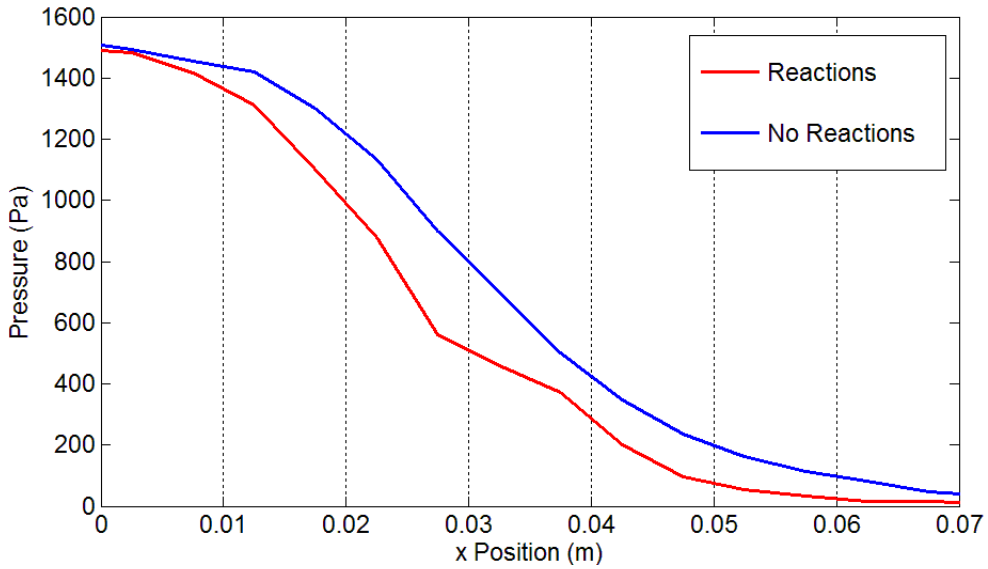

Figure 6.24 Comparison between Pressure Deriving Sparta Simulations with and without Reactions

Radiate Heat Flux

The high temperature gas encountered in the shock layer formed over an atmospheric entry vehicle is composed of a collection of molecules, atoms, and electrons. Each of these particles can possess thermal energy in a variety of forms: molecules, atoms and electrons can all have translational energy, molecules and atoms can possess electronic energy due to presence of bound electrons, and molecules can possess vibration and rotational energy due to the extra degrees of freedom.

A dramatic increase in thermodynamic energy is experienced by a set of atmospheric gases as it is processed by the bow-shock of an atmospheric entry spacecraft. Although this energy first manifests as an increase in translation motion of the atmospheric molecules, collision interactions between particles quickly give rise to a cascade of chemical kinetic processes. In Figure 6.25 a schematic representation of these processes occurring in the shock layer and near the surface of a re-entry capsule at the max heating conditions is shown. Two different regions of the flowfield are shown: (1) the shock layer, and (2) the ablation layer. The TPS material pyrolyses and the products form an ablation layer over the surface due to the strong heating environment experienced by the vehicle surface. This study does not want to deal with the material used in the thermal shield so will concentrate on the shock layer where the influence of the ablating surface is negligible.

Figure 6.26 illustrates the key chemical kinetic processes happening along the stagnation line of a vehicle with a non-ablating TPS re-entering the Earth's atmosphere. Most of the kinetic energy of the freestream particles (in the vehicle's frame of reference), across the strong shock formed over the vehicle, is rapidly converted into translational energy as they collide with the more dense shock layer gas. Inter-particle collisions then excite the rotational, vibrational and electronic modes of the molecules, and translational energy begins to relax. Rotational and translational energy modes, due to efficient energy transfer (in the order of tens of collisions), quickly equalize, while vibrational excitation is considerably slower (thousands of collisions). The molecules quickly build up large amounts of vibrational energy, until the internuclear bonds are overcome and dissociation occurs. Further collisional excitation among the pool of molecules and atoms excites the bound electrons to elevated states, and the gas radiates electromagnetic energy as the electrons spontaneously decay to less energetic states.

After many collisions have occurred, sufficiently far behind the shock, the plasma reaches a state of local thermodynamic equilibrium (LTE). If the 'equilibrium' gas emits more than the radiations absorbed, however, LTE is never completely reached and the decay of electronic states will continuously bleed off energy from the shock layer. Knowledge of the precise thermodynamic state of the plasma throughout this entire excitation and relaxation process is required for

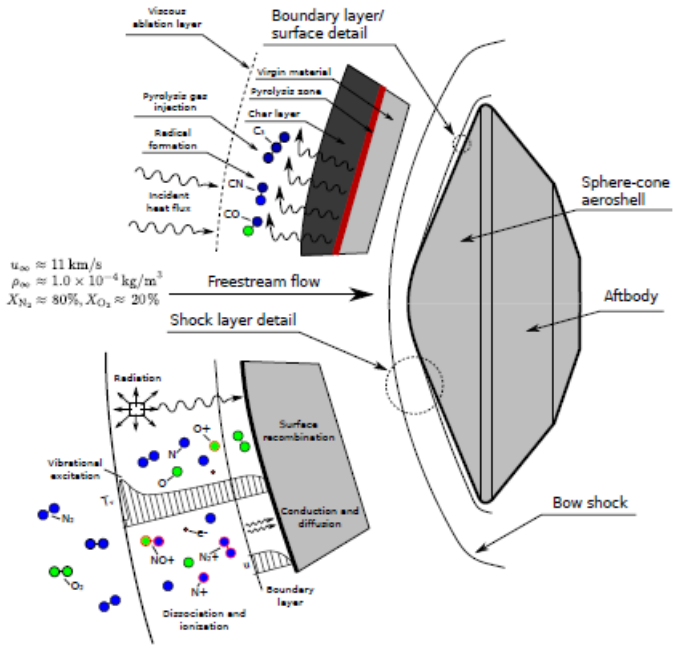

Figure 6.25: Aerothermodynamic Processes Occurring in the Shock Layer and on the Surface of a Re-entry Capsule at Peak Heating Conditions [80]

accurate radiative heat-flux calculations. The physical models which describe these processes, due to the complexity of them, have a large degree of uncertainty, so the radiative heat-flux incident on the vehicle surface is also highly uncertain.

The amount of energy contained in each of these thermal modes is dependent on the particle's quantum state. The most complete way to determine the energy of the plasma would be to solve for the wavefunction of all particles via the Schrödinger equation. Due to the enormous number of particles present, however, this approach is not feasible and some models must be considered.

Given sufficient collisions between particles, the plasma tends towards a situation where all energy modes are describable by equilibrium distributions at a single temperature. If also the chemical equilibrium is achieved, the complete thermodynamic state can be described as a function of p, T and the elemental composition. This is the One-temperature model and it is the one used for the evaluation of the convective heat flux.

However experiments performed [19] revealed that each of the internal energy modes appeared to be governed by separate equilibrium temperatures. The electronic and vibrational temperatures were found to exhibit diffusive excitation, rising to a peak then decaying to the equilibrium temperature, while the rotational temperature was found to be rapidly excited to the level expected for the translational temperature. As a consequence of these results Park was motivated

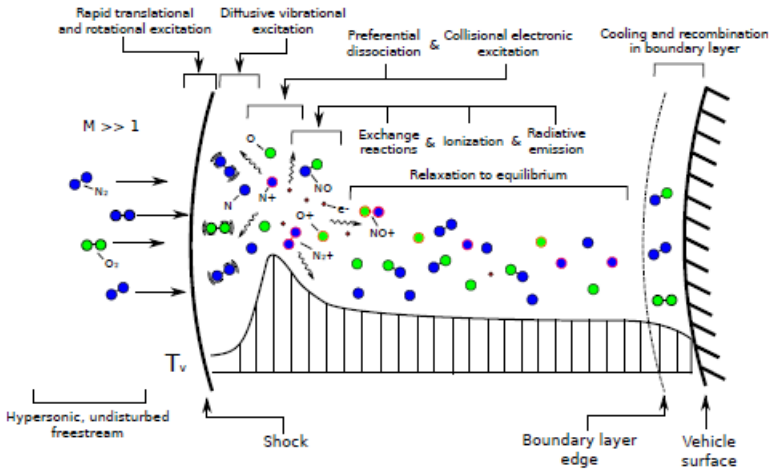

Figure 6.26: Chemical Kinetic Processes along the Stagnation Streamline for Earth Re-entry [81]

to formulate a new model, where heavy particle translation and rotation are described by one temperature (translation / rotation temperature), and vibration, electron and electronic excitation by another (vibration / electron / electronic temperature). This is the Two-temperature model. This model is used to evaluate the radiate heat flux in the bigger part of the software developed for this target and it is also the one implemented in the DSMC solver of OpenFOAM and apparently also Sparta. However, evaluation of the radiate heat flux is not what is going to be studied. For the moment the aim is just to provide all the useful data to do it, that is the translation / rotation and vibration / electron / electronic temperatures obtained from the Sparta simulation, which are shown in Figure 6.27 and 6.28. In Figure 6.27 the overall temperature is shown, but, as said after the comparison with the OpenFOAM data, it seems to be the translation / rotation temperature. More details will be supplied in the next Paragraph 6.5 regarding this matter.

6.5 Experimental Data Comparison

The final validation of the program for high re-entry studies is completed by the comparison with experimental data collected by the Hayabusa capsule during its re-entry at the point studied, H3.

The data collected by Hayabusa are the spectrum of the radiate heat flux. This kind of data, as presented in the previous Paragraph 6.4, are derivable from translation / rotation and the

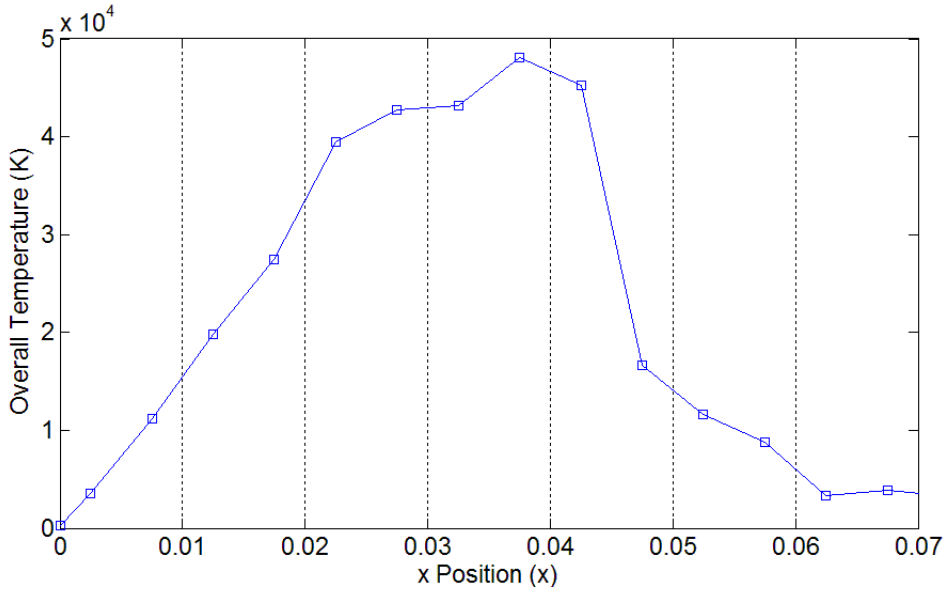

Figure 6.27: Overall Temperature Curve Evaluated using to Sparta Simulation with Chemical Reactions

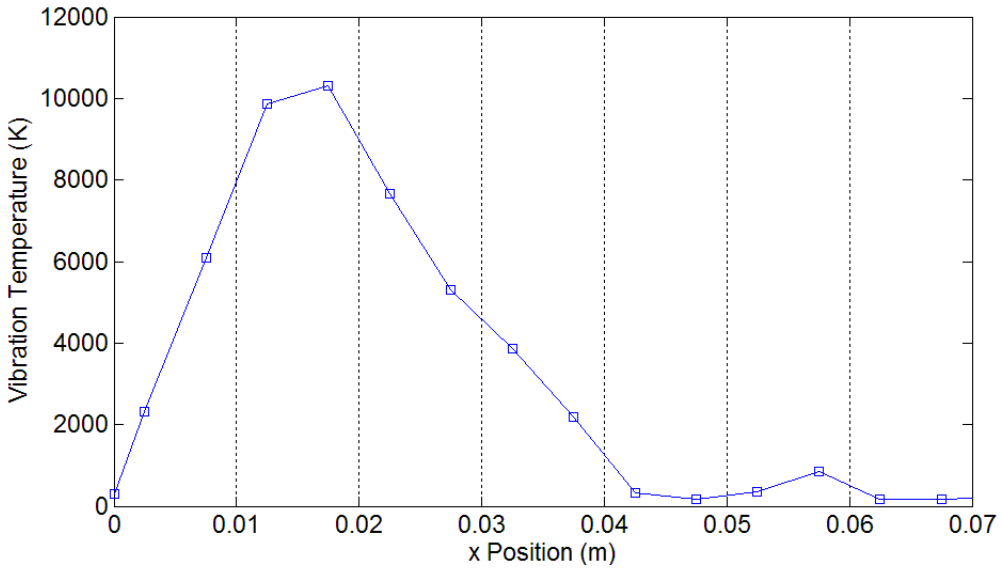

Figure 6.28: Vibration Temperature Curve Evaluated using to Sparta Simulation with Chemical Reactions

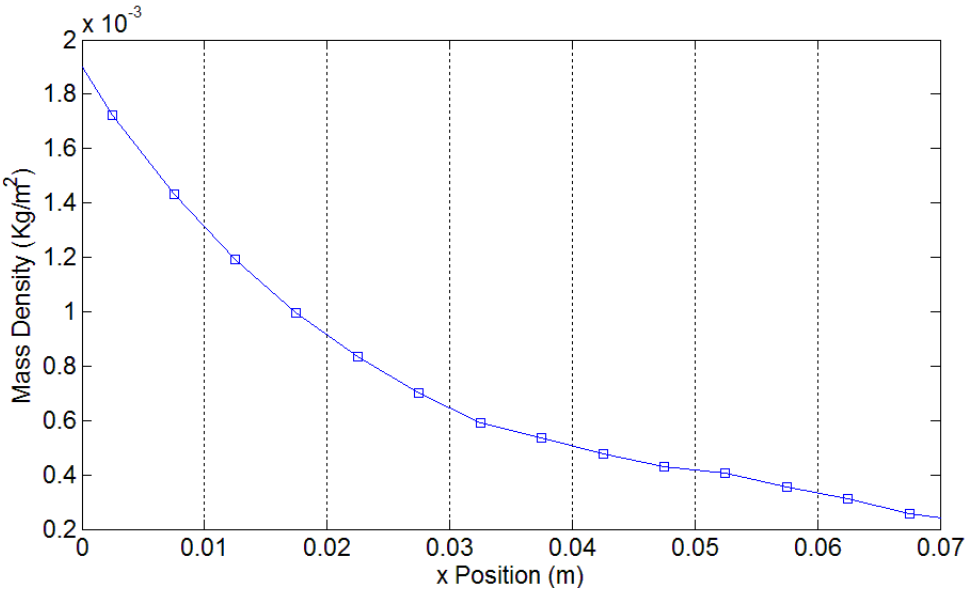

Figure 6.29: Mass Density Approaching Hayabusa's Surface

vibration / electron / electronic temperatures, pressure and mass fraction solving the relative wave equations.

The derivation of the radiate heat flux will be the next step of this research, so will not be dealt with here. However it is possible to find another source of comparison in a simulation done with a CFD software which performs simulations using Navier-Stockes equations, Eilmer3. In fact the case analyzed is in a limbo between the continuum regime and the free molecular regime. In particular H3 is in the regime called slip regime, where the fluid is slightly rarefied. Anyway when the fluid arrives in the zones near the capsule, it starts to become more and more dense because of the obstacle represented by the capsule which stops the motion of the particles and makes them concentrate there. In fact the density grows approaching the surface as shown in Figure 6.29. In addition the mean free path varies in the zones near the surface. Instead Figure 6.30 shows the Knudeus number found using as a characteristic length of the problem, the radius of the circular part of the Hayabusa capsule, which is about 0.18 m. If Figure 2.1 is considered, which shows the various flow regimes according to the Knudeus number, it is possible to see that in the proximity of the surface the problem belongs completely to the Continuum regime. Therefore the Eilmer3 software, which uses the Navier-Stockes equations, works in a proper regime.

However care must be taken in using the Navier-Stockes equations in such rarefied conditions, and should always be checked to verify if they are appropriate or not. As it is possible to see from Figure 6.30 there is only a small zone where Navier-Stockes equations can be successfully

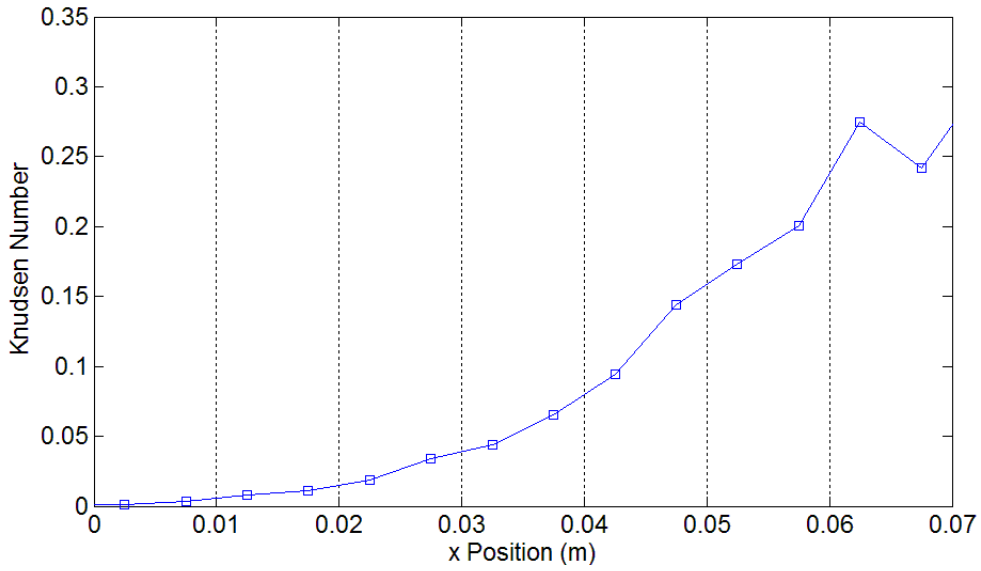

Figure 6.30: Knudsen Number Approaching Hayabusa's Surface

apply with certainty. In fact the free stream field is in a transition regime, so good results are not always guarantee and the back side of the capsule is an extremely rarefied zone, as a consequence of the higher density in the front, where valid results of the Navier-Stockes equations are never possible. Besides, the mean free path increases rapidly considering the wide range of altitude taken into consideration. For example, from the altitude of point H3, which is about 79 Km, to 89 km, so 10 km more, the mean free path increases by one order of magnitude. If the same capsule is considered, this means that it is out with a regime where the Navier-Stockes equation can still work. However the variation of the regime can happen also at the altitude considered if the body studied is sufficiently smaller than the Hayabusa capsule.

Eilmer3 gives reliable results, in fact it is already widely used and tested in fluid dynamic simulations. The geometry used in this simulation is the same one used in the DSMC, but the domain considered is smaller with respect to the latter. This is because a CFD simulation which uses Navier-Stockes equations needs a very refined mesh, in particular approaching the surface, so a big domain drastically increases the computational resources used. Nevertheless, as said before, the Navier-Stockes equations are able to describe correctly the phenomena only in the proximity of the surface where the Knudeus number is sufficiently low.

The data evaluated with the Eilmer3 are the Mach Number, pressure, vibration temperature and translation temperature.

From Figure 6.31 to 6.34 the comparison between the data of the two software is shown.

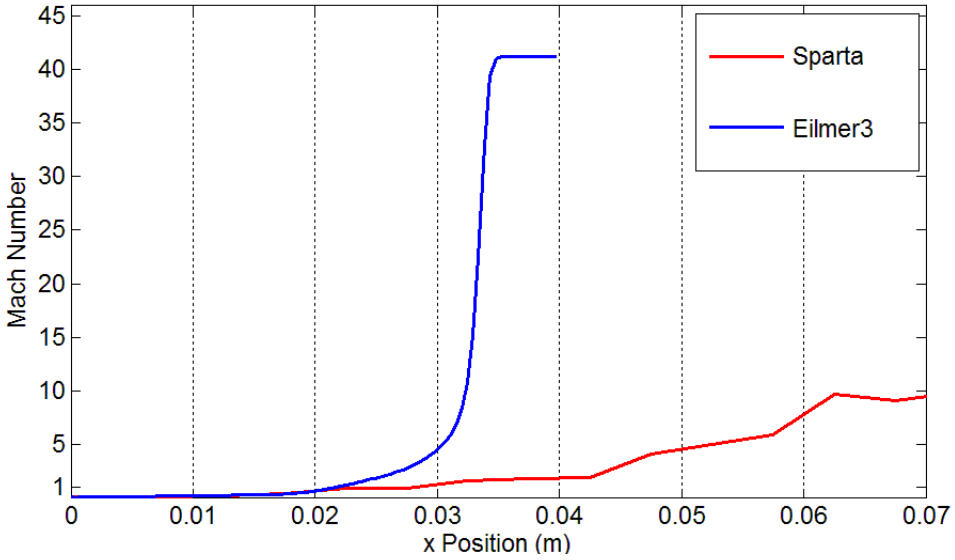

Figure 6.31: Mach Number Comparison between Sparta and Eilmer3 Simulation

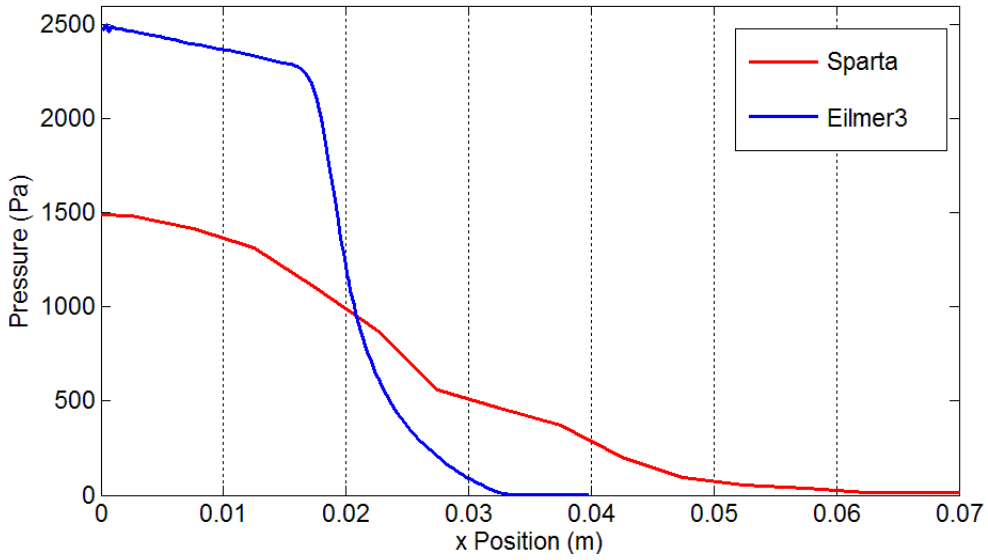

Figure 6.32: Pressure Comparison between Sparta and Eilmer3 Simulation

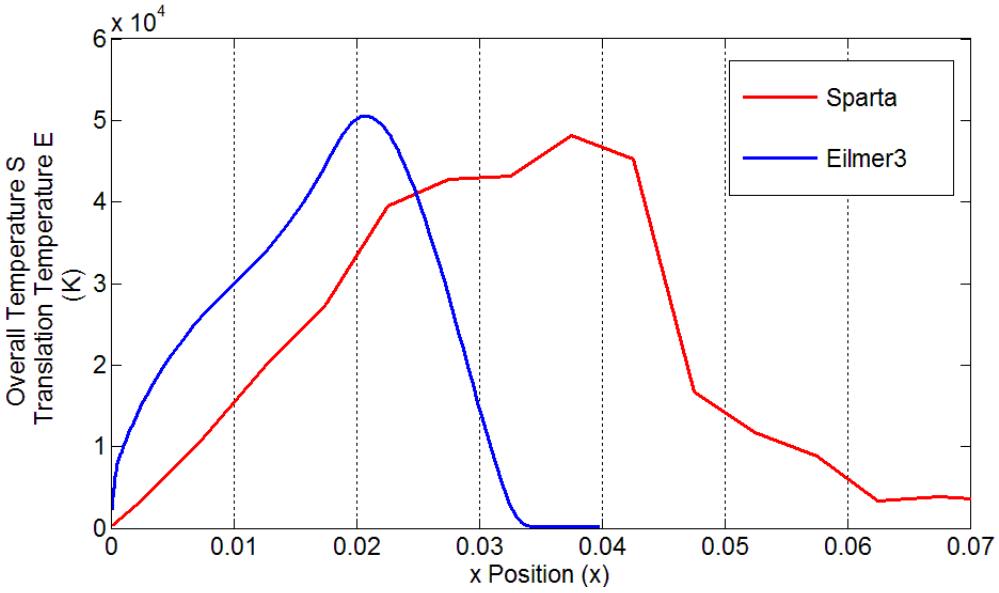

Figure 6.33: Comparison between Sparta Overall Temperature and Eilmer3 Translation Temperature

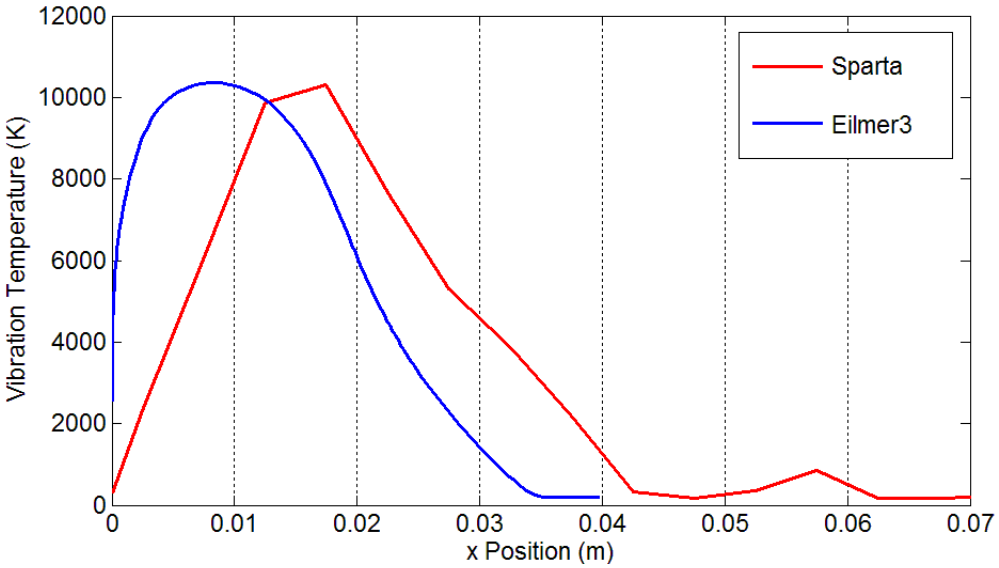

Figure 6.34: Vibration Temperature Comparison between Sparta and Eilmer3 Simulation

It is possible to observe that the Sparta curves are very similar to the Eilmer3 ones in their shapes, even if they are less refined. However it is important to remember that here the simulations are run with a number of particles per cell equal to one, which is not the best number discovered in the sensitivity analysis, but it is the best achieved with the resources available in the laboratory. Anyway more details regarding this problem, as said, will be provided in Appendix 1.

It is possible to notice that the portion of the DSMC temperature slopes with a negative gradient are always farther from the surface with respect to the Eilmer3 ones. Also the part of the pressure slopes where the higher gradient is present, which indicates the discontinuity created by the shock layer, ends in a position further from the surface with respect to the one of the Eilmer3 pressure. This means the shock in the Sparta simulations is wider with respect to the Eilmer3 one and this difference is of about 2 cm. It is not possible to give more accurate results in the depth of the shock layer because the quality of the DSMC curves do not allow for this. The difference in the width of the shock layer is probably due to some incorrect results obtained from the software Sparta because the best simulation setting is not used. Nevertheless the difference can be also caused by Eilmer3 and in particular by its mesh. In fact the results from a CFD simulation are very dependent on the quality of the mesh. In particular they cannot describe correctly the strong variations in the physical parameters present in the shock layer if a very refined mesh is not present there. Therefore a CFD mesh must be built recursively, trying, each time, to refine more the zone where the gradient of the thermodynamic parameters are stronger, according to the results from the previous simulation. This iteration work is not done in the present study for reasons of time, but it could curtail the distance between the width of the shock layer obtained from the two simulations.

However the absolute value of the temperatures considered are very close in the Sparta and Eilmer3 simulations. Instead the Sparta pressure values are lower with respect to the Eilmer3 ones, but such a difference was also found with respect to the OpenFOAM one. In fact it has already been said that Sparta does not produce reliable pressure results, in their absolute values. Instead the shape seems to be correct. Moreover the final values of the pressure seem to be equivalent with and without reactions, as can be seen from the figures in the previous chapters and confirmed by the comparison made between the pressure with and without reactions in Paragraph 6.4. Consequently it is also possible to make a comparison between the OpenFOAM and Eilmer3 pressure which is shown in Figure 6.35. Here it is possible to see that the two pressure curves are similar in the final values even if the shock layer is wider according to the OpenFOAM graph. This confirms that the results produced by OpenFOAM are reliable.

Finally, with another source of comparison it is possible to clarify the question about Sparta temperature. In fact there is no doubt that Eilmer3 and OpenFOAM use the Two-temperature model (in the OpenFOAM case also the One-temperature model is implemented, in fact it is

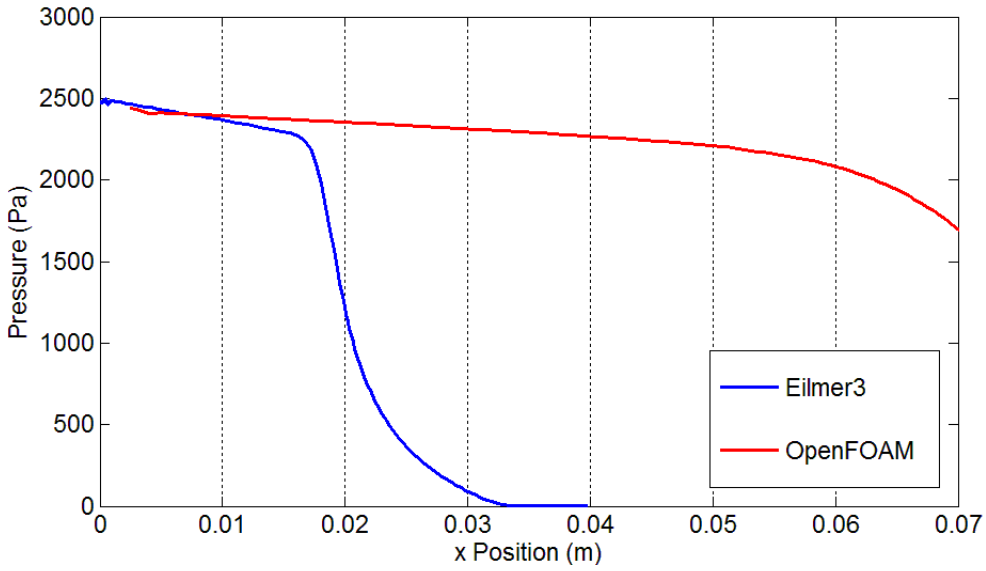

Figure 6.35 Pressure Comparison between Eilmer3 and OpenFOAM without Reactions Simulation

possible to extract an overall temperature) as specified in the documentation, and that translation temperature is the translation / rotational temperature and vibration and internal are the vibration / electron / electronic temperature respectively in Eilmer3 and OpenFOAM. In Sparta the Two-temperature model is used too, in fact it is possible to extract two temperatures from the simulation. Analyzing the comparison with respect to OpenFOAM, it seems that the Sparta overall temperature does not have the same physical meaning as the OpenFOAM one and seems to match more with the OpenFOAM translation temperature. Instead the Sparta vibration temperature seems to be the vibration / electron / electronic temperature. Comparing the Eilmer3 temperatures with the Sparta ones the hypothesis is confirmed, as it is possible to see from the Figure 6.31. Therefore in Sparta, referring to the Two-temperature model, what is called overall temperature is the translation / rotational temperature and what is called vibration temperature is the vibration / electron / electronic temperature. This use of the Sparta overall temperature in the previous paragraph, as the temperature of One-temperature model, is justified by the similarity between the overall temperature in the One-temperature model and the translation / rotational in the Two-temperature model. In particular this is true for the temperature in proximity of the capsule surface, as it is possible to see from the OpenFOAM data in Paragraph 6.2, where all the types of temperatures considered are present. In fact the data used in the evaluation of the convective heat flux are the values of the temperature just beyond the capsule layer.

7 Conclusions

The aim of studying and finding the best setting of both the OpenFOAM and Sparta DSMC solver, is achieved and shown in the relative chapters. Now the software are more easily accessible for the Interdisciplinary Aerodynamic Group and for anyone interested in using them.

Validation and verification studies of the new DSMC codes have been undertaken for both inert and chemically-reacting (the latter only for Sparta, because in OpenFOAM a chemistry model is not yet implemented in the *dsmcFoam* solver), hypersonic rarefied flows. They have been assessed against other numerical and analytical solutions for equilibrium conditions. The results for inert flows showed close agreement for temperatures and pressure with analytical counterparts. However, for Sparta pressure values, further studies were found to be necessary in order to correctly match with the OpenFOAM and analytical results.

In the comparison of the two software analyzed, Sparta reveals some limits in the solidity of the code and some uncertainty in the results. Moreover it used a less optimized post-processing system with respect to the OpenFOAM one. On the other hand it is the only one, between the two considered, to have implemented a chemistry reaction model, so it is the only one useful in a entry atmosphere study.

The Sparta simulations with chemically-reacting flows demonstrated excellent agreement compared with the results from an alternative code, Eilmer3, except for the translation of the slopes obtained farther from the capsule surface with respect to the term of comparison. This is probably due to the set up used in Sparta, which is not the best because of computational memory problems.

The inclusion of chemical reactions in the *dsmcFoam* calculations resulted in an alteration of the flow structure with a reduced shock stand-off distance, a significant reduction in the overall temperature in the shock layer, and a substantial decrease in the predicted convective heat flux to the vehicle surface when compared with the inert gas case, as expected, because of the activation of endothermic dissociation reactions.

Finally the results presented in this thesis clearly show a new tool of investigation in the field of fluid-dynamics is available and reliable, that is the direct simulation Monte Carlo method. It provides an alternative to the classic CFD in the analysis of slightly rarefied fluids, with extremely low resources consumption, but at the same time producing acceptable results. In fact, even if the computational resources used for a single DSMC can be comparable to the ones of CFD, the mesh creation is simpler with respect to the latter and an iteration in the simulations to model the mesh zones with higher thermodynamic gradients is not necessary. In addition, the DSMC is the best method to provide results in the high rarefied flow.

7.1 Future Work

The last step to officially validate the DSMC solver is the comparison with the experimental data. Considering that the data collected by the Hayabusa capsule at the point analyzed are radiative spectra, a further study is necessary to extract them from the data obtained from the DSMC. This is possible only for the software Sparta for the moment.

Moreover, the OpenFOAM team of developers, application specialists, trainers and testers are implementing the chemistry model for the *dsmcFoam* solver, which will be available in a short time after the publication of this thesis. Considering this, running a DSMC with chemical reactions will be possible also for the software OpenFOAM. As a consequence of this, the validation process can be performed also for the OpenFOAM DSMC solver and a complete comparison between the two software considered can be made.

The future work proposed by the author to complete the work consists of the following steps:

- Extraction of the radiate spectra starting from the data obtained from the Sparta simulation which are all that is necessary to undertake this study.
- Final validation of the Sparta DSMC solver with the comparison of the radiate spectra derived from the Sparta results with the one measured by the Hayabusa.

- Performing the simulation considered in this study and extracting the same results using OpenFOAM with the chemistry model implemented.
- Repeating the first two steps using the results derived from the step 3, to validate the OpenFOAM DSMC solver.

In the near future the research contained in this thesis could be the catalyst for further investigations starting from numerical trials of the methodology shown. The most useful for the re-entry analysis is the following. It consists in the implementation, inside the DSMC solver, of surface chemistry analysis, outgassing and surface ablation from which the direct evaluation of convective and radiate heating is possible. Another possible way to obtain the same result is to couple already existing software, used to simulate surface chemistry, outgassing and ablation with Sparta or OpenFOAM DSMC solver which provide them all with the necessary starting data for the work.

References

[1] G.A. Bird. Molecular gas dynamics and the direct simulation of gas flows, 1994.

[2] S. Chapman and T.G. Cowling. The mathematical theory of non-uniform gases: an Account of the kinetic theory of viscosity, thermal conduction and diffusion in gases, 1991.

[3] I. D. Boyd, G. Chen, and G. V. Candler. Predicting failure of the continuum fluid equations in transitional hypersonic flows. Physics of Fluids, 1995.

[4] W. Wang and I. D. Boyd. Predicting continuum breakdown in hypersonic viscous ows. Physics of Fluids, 2003.

[5] D. Burnett. The distribution of velocities in a slightly non-uniform gas. In Proceedings of the London Mathematical Society, volume 39, 1935.

[6] D. Burnett. The distribution of molecular velocities and the mean motion in a non-uniform gas. In Proceedings of the London Mathematical Society, volume 40, 1936.

[7] C. H. Campbell, B. Anderson, G. Bourland, S. Bouslog, A. Cassady, T. J. Horvath, S. A. Berry, P. A. Gnoffo, W. A. Wood, J. J. Reuther, D. M. Driver, D. C. Chao, and J. Hyatt. Orbiter return to flight entry aeroheating. 9th AIAA/ASME Joint Thermophysics and Heat Transfer Conference, number AIAA Paper 2006-2917, 2006.

[8] X. Zhong, R. W. MacCormack, and D. R. Chapman. Stabilization of the Burnett equations and application to hypersonic flows. AIAA Journal, 1993.

[9] K. A. Comeaux, D. R. Chapman, and R. W. MacCormack. An analysis of the Burnett equations based on the second law of thermodynamics. 33rd Aerospace Science Meeting and Exhibit, volume AIAA 95-0415, 1995.

[10] H. K. Cheng and G. Emanuel. Perspective on hypersonic nonequilibrium flow. AIAA Journal, 1995.

[11] Ojas Joshi. Fluid-structure thermal coupling and ablation effects in atmospheric entry. PhD thesis. École polytechnique fédérale de Lausanne. Lausanne, 2014.

[12] Rodrigo Cassineli Palharini. Atmospheric Reentry Modelling Using an Open-Source DSMC Code. PhD thesis, University of Strathclyde. Strathclyde, 2014.

[13] R. K. Agarwal and K. Yun. Burnett equations for simulation of transitional flows. Applied Mechanics Reviews, 2002.

[14] C. Cercignani. Rarefied gas dynamics: from basic concepts to actual calculations, 2000.

[15] D. C. Rapaport. The Art of Molecular Dynamics Simulation, 2014.

[16] D. Frenkel and B. Smit. Understanding Molecular Simulation, 2002.

[17] G. A. Bird. Molecular gas dynamics, 1976.

[18] A. Roshko. Some measurements of flow in a rectangular cutout. Technical Report NACA, 1955.

[19] J. L. Shideler, G. L. Webb, and C. M. Pittman. Verification tests of durable thermal protection system concepts. Journal of Spacecraft and Rockets, 1985.

[20] M. H. Bertran and Wiggs. M. M. Effect of surface distortions on the heat transfer to a wing at hypersonic speeds. AIAA Journal, 1963.

[21] M. A. Pulsonetti and W. A. Wood. Computational aerothermodynamic assessment of space shuttle orbiter tile damage - open cavities. 38th AIAA Thermophysics Conference, 2005.

[22] F. J. Alexander, A. L. Garcia, and B. J. Alder. Cell size dependence of transport coefficients in stochastic particle algorithms. Physics of Fluids, 1998.

[23] Sparta website. URL *http://www.sparta.sandia.gov/*.

[24] JAXA website. URL *http://www.isas.jaxa.jp/*.

[25] F. J. Alexander, A. L. Garcia, and B. J. Alder. Erratum: Cell size dependence of transport coefficients in stochastic particle algorithms. Physics of Fluids, 2000.

[26] G. A. Bird. Direct simulation of highvorticity gas flows. Physics of Fluids, 1987.

[27] A. G. Garcia and W. A. Wagner. Time step truncation error in direct simulation Monte Carlo. Physics of Fluids, 2000.

[28] N. G. Hadjiconstantinou. Analysis of discretization in the direct simulation Monte Carlo. Physics of Fluids, 2000.

[29] K. A. Koura. Null-collision tecnique in the direct-simulationMonte Carlo method. Physics of Fluids, 1986.

[30] K. A. Koura. Improved null-collision technique in the direct simulation Monte Carlo method: application to vibrational relaxation of nitrogen. Computer and Mathematics with Applications, 1998.

[31] G. A. Bird. Perception of numerical methods in rarefied gasdynamic. Progress in Astro- nautics and Aeronautics, 1989.

[32] T. Abe. Generalized scheme of the no-time-counter scheme for the DSMC in rarefied gas flow analysis. Computer and Fluids, 1993.

[33] J.C. Maxwell. On stresses on rarefied gases arising from inequalities of temperature. Philosophical Transactions of the Royal Society of London, 1879.

[34] R. M. Logan and R. E. Stickney. Simple classical model for the scattering of gas atoms from a solid surface. Journal fo Chemical Physics, 1966.

[35] Nasa website. URL *http://www.nasa.gov/*.

[36] ANSYS website. URL *http://www.ansys.com/*.

[37] J. J. Hinchen and W. M. Foley. Scattering of molecular beams by metallic surfaces. 5th International Symposium on Rarefied Gas Dynamics, 1966.

[38] C. Cercignani and M. Lampis. Kinetic models for gas-surface interactions. Transport Theory and Statistical Physics, 1971.

[39] C. Cercignani and A. Frezzotti. Numerical simulations of supersonic rarefied gas glows past a flat plate: effects of the gas-surface interaction model on the flowfield. Progress in Aeronautics and Astronautics, 1989.

[40] R. G. Lord. Application of the cercignani-lampis scattering kernel to the direct simulation Monte C calculations. 17th International Symposium on Rarefied Gas Dynamics, 1990.

[41] R. G. Lord. Some extensions of the cercignani-lampis gas-surface interaction model. Physics of Fluids A: Fluid Dynamics, 1991.

[42] R. G. Lord. Some further extensions of the cercignani-lampis gas-surface interaction model. Physics of Fluids, 1995.

[43] G. A. Bird. Monte-Carlo simulation in an engineering context. 12th International Symposium on Rarefied Gas Dynamics, 1981.

[44] K. Koura and H. Matsumoto. Variable soft sphere molecular model for inversepowerlaw or Lennard Jones potential. Physics of Fluids, 1991.

[45] K. Koura and H. Matsumoto. Variable soft sphere molecular model for air species. Physics of Fluids, 1992.

[46] H. A. Hassan and D. B. Hash. A generalized hardsphere model for monte carlo simulation. Physics of Fluids, 1993.

[47] ANSYS. ANSYS Mechanical User's Guide, 2013.

[48] D. B. Hash, H. A. Hassan, and J. N. Moss. Direct simulation of diatomic gases using the generalized hard sphere model. Journal of Thermophysics and Heat Transfer, 1994.

[49] J. A. Kunc, D. B. Hash, and H. A. Hassan. The GHS interaction model for strong attractive potentials. Physics of Fluids, 1995.

[50] D. Baganoff and J. McDonald. A collision selection rule for a particle simulation method suited to vector computers. Physics of Fluids A: Fluid Dynamics, 1990.

[51] C. Borgnakke and P. S. Larsen. Statistical collision model for Monte Carlo simulation of polyatomic gas mixture. Journal of Computational Physics, 1975.

[52] I. D. Boyd. Analysis of rotational nonequilibrium in standing shock waves of nitrogen. AIAA Journal, 1990.

[53] I. D. Boyd. Rotational and vibrational nonequilibrium effects in rarefied hypersonic flow. Journal of Thermophysics and Heat Transfer, 1990.

[54] F. E. Lumpkin III, B. L. Haas, and I. D. Boyd. Resolution of differences between collision number definitions in particle and continuum simulations. Physics of Fluids A: Fluid Dynamics, 1991.

[55] B. L. Haas, J. D. McDonald, and L. Dagum. Models of thermal relaxation mechanics for particle simulations. Journal of Computational Physics, 1993.

[56] F. Bergmann and I. D. Boyd. New discrete vibrational energy model for the direct simulation Monte Carlo method. Progress in Aerospace Science, 1994.

[57] G. A. Bird. A comparison of collision energy-based and temperature-based procedures in DSMC. 26th International Symposium on Rarified Gas Dynamics, volume 1084, 2008.

[58] Iain D. Boyd. Direct Simulation Monte Carlo for Atmospheric Entry 2. Code Development and Application Results. 2009

[59] Scanlon, White, Craig, Borg, Palharini. Open source Direct Simulation Monte Carlo (DSMC) Chemistry Modelling for Hypersonic Flows. AIAA Journal, 53. 2014

[60] C. Rebick and R. D. Levine. Collision induced dissociation: A statistical theory. Journal of Chemical Physics, 1973.

[61] K. A. Koura. A set of model cross sections for the Monte Carlo simulation of rarefied real gases: atom-diatom collisions. Physics of Fluids, 1994.

[62] I. D. Boyd. A threshold line dissociation model for the direct simulation Monte Carlo method. Physics of Fluids, 1996.

[63] M. A. Gallis. Maximum entropy analysis of chemical reaction energy dependence. Journal of Thermophysics and Heat Transfer, 1996.

[64] G. A. Bird. Simulation of multi-dimensional and chemically reacting flows (past space shuttle orbiter). 11th International Symposium on Rarefied Gas Dynamics, 1979.

[65] I. D. Boyd. Assessment of chemical nonequilibrium in rarefied hypersonic flow. 28th Aerospace Sciences Meeting, number AIAA Paper 90-0145, 1990.

[66] T.J. Scanlon, E. Roohi, C. White, M. Darbandi and J. M. Reese. An Open Source, Parallel DSMC Code for Rarefied Gas Flows in Arbitrary Geometries.

[67] I. D. Boyd. Analysis of vibrational-dissociation-recombination processes behind strong shock waves of nitrogen. Physics of Fluids A: Fluid Dynamics, 1992.

[68] B. L. Hass and I. D. Boyd. Models for direct Monte Carlo simulation of coupled vibrational-dissociation. Physics of Fluids A: Fluid Dynamics, 1993.

[69] M. A. Gallis, R. B. Bond, and J.R. Torczynski. A kinetic-theory approach for computing chemical-reaction rates in upper-atmosphere hypersonic flows. Journal of Chemical Physics, 2009.

[70] G. A. Bird. Chemical reactions in DSMC. 27th Symposium on Rarefied Gas Dynamics. 2010.

[71] G. A. Bird. The quantum-kinetic chemistry model. 27th International Symposium on Rarefied Gas Dynamics. 2010.

[72] G. A Bird. The Q-K model for gas phase chemical reaction rates. Physics of Fluids, 2011.

[73] I. Wysong, S. Gimelshein, N. Gimelshein, W. McKeon, and F. Esposito. Reaction cross sections for two direct simulation Monte Carlo models: accuracy and sensitivity analysis. Physics of Fluids, 2012.

[74] T. J. Scanlon, E. Roohi, C. White, M. Darbandi, and J. M. Reese. An open source, parallel, DSMC code for rarefied gas flows in arbitrary geometries. Computer and Fluids, 2010.

[75] OpenFOAM website. URL *http://www.openfoam.com/*.

[76] M. A. Rieffel. A method for estimating the computational resquirement of DSMC simulations. Journal of Computational Physics, 1999.

[77] NOAA/NASA/USAF. U. S. Standard atmosphere. U.S. Government Printing Office, 1976.

[78] T. Rivell. Notes on earth atmospheric entry for mars sample return missions, NASA, 2006.

[79] Automated Data Collection Methods website. URL *http://www.ntl.bts.gov/DOCS/ch5.html.*

[80] D. F. Potter. Modelling of radiating shock layers for atmospheric entry at Earth and Mars. Phd thesis, University of Queensland, Brisbane. Australia, 2010.

[81] R. Savajano, D. F. Potter, O. Joshi, and P. Leyland. Radiation Analysis for Two Trajectory Points of the Fire II Entry. International Journal of Aerospace Engineering Vol. 2012. Article ID 597930, 2012.

[82] Università degli Studi di Napoli Federico II, Tommaso Astarita. Flu_7_ONDE D'URTO. URL *http://www.unina.it/.*

Appendix 1

In this appendix some answers are tried to give regarding the problem encountered during the performance of a restricted number of simulations, as anticipated in previous chapters.

In particular only Sparta shows difficulties to perform some kind of simulations because of the apparent lack of computational resources, instead all the OpenFOAM simulations work correctly. As presented in Chapter 5, only varying the number of particles per cell some problems were encountered.

In the set of simulation without reactions, the failure happens starting with a number of particles per cell equal to 50. Instead, in simulations with chemical reactions the problem arose already with 10 particles per cell. The decrease of the number of particles per cell, starting from which the simulation crashed passing from simulations without reactions to with, can be expected considering that the chemical reactions increase the RAM use. However the use of memory was drastically increased for the simulation with 10 particles per cell with chemical reactions with respect to the one in simulation without reactions. The latter with 256 Gb of RAM works successfully, the one with reactions cannot work with a 4 Tb RAM use. It seems that the use of chemical reactions makes the computational memory request increasing exponentially.

In the try of discovering the RAM needed for each particles to have an estimation of the amount of memory necessary to run a simulation with chemical reactions and a number of 10 particles per cell, many tests are made using the laboratory laptop. In these tests the simulation with 10 particles per cell and chemical reactions included is discovered being able to run, differently to what happened in the cluster Bellatrix where it crashed before inserting particles in the domain. Clearly the laboratory laptop can encounter some damages in carrying out such a

whole simulation because the computational resources request are too high. On the other hand this is a poof of the fact that the incapability of running certain simulations is not for the lack of the computational resources, but must be find in some others fields.

The hypothesis made is that the programming language used in writing the software encounters some problems when it has to subdivide the domain and launch the calculation in a cluster like Bellatrix. However this hypothesis cannot explain the reason of why some others simulations performed on Bellatrix and where the domain is equally subdivided can work.

Eventually it is possible to conclude that the problem is more complex than expected and a more deep analysis also regarding the informatics point of view is necessary to give some more certain answers.

Appendix 2

In this appendix the results of the OpenFOAM two-dimensional simulation without reactions for different end time are reported, starting from 0.001 s to 0.005 s. The same results obtained with OpenFOAM three-dimensional simulation using the end time chosen in Paragraph 5.1.5 are reported.

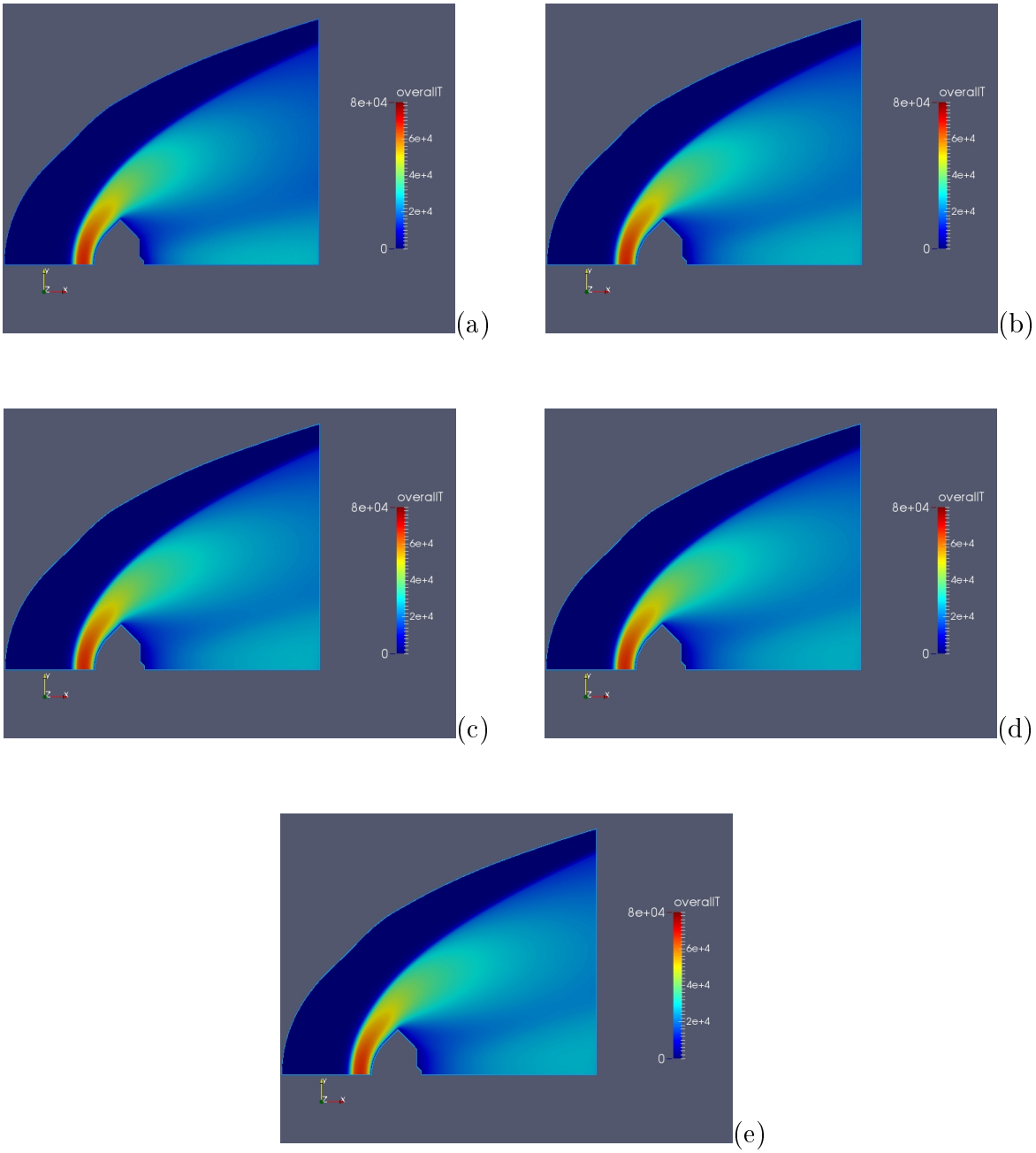

Figure A.1 Overall Temperature Deriving from OpenFOAM Two-Dimensional Simulations without Reactions Starting from an End Time of 0.001 s (a) to 0.005 s (e)

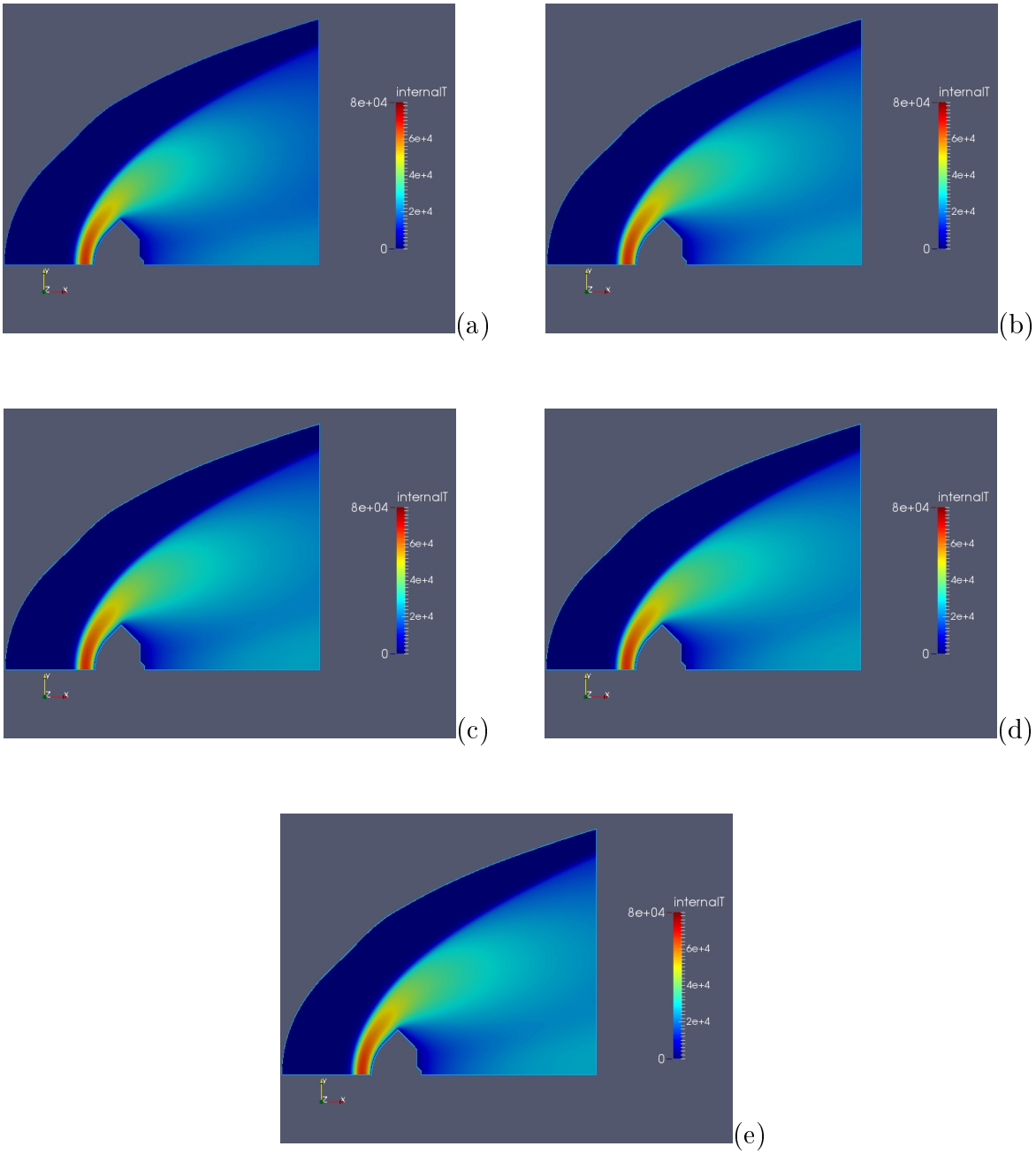

Figure A.2 Vibration / Electron / Electronic Temperature Deriving from OpenFOAM Two-Dimensional Simulations without Reactions Starting from an End Time of 0.001 s (a) to 0.005 s (e)

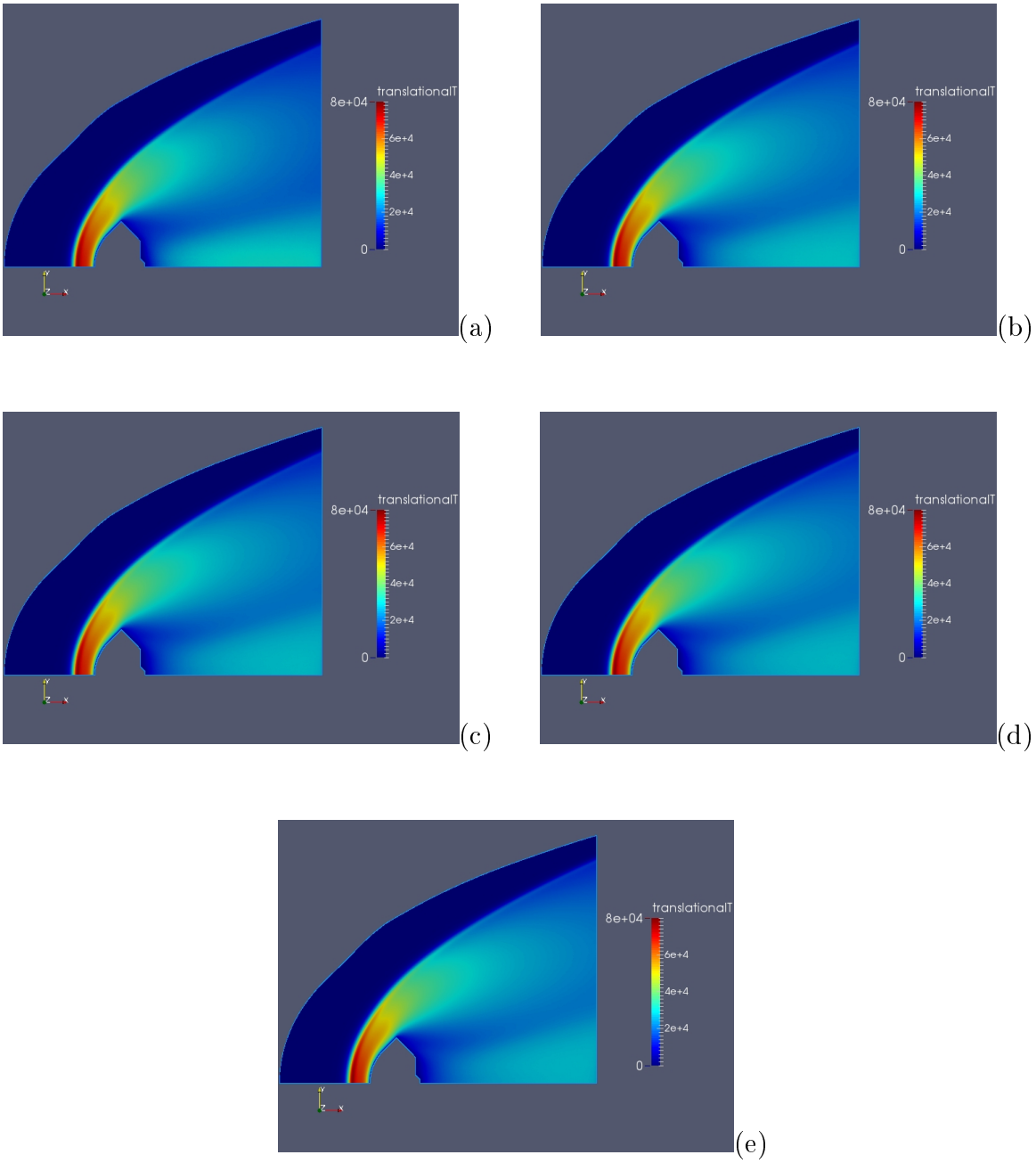

Figure A.3 Translation / Rotational Temperature Deriving from OpenFOAM Two-Dimensional Simulations without Reactions Starting from an End Time of 0.001 s (a) to 0.005 s (e)

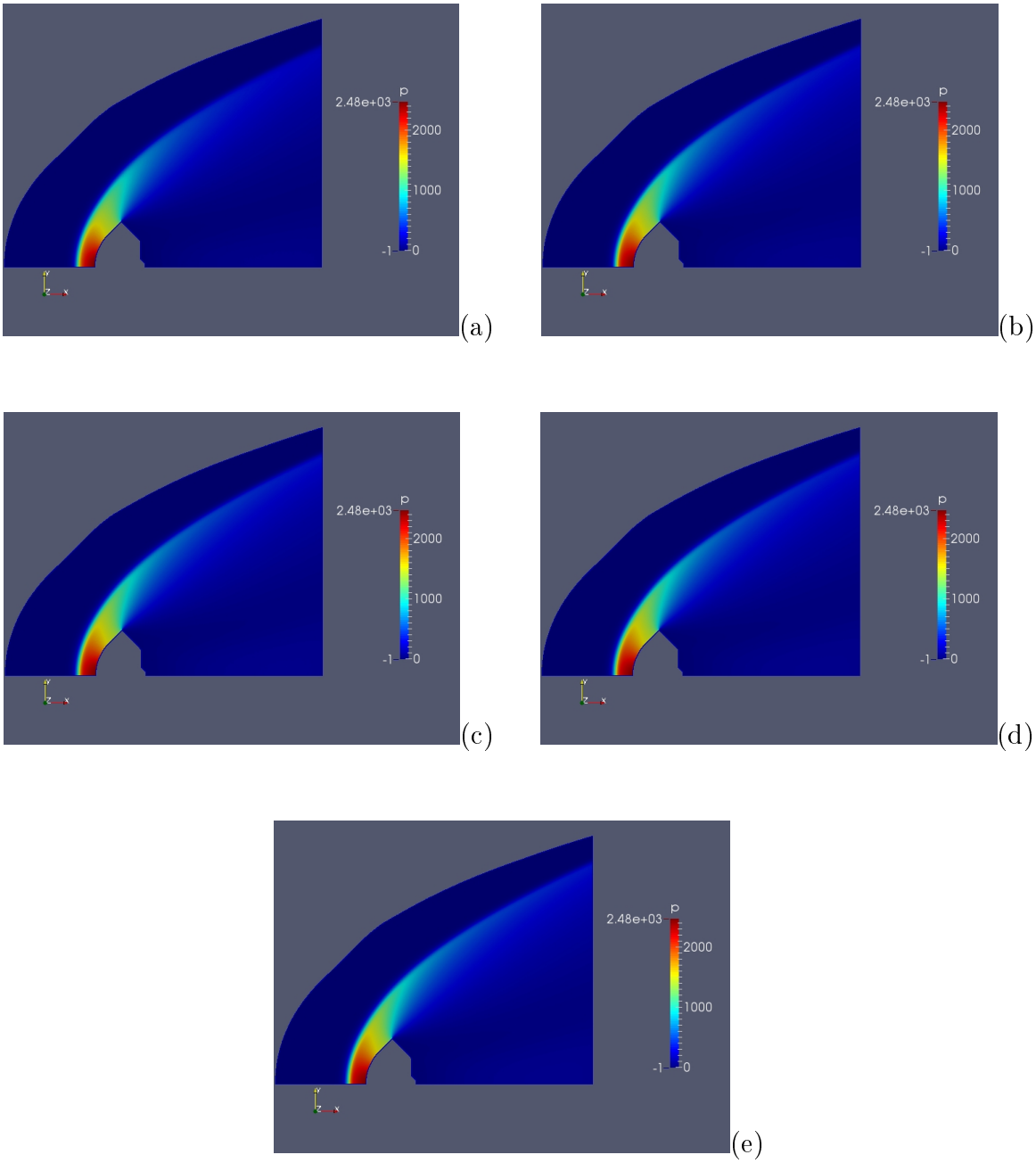

Figure A.4 Pressure Deriving from OpenFOAM Two-Dimensional Simulations without Reactions Starting from an End Time of 0.001 s (a) to 0.005 s (e)

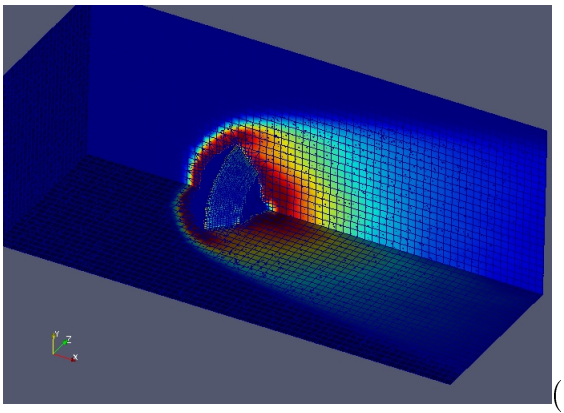
(a)

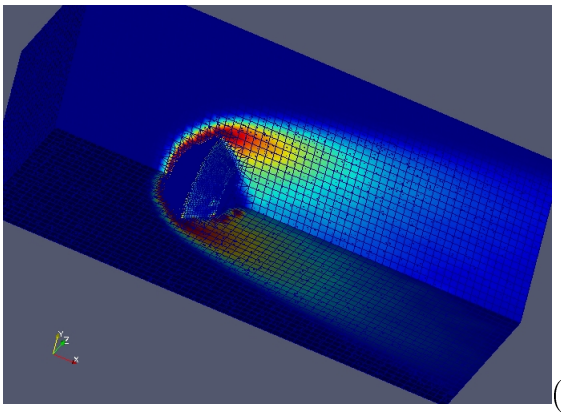
(b)

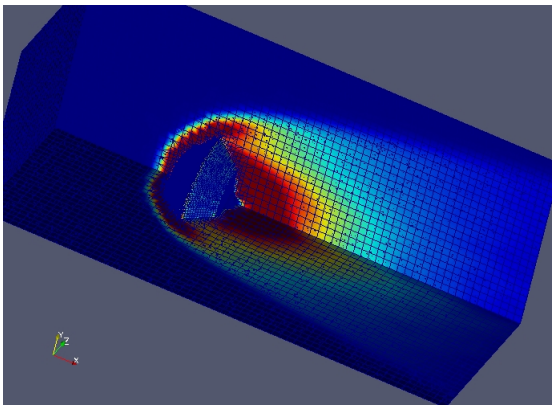
(c)

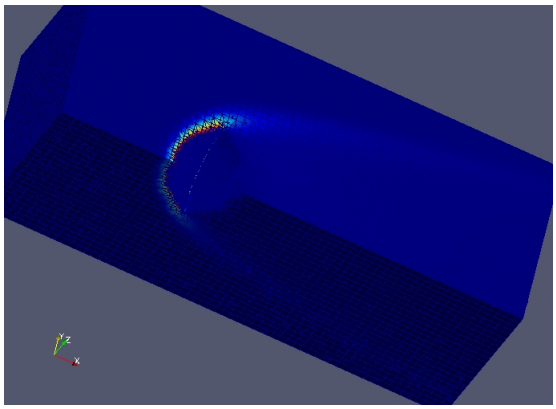
(d)

Figure A.5 Overall Temperature (a), Vibration / Electron / Electronic Temperature (b), Translation / Rotational Temperature (c) and Pressure (d) Deriving from OpenFOAM Three-Dimensional Simulations without Reactions for an End Time of 0.001 s